DESIGN AND ANALYSIS OF EX-VIVO MINIMALLY INVASIVE ROBOTIC SYSTEM FOR ANTEBRACHIUM LACERATION SUTURING TASK

A thesis submitted to the
University of Petroleum and Energy Studies

For the award of
Doctor of Philosophy
in
Electrical and Electronics Engineering

BY
Varnita Verma

October 2020

SUPERVISOR
Dr. Piyush Chauhan
Dr. Mukul Kumar Gupta

Department of Electrical and Electronics Engineering
School of Engineering
University of Petroleum & Energy Studies,
Dehradun – 248007: Uttarakhand

DESIGN AND ANALYSIS OF EX-VIVO MINIMALLY INVASIVE ROBOTIC SYSTEM FOR ANTEBRACHIUM LACERATION SUTURING TASK

A thesis submitted to the
University of Petroleum and Energy Studies

For the award of
Doctor of Philosophy
in
Electrical and Electronics Engineering

BY
Varnita Verma
(SAP ID- 500056857)

October 2020

SUPERVISOR
Dr. Piyush Chauhan
Assistant Professor (Selection Grade)
Department of Informatics

CO-SUPERVISOR
Dr. Mukul Kumar Gupta
Assistant Professor (Selection Grade)
Department of Electrical and Electronics Engineering
University of Petroleum and Energy Studies
Dehradun, Uttarakhand

Department of Electrical and Electronics Engineering
School of Engineering
University of Petroleum &Energy Studies,
Dehradun – 248007: Uttarakhand

DECLARATION

I declare that the thesis entitled "**Design and Analysis of Ex-Vivo Minimally Invasive Robotic System for Antebrachium Laceration Suturing Task"** has been prepared by me under the guidance of **Dr. Piyush Chauhan**, Assistant Professor (Selection Grade) of Department of Informatics and **Dr. Mukul Kumar Gupta**, Assistant Professor (Selection Grade) of Department of Electrical and Electronics Engineering, University of Petroleum & Energy Studies. No part of this thesis has formed the basis for the award of any degree or fellowship previously.

Varnita Verma

Department of Electrical and Electronics Engineering,
School of Engineering
University of Petroleum & Energy Studies
Dehradun-248007: Uttarakhand

Date:

UPES
UNIVERSITY WITH A PURPOSE

Great Place To Work. Certified APR 2019–MAR 2020 INDIA

CERTIFICATE

I certify that **Varnita Verma** has prepared her thesis entitled "**Design and Analysis of Ex-Vivo Minimally Invasive Robotic System for Antebrachium Laceration Suturing Task,**" for the award of a Ph.D. degree from the University of Petroleum & Energy Studies, under my guidance. She has carried out the work at the Department of Electrical and Electronics Engineering, University of Petroleum & Energy Studies, Dehradun.

Piyush Chauhan 22/10/2020

Supervisor

Dr. Piyush Chauhan

Assistant Professor (Selection Grade)
Department of Informatics
University of Petroleum and Energy Studies
Dehradun, Uttarakhand

Co-Supervisor

Dr. Mukul Kumar Gupta

Assistant Professor (Selection Grade)
Department of Electrical and Electronics Engineering
University of Petroleum and Energy Studies
Dehradun, Uttarakhand

Date: 22/10/2020

CORPORATE OFFICE: 210, 2nd Floor, Okhla Industrial Estate, Phase III, New Delhi - 110 020, India.
T: +91 11 41730151/53, 46022691/5
F: +91 11 41730154

ENERGY ACRES: Bidholi Via Prem Nagar, Dehradun - 248 007 (Uttarakhand), India.
T: +91 135 2770137, 2776053/54/91, 2776201
F: +91 135 2776090/95

KNOWLEDGE ACRES: Kandoli Via Prem Nagar, Dehradun - 248 007 (Uttarakhand), India.
T: +91 8171979021/2/3, 7060111775

ABSTRACT

Open surgery generally involves making a large cut to visualize the operative field and to ingress human internal tissues. Minimally invasive surgery (MIS) is a fetching alternative to the surgery whereby same operations are performed using the specialized instruments designed to fit into the body through multiple very small-sized holes instead of one large cut.

Simple techniques in open surgery such as suturing of surgical wounds become time-consuming and inconsistent tasks. The suturing task is performed repeatedly and consumes a majority of the time during surgery, to make it autonomous will increase the efficiency, uniformity and standardize the quality of suturing outcome with minimum human intervention and in less duration of time. The Automatic suturing robot will perform the basic suturing task with the help of advanced computer vision techniques and actuator control techniques.

The Antebrachium Laceration Suturing Robot (ALSR) consists of a bedside light weighted 6 DOF robotic arm with the actuated suturing tool Endo stitch attached with the robotic arm as an end effector. The Endo stitch handles three actuators in which the first actuators is to drive the circular needle and the second is to lock the needle between jaws of the endo stitch. The kinematics and dynamics of the system are computed in order to identify and control the motion analysis of the ALSR. The implementation of different control algorithms is used in order to achieve zero tracking error and robust trajectory tracking. The CAD model design of the novel ALSR was developed. The virtual surgical simulation is conducted to validate the control of trajectory tracking control. The antebrachium skin laceration has been depicted using tissue phantom. The interactive image segmentation has been used to detect the skin laceration on targeted tissue phantom. The detected skin laceration was considered as the desired trajectory for ALSR. The various controls were implemented to achieve accurate position control to perform the suturing task. The technical evaluation of the proposed robot is carried out using a co-simulation platform. The primary goal of this

research is to explore how the collaboration of dynamics analysis, control technique, and Image processing that can help in the precise micro motions of suturing robot. This thesis focuses on reducing the time of surgery by automating the simple suturing task which takes time to stitch the different layers of human/animal skin with the help of advanced algorithms and control techniques.

ACKNOWLEDGMENT

I would like to thank all the people who supported me, undertaking this research. I would first like to thank my advisors, Dr. Piyush Chauhan and Dr. Mukul Kumar Gupta, for their continuous guidance, support and encouragement. Their passion and persistence in science have always encouraged me during my research. In my first year, Dr. Mukul Kumar Gupta spent enormous efforts guiding me on research and never lost his patience when my simulation was not going well. I am thankful to my advisors for patiently listening to all of my puerile ideas and showing immense faith in me throughout.

In addition to my Supervisor, I would like to express my profuse appreciation and thankfulness to Dr. S. J. Chopra (Chancellor), Dr. Sunil rai (Vice-Chancellor), Dr. Kamal Bansal (Dean) and Dr. Jitendra Kumar Pandey (Assoc. Dean - Research) for their support in helping me pursue my research at the University of Petroleum & Energy Studies (UPES). I would also like to acknowledge the funding support received from the Research & Development Department, UPES, under SEED grant scheme, which was instrumental in my graduate research and getting this dissertation completed in time.

I would also like to mention my gratitude to the HOD and the faculty colleagues of the Electrical and Electronics Department for motivation and cooperation. I would like to acknowledge the in-house Robotics and Sensor lab, Image processing lab, Mechatronics Lab and Bosch Center of Excellence at UPES, Dehradun for providing facilities to conduct my research experiments. I am also grateful to the lab staff and their support at our Institute (UPES).

A sincere note of thanks to Dr. Deepak Bharadwaj, Mr. Anil Kumar, Dr. R. Gowri, Dr. N. Prashanti, Dr. Amit Kumar Mondal for their valuable suggestions and guidance at every stage of this work. I am deeply thankful to all my colleagues at the University of Petroleum and Energy Studies: Mr. Debajyoti Bose, Mr. Akash Gupta, Ms. Meera C. S, Mr. Caneon Kurien, Mr.

S.R.V.S Prasanna, Mr. P. Sairam, Ms. B. Aslesha, Ms. Srawanthi Medhi, Mr. Satyajith Chowdhary, Mr. Glen B. H, Mr. K. Balaji and Mr. Chakradhar for their invaluable comments and suggestions during group meetings. Special thanks to Kashyap, Alex and Vikas Thapa for their support in my journey.

Finally, I would like to thank my parents Smt. Sandhya Verma and Shri. Arvind Prakash Verma for their immense support and love at every stage of my life. Completing this degree would never be possible without their love and encouragement. I especially want to thank my siblings, Miss Arpita Verma and Mr. Kushagra Verma, for their steadfast support. I become brave enough to face the toughness of life because of their encouragement and motivation.

To my Family

and

My Late Grandfather “Shri. Jay Prakash Verma”

TABLE OF CONTENT

DECLARATION ..... **ii**
CERTIFICATE ..... **iii**
ABSTRACT ..... **iv**
ACKNOWLEDGMENT ..... **vi**
TABLE OF CONTENT ..... **ix**
LIST OF FIGURE ..... **xii**
LIST OF TABLE ..... **xiv**
NOMENCLATURE ..... **xv**
ABBREVIATIONS ..... **xvi**
CHAPTER 1 INTRODUCTION **1**
1.1 MOTIVATION 1
1.2 PROPOSED METHODOLOGY 3
1.3 PRINCIPLE CONTRIBUTION 5
1.4 THESIS ORGANIZATION 5
CHAPTER 2 LITERATURE REVIEW **7**
2.1 APPLICATION OF ROBOTICS IN HEALTHCARE 7
2.2 MECHANICAL DESIGN CONSIDERATION 11
2.3 CONTROL PARADIGMS 12
2.3.1 HANDS-ON COMPLIANT CONTROL 13
2.3.2 TELE-OPERATIVE CONTROL 13
2.3.3 PRE-PROGRAMMED, SEMI–AUTONOMOUS CONTROL 18
2.4 SURGICAL SIMULATION 19
2.5 PROBLEM STATEMENT 22
CHAPTER 3 GENERIC KINEMATIC AND DYNAMIC MODELING OF N- DOF ROBOT MANIPULATOR **24**
3.1 MATHEMATICAL MODELLING: 25
3.2 GENERIC KINEMATIC MODEL FOR N-DOF: 26

3.3 THE N-DOF GENERIC DYNAMICS MODEL BY NEWTON EULER: 28
3.3.1 FORWARD COMPUTATION FOR VELOCITY AND ACCELERATION: 30
3.3.2 BACKWARD COMPUTATION FOR FORCE AND MOMENTS 33
3.4 GENERIC SEPARATION ALGORITHM (GSA): 36
3.5 MODEL EVALUATION: 37
3.6 SUMMARY: 41
CHAPTER 4 KINEMATIC AND DYNAMIC MODELING OF ANTEBRACHIUM LACERATION SUTURING ROBOT 42
4.1 KINEMATIC MODELING OF ANTEBRACHIUM LACERATION SUTURING ROBOT (ALSR) 43
4.1.1 FORWARD KINEMATICS 45
4.1.2 INVERSE KINEMATICS 50
4.2 ANTEBRACHIUM LACERATION SUTURING ROBOT DYNAMIC FORMULATION 51
4.3 SUMMARY 53
CHAPTER 5 SKIN LACERATION DETECTION 54
5.1 REVIEW OF IMAGE SEGMENTATION IN MEDICAL DIAGNOSIS 55
5.2 SKIN LACERATION DETECTION TECHNIQUE 55
5.2.1 IMAGE ACQUISITION 56
5.2.2 IMAGE PRE-PROCESSING 56
5.2.3 FEATURE EXTRACTION 58
5.3 GEODESIC SEGMENTATION 59
5.4 EUCLIDEAN DISTANCE SEGMENTATION 60
5.5 RESULT 63
5.6 SUMMARY 67
CHAPTER 6 TRAJECTORY TRACKING CONTROL 68
6.1 CONTROL: PD, PID AND COMPUTED TORQUE CONTROLLER ANALYSIS 69

6.2 COMPARATIVE RESULTS OF PD AND PID CONTROLLER WITH REFERENCE TO CTC CONTROLLER AND ITS CASES....72
6.3 PERFORMANCE ESTIMATION....72
6.4 DISTURBANCE MODELLING FOR ALSR....77
6.5 DISTURBANCE OBSERVER BASED CONTROL SCHEME OF THE ALSR....79
6.6 SIMULATION STUDY OF DISTURBANCE OBSERVER....82
6.7 CO SIMULATION ANALYSIS AND RESULTS....88
6.8 SAFETY ASPECTS....95
6.9 SUMMARY....95
CHAPTER 7 CONCLUSION AND FUTURE SCOPE....96
7.1 CONTRIBUTION....96
7.2 FUTURE WORK....97
REFERENCES....99
APPENDIX A....113
LIST OF PUBLICATIONS....114

LIST OF FIGURE

Figure 1.1. Laparoscopic surgery through DA-Vinci Robot [8].....3
Figure 1.2: Proposed system methodology flow diagram for ALSR.....4
Figure 2.1: Robot Assistive surgery (Modified from Okamura, Allison M. 2010)[15].....8
Figure 2.2: Different Types of End-Effector tools [36], [37] 13
Figure 3.1: Possible position of joint Vector of joint i-1 [42] 28
Figure 3.2: Representation for preceding two links of n-DOF GDM.....29
Figure 3.3: Flow chart of dynamic calculation 35
Figure 3.4: The flow chart representation of the Generic Separation Algorithm 37
Figure 3.5: Structural Representation of two-link 2R configuration robot.....38
Figure 3.6: Structural Representation of a two-link RT configuration robot. .39
Figure 3.7: Structural Representation of a two-link TT configuration robot...40
Figure 4.1. RRPR Robot Manipulator (Center of Excellence Laboratory, U.P.E.S., Dehradun,India) 43
Figure 4.2: CAD model of the Antebrachium Laceration Suturing Robot (ALSR).....45
Figure 4.3: Frame assignment of the Antebrachium Laceration Suturing Robot (ALSR).....46
Figure 5.1: Skin Phantom 56
Figure 5.2: HSV Image of Skin Phantom 57
Figure 5.3: Interactive selection of desired HSV color space.....58
Figure 5.4: Flow chart for Skin laceration detection system. 62
Figure 5.5: Laceration segmentation of Phantom using Euclidean Distance Metric algorithm with varying Tolerance. 63
Figure 5.6: Laceration segmentation of Phantom using Geodesic Distance Metric algorithm with varying Tolerance. 64
Figure 5.7: Comparative analysis of Total pixels required for each Euclidean and Geodesic Distance metric algorithm for laceration detection. 66
Figure 5.8: Segmentation of Skin laceration.....66
Figure 6.1: Block Diagram of PD–Computed Torque Control (PD-CTC).....69
Figure 6.2: Computed Torque Control (CTC) at different cases and Desired Input Step Trajectory for (a) Link 1 Joint Angle, (b) Link 2 Joint Angle, (c) Link 3 Joint Displacement, and (d) Link 4 Joint Angle.....74
Figure 6.3: Computed Torque Control (CTC), Proportional-Derivative Control (PD), Proportional Integrated Derivative Control (PID) and Desired Input Step

Trajectory for (a) Link 1 Joint Angle, (b) Link 2 Joint Angle, (c) Link 3 Joint Displacement and (d) Link 4 Joint Angle. 76
Figure 6.4: Block Diagram of the disturbance observer scheme for the surgical robot 80
Figure 6.5: Modelling of disturbance observer assisted surgical manipulator 82
Figure 6.6: Time Trajectory position tracking of each link of the manipulator (a), (b), (c) and (d) with and without Observer. 83
Figure 6.7: Position tracking error profile for link 1 (a), link 2 (b), link 3(c), and link 4 (d) in laceration tracking. 84
Figure 6.8: Joint disturbance tracking profile for each joint of the surgical manipulator 85
Figure 6.9: Disturbance tracking error in each joint of a surgical manipulator 86
Figure 6.10: Task space coordinate (XYZ) of the end effector during laceration tracking operation..... 87
Figure 6.11: Co-simulation experiment of ALSR in Matlab/ADAMS interface 90
Figure 6.12: Co-simulation experiment of ALSR invoking ADAMS platform through MATLAB shows the suturing operation 90
Figure 6.13: Suturing task-specific joint angle position tracing by ALSR..... 91
Figure 6.14: Hardware model of ALSR..... 92
Figure 6.15: Sutured skin phantom..... 93
Figure 6.16: Interaction force estimation setup 93
Figure 6.17: Contact force on end effector 94
Figure 6.18: ALSR suture needle displacement in the workspace 94

LIST OF TABLE

Table 2.1: Pros and Cons of different assistive devices.....9
Table 2.2: Comparative Study of different Robotic Solutions 15
Table 2.3: Different Simulators for treatment of different diseases 20
Table 2.4: Different Suturing tools and their operations [60].....21
Table 3.1: D-H parameter of n-DOF Generic Kinematic model. 27
Table 3.2: D-H Parameters for 2R Planar.....38
Table 3.3: D-H Parameters for RT Planar robot manipulator.....39
Table 3.4: D-H Parameters for TT Planar robot manipulator.....40
Table 4.1: ALSR Robot Parameters and Their Value.....46
Table 4.2: D-H Parameter of the ALSR Manipulator.....47
Table 5.1: Comparison table for Euclidean distance matric with respect to Geodesic Distance Metric.....65
Table 6.1: Comparison table of Computed Torque Control (CTC) of different cases followed with their respective Steady State Error (SS Error) and Root Mean Square Error (RMS Error) 74
Table 6.2: Different control techniques: CTC, PD and PID with their respective gains.....76
Table 6.3: Root Mean Square (RMS) Error of system and Steady State (SS) Error at each joint of the system at different control techniques. 77
Table 6.4: Illustrate the RMS value of position tracking error and disturbance tracking error while performing the surgical task by the manipulator.....87
Table 6.5: Generalised Antebrachium Skin Properties.....89

NOMENCLATURE

$\boldsymbol{\theta_i}$	Generic Joint Angle of link i
$\boldsymbol{d_i}$	Joint offset of link i
$\boldsymbol{a_i}$	length of link i
$\boldsymbol{\alpha_i}$	Joint Twist in link i
$\boldsymbol{M(q)}$	Inertia Matrix
$\boldsymbol{N(q,\dot{q})}$	Coriolis and Centripetal Matrix
$\boldsymbol{G(q)}$	Gravity Matrix
$\boldsymbol{m_i}$	Mass of Augmented link,
$\boldsymbol{P_{ci}}$	Generic Center of Mass Coordinate
$\boldsymbol{I_i}$	Inertia Tensor of Augmented Link,
$(\boldsymbol{R_i^{i-1}})^{\boldsymbol{T}}$	Transposed Rotation Matrices of Augmented Link
$\boldsymbol{P_i^{i-1}}$	Generalized position Vector
$\boldsymbol{\dot{P}_i^{i-1}}$	Linear velocity for a generic augmented link
$\boldsymbol{\ddot{P}_i^{i-1}}$	Linear acceleration for a generic augmented link
$\boldsymbol{\omega_i^i}$	Angular velocity of augmented joint
$\boldsymbol{\dot{\omega}_i^i}$	Angular acceleration of augmented joint
$\boldsymbol{v_i^i}$	Linear velocity of augmented joint
$\boldsymbol{\dot{v}_i^i}$	Linear acceleration of augmented joint
$\boldsymbol{\dot{v}c_i^i}$	Linear acceleration of center of mass of n link.
$\boldsymbol{F_i^i}$	Total external force acting on each link
$\boldsymbol{N_i^i}$	Total moment of inertia force acting on each link
$\boldsymbol{f_i^i}$	Force acting on each link.
$\boldsymbol{\eta_i^i}$	Moment of Inertia acting on each link

ABBREVIATIONS

RRPR	Two Revolute One Prismatic and One Revolute Joint
ALSR	Antebrachium Laceration-Suturing Robot
BBST	Bounding Box Based Segmentation Technique
CAD	Computer Aided Design
CAS	Computer-Assisted Surgery
CTC	Computed Torque Control
D-H	Denavit-Hartenberg
DOB	Disturbance Observer
DOF	Degree of Freedom
EOG	Electrooculography
GDM	Generic Dynamic Model
GKM	Generic Kinematic Model
GSA	Generic Separation Algorithm
GSI	Giga Scale of Integration
HAL	Hybrid Assistive Limb
MBST	Marking Based Segmentation Technique
MIS	Minimally Invasive Surgery
MTM	Master Tool Manipulator
PD	Proportional-Derivative
PID	Proportional Integration Differentiation
PSM	Patient Side Manipulator
RAI	Robotic Assosiation Institute
RAS	Robotic Assistive Surgery
RMS	Root Mean Square
ROI	Region Of Interest
SCARA	Selective Compliance Assembly Robot Arm
SENARIO	SENsor- Aided intelligent wheelchaiR navigatIOn

STAR	Smart Tissue Anastomosis Robot
ULSI	Ultra Large Scale Of Integration
VLSI	Very Large Scale Of Integration
VR	Virtual Reality

CHAPTER 1 INTRODUCTION

The accelerated involvement of automation in various field to make human life simpler, give rise to surplus issues, which required attention. The rapid development of industrial automation produces a huge demand for robot manipulators in their workspace. Similarly in the field of surgery, the different manipulators were involved to perform various tasks in pre, post and during surgery. The basic operating task frequently involved during the surgery is Suturing. To approximate or ligate the tissue using sutures termed as suturing and to automate this task for Antebrachium laceration the Antebrachium Laceration Suturing Robot (ALSR) was developed. The thesis illustrates the systematic procedure for the design of manipulator and end effector, performance estimation of different control schemes for the competition of suturing task. The chapter introduces the aspects related to this topic, outline, and thesis organization of this dissertation.

1.1 MOTIVATION

Open surgery generally involves making a large cut to visualize the operative field and to ingress human internal tissues. Minimally invasive surgery (MIS) is a fetching alternative to surgery whereby the same operations are performed using specialized instruments designed to fit into the body through multiple very small-sized holes instead of one large cut. It can minimize pain and decrease the recovery time and cost, but also offers more technical difficulties to surgeons. Indulgence of robotic technology in surgery changed the experience of the surgeon during surgery. Various image-guided surgical robots were used by capturing the real-time tool status from advanced imaging techniques such as CT Scan, Magnetic Resonance Imaging (MRI), etc. After any MIS or open surgery, the majority of the time consumed by the surgeon in operation theater

is because of tedious multiple-layer skin closure. The classical method of skin closure technique is manual suturing, which intends the surgeon to directly see the operating site and perform suturing manually. The manual suturing involves several practical challenges and limitations such as limited access to the operating site in case of in-vivo suturing, intense concentration is required from the surgeon, accuracy, and precision of sutures were entirely dependent on the surgeon's manipulability. Large blood loss can happen while performing in-vivo manual suturing. Proper training is required to perform manual suturing. To overcome limitations of manual suturing the different Hand-Held Suturing Devices (HHSD) was developed which enables the surgeon to manipulate the control of the device with a manual shifting mechanism. This brings the shift of technology from open surgery to Minimally Invasive Surgery (MIS). HHSD technique brings the challenge to the surgeon to stay in an awkward position for a longer duration that made the surgeon tired and more vulnerable to human errors and hand tremors. Robot-Assisted Surgery (RAS) brings the surgeon into a semi-comfortable position of operation which has a Master tool Manipulator console with a virtual imaging attachment. In manual, HHSD and RAS suturing operation entirely depend on the surgeon's hand and eye coordination and experience.

Human being who were performing task with sharp tools and machinery are more susceptible to antebracium skin laceration while performing industrial task. The Antebrachium is more vulnerable to cuts and deep laceration while performing different tasks in industries or daily routine work. In order to provide solutions to antebrachium laceration for the speedy recovery of employees, shorter hospital stay, less blood loss, less operating time for ex-vivo skin laceration, and limited or no dependence on surgeons manipulability a robotic system is required. This brings a new domain of specific application robots for wound closure.

The objective of the thesis is to design a novel suturing robotic for Antebracium Ex-vivo skin laceration that can provide a feasible solution for skin closure.
The research is intended to perform an automatic suturing in a simulation model in which trajectory planning of the robot end-effector will be taken into account, accordingly suturing of cut will be done. Using this simulation model that helps surgeons to simulate the surgery which is going to be performed[1][2][3]. The Simulation model development will help the surgeon to assess suture points and implement it in the simulation model irrespective of the surgeon's training, experience and working condition. The lack of skill and expertise in operating the laparoscopic surgery leads to difficulty in operating it quickly and efficiently[4][5]. Availability of less number of skilled surgeons in the market increases the cost of simple operation task like suturing. The integration of robotics in surgery with automation makes the system more reliable and improve operations performance[6][7].

Figure 1.1. Laparoscopic surgery through DA-Vinci Robot [8]

1.2 PROPOSED METHODOLOGY

The goal of the research is to reduce the operating time of surgery, potential access to robots during surgery and to develop the automatic suturing robot simulation model for complex suturing tasks[9][10].

Figure 1.2 shows the proposed system methodology flow diagram for novel Antebrachium Laceration Suturing Robot (ALSR). The flow diagram consists of four sections which is discussed in four chapters. The first section is laceration detection where with the use of machine vision and interactive image segmentation, the antebrachium skin laceration way points has been estimated. These coordinated were fed to the second section consists of kinematic modeling where inverse kinematic modelling has been used to estimate the joint motion of ALSR. The estimated joint motion of ALSR is taken as the desired motion and provided this as an input to the DOB control to perform the trajectory tracking control of ALSR. The fourth section consists of ALSR itself having torque as an input to actuators and sensors provide the actual joint variables which is again fed back to the DOB based CTC control to achieve zero tracking error.

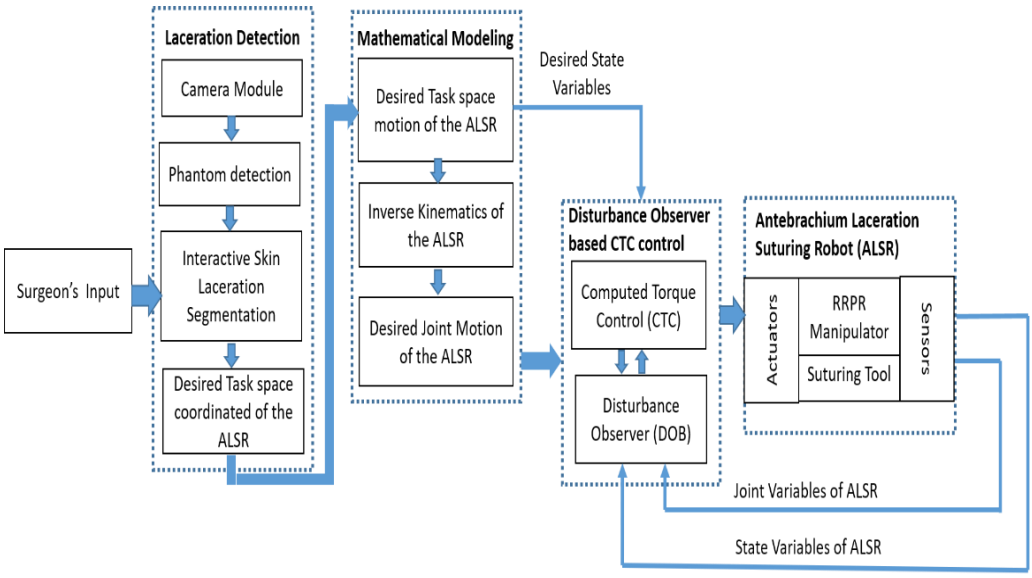

Figure 1.2: Proposed system methodology flow diagram for ALSR

1.3 PRINCIPLE CONTRIBUTION

The principal contribution of this research is the design of a novel robotic system for the suturing of antebrachium skin laceration. This research aims to provide an automatic suturing robot for ex-vivo skin laceration. This can be operated by a novice surgeon for small antebrachium laceration.

- Design of a novel suturing robot for the antebrachium laceration suturing application.
- The extraction of the desired trajectory waypoints by using interactive skin laceration segmentation techniques.
- Derivation of disturbance observer-based assisted control for the disturbance compensation and accurate joint torque estimation. This observer model can be used for disturbance estimation in other manipulators by providing joint velocity and joint acceleration.
- Development of a virtual simulation environment to analyzing the feasibility test of the designed robot at a low cost. The testing of control algorithms using virtual simulation.
- Development of hardware model for the proof of concept.

1.4 THESIS ORGANIZATION

The decomposition of the entire research work is in the form of chapters. Following are the organization of chapters is the sequential problem-solving structure to form the thesis.

- Chapter 2 illustrates the review of the vast literature of robotics in surgery, related to their robot selection, proposed methods and their limitations.
- In Chapter 3, the generalized robot kinematics and dynamics (GKM & GDM) of the n-DOF robot manipulator were discussed.

- Chapter 4 the design and computation of kinematics and dynamics of Antebrachium Laceration Suturing Robot (ALSR) based on GKM and GDM were computed.
- Chapter 5 The Skin Laceration detection and Segmentation were discussed using the Image Segmentation technique to have the desired trajectory for ALSR.
- Chapter 6 presents the results of the performance analysis of various control schemes to obtained precise trajectory tracking of skin laceration for suturing. The work is concluded in Chapter 7, with the conclusion and an enumeration of the possible extension of the present work for future research.

CHAPTER 2 LITERATURE REVIEW

The chapter gives an overview of the previous studies conducted in the field of surgical robotics. Robotics is one of the emerging and innovative fields of research in universities for the last two decades. The robot was first introduced in 1920 by Karl Capek. There is no fixed definition of the robot but as per the Robot Institute of America (RIA): A robot is a programmable multifunctional manipulator designed to move material, parts, tools, or specialized devices through variable programmed motions for the performance of a variety of task. Robotics is the engineering science and technology that has applications mainly in the area of Military applications, intelligent home applications, industrial automation, health services, and Outer space applications[11]–[14]. The robotic unmanned spacecraft is used as the key to exploring the stars, planets, etc.

With the development of electronic technology like the very large scale of integration (VLSI), the ultra large scale of integration (ULSI) and the Giga scale of integration (GSI) and new sensor robots are using in very new areas. Robotics now play a vital role in the area like Aerial Robotics, Assistive living, Bioenergy and Self-Sustainable, Biomimetic and neuro-robotics, Medical robotics, Nonlinear robotics, Robot vision, Safe human-robot interaction, Self-repairing robotics systems, Smart automation, Soft robotics, Swarm robotics, Unconventional computation, etc.

2.1 APPLICATION OF ROBOTICS IN HEALTHCARE

The synergy between healthcare and robotics is deeply intertwined in the field of surgery, which provides great aid to the surgeon’s hand. Overall assessment of surgical care includes simulation training, preoperative planning and rehearsal, intraoperative navigation, post-operative assessment, open surgery, minimal invasive and remote surgery. The robotic surgery reduces surgical trauma, diminishes tissue damage, improves the recovery period of the patient,

appreciates the operation without tremor and favors precise micro motions aided with micro-forces.

Robotic Assistive Surgery (RAS) includes a motorized system to control the motion of the intervention suite. However, in Computer Assisted Surgery (CAS), the computer interface assists to doctor and controlling the intervention suite manually. CAS is generally used for the detection of tools, motion planning, identification of cut, cancer cells, etc. RAS considers the robot as the patient side manipulator (PSM) that can be autonomous or telemetry, controlled by the Master tool manipulator (MTM) which gave manipulability capability to the doctor intelligence can be seen in Figure 2.1. In CAS, the end tool operating the person is directly manipulated by the surgeon's hand while in RAS the operating end tool is a robotic arm controlled by the surgeon's Inputs this is the major difference between CAS and RAS.

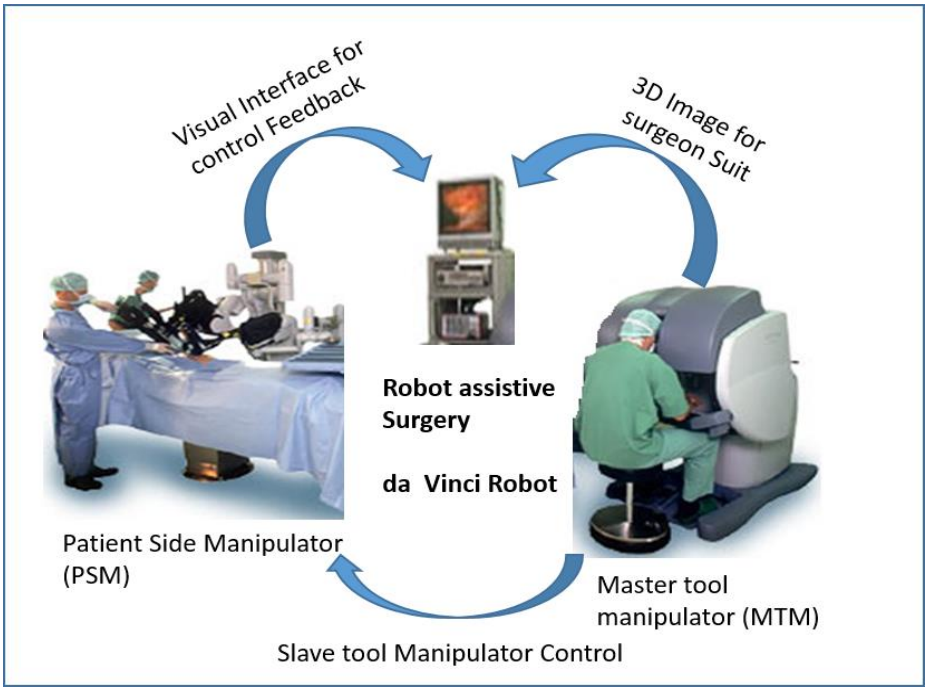

Figure 2.1: Robot Assistive surgery (Modified from Okamura, Allison M. 2010)[15]

RAS provides human dexterity and ergonomics make the system more reliable with less tremors and more robust to human errors. The upcoming technology not only focuses on the enhancement of MIS surgery but also focused on the localization of foreign bodies. The different assistive robots are used to provide aid to elderly or handicapped people like Cody, Hybrid Assistive Limb (HAL) and many more. The pros and cons of the assistive robot can be seen in Table 2.1

Table 2.1: Pros and Cons of different assistive devices

Assistive Device	Salient pts.	Limitations
SENsor- Aided intelligent wheelchaiR navigatIOn (SENARIO) [16]	a) High level navigation to wheel chair. b) Works in semi autonomous with the help of joystick or voice commands. c) In autonomous modes, follows recorded paths.	a) In autonomous mode, navigation is limited to defined paths. b) Voice commands need proper filtering of noise, due to the shivering voice of the elderly people.
VAHIM [17]	a) Works in manual mode with anti-collision system. b) In assisted manual mode, it uses wall following or obstacle detection. c) In automatic mode, it uses globally planned paths.	
Wheelesley[18]	a) Equipped with graphical user interface in place of joystick.	For people with limited upper body mobility
Navcha [19], [20], SIAMO, Rolland	a) Automated navigation system.	
Kuno [21]	a) Caregiver following wheel chair	
Electrooculography (EOG) [22], [23]	a) These wheelchairs works based on the	

	retina movement of the user. b) Electrodes are placed around the eye to capture the eye movement.	
Direction gazing [24], [25]	a) Works on the movement of camera (placed in active or passive way) mounted with the wheelchair or user's head.	
Brain actuated [26], [27]	a) Works on Brain-computer interface. b) EEG signals via passive electrodes are used to capture the brain signals.	a) Aged people may find it difficult to use.
ROAD [28]	a) Assists users in standing up, sitting down, and locomotion. b) Robot is connected via ceiling and provides locomotion over a predefined path.	a) Most of the operations are addressed for lower limb rehabilitation. b) Infrastructural upgradation required. c) Navigation is limited to defined paths.
Robot for Interactive Body Assistance (RIBA) (developed by RIKEN-TRI Collaboration Center for Human-Interactive Robot Research) [29]	a) Strong and versatile to lift up patients. b) Could be used for modifying lifting trajectories, caregiver's instructions, voice commands, etc.	a) Highly sophisticated b) Risk of slippage from robotic arms (user safety).
Intelligent Sweet Home (ISH) [30], [31]	a) A smart house consists of various assistive robotic subsystems such as an intelligent bed, robotic hoists,	a) Highly sophisticated b) Need modifications to infrastructures

	intelligent wheelchair, etc. b) All the devices are connected.	
Home Lift, Position and Rehabilitation (HLPR) (developed by National Institute of Standards and Technology, USA)[32]–[35]	a) Multipurpose assistive chair for locomotion, transfer to toilet or bed, lift assistance and rehabilitation. b) Autonomous navigation	a) Highly sophisticated b) Dimensions of HLPR is constrained for operations in small spaces.

2.2 MECHANICAL DESIGN CONSIDERATION

Specific applications of the robot decide its design and structure. The design of a robot for surgical task need to have high precision, high stiffness and limited dexterity, which is suitable for needle placement in a sensitive organ like eyes, heart, brain, etc., orthopedic bone shaping, tumor removal and many other applications. The robot used for surgery usually has high gear ration, low speed, and low back-drivability. On the other hand, a robot used for Minimally Invasive Surgery (MIS) and complex surgery for soft tissues need to have high dexterity, compactness, and responsiveness. The robot usually has high speed, high back drivable mechanism, and low stiffness.

Earlier the industrial robots were modified and adapted to the medical implementation. This helps the researcher to reduce cost and time for the development of the robot, increase rapid prototyping with high reliability with modification to assure safety and sterility. These specialized end-effector tools are required for tool holding, positioning, sniping, suturing, etc. which will decrease the task of assisting individuals and provides the satisfaction of control over surgery. The different control techniques are used to interface between the surgeon and surgical tools like a joystick, visual tracking, voice recognition, which makes

surgeons operate more intuitively. The perfect example of foot-actuated joystick and voice recognition is Aesop endoscopic positioner. Aesop and Zeus robots are capable of pivot along with the insertion point whereas the rotation of tool end effector at its distal point provides more tranquility to the surgeon. The above techniques were used by the DaVinci robot, which is commercially very successful.

The variety of designs were proposed by numerous research groups who focused on the development of a robot that can provide high performance in a constrained environment. This introduces Minimal Invasive Surgery (MIS) to operate at a quarter-inch incision to reduce the loss of healthy tissues. For the construction of instruments for MIS investigated on different technologies such as cable-actuated wrists, shape memory alloy actuators, Micro hydraulic systems and electroactive polymers.

The placement of the robot also plays an important role during surgery. Usually, the robots are mounted on the operation theatre floor, ceiling, or bedside of the patient. The mount of the robot is necessary to ensure that even if the patient moves the relative motion of the patient and the robot should not be changed. The robotic system was embedded with different sensory technology that helps in estimating the pose of the end effector, imaging environment, and different constraints. The robot should be able to maneuver along the patient's contour. The workspace of the robot should be free from geometrical constraints. Secondly, the images captured for processing should not interfere with the robot structure or actuators.

2.3 CONTROL PARADIGMS

The control of a surgical robot places a crucial role without which the robot cannot be considered safe and may lead to death. The placement of different sensors, dynamics tools, and vision systems was mounted on a robot, which is controlled by the doctor w.r.t patient. Usually, the control of the robot can be done through the below three ways:

2.3.1 HANDS-ON COMPLIANT CONTROL

Figure 2.2 shows the robotic tool or control handle, which is grasped by the surgeon's hand to locate the position of the robotic end-effector. It is dependent on the surgeon's eye-hand coordination. The force sensors provide intuitive feedback to the surgeon by providing, visual or sensory feedback. Robodoc, EndoBot, and many others are used for this purpose. The coordinates of the end-effector can be continuously sent to the server for the track of operation.

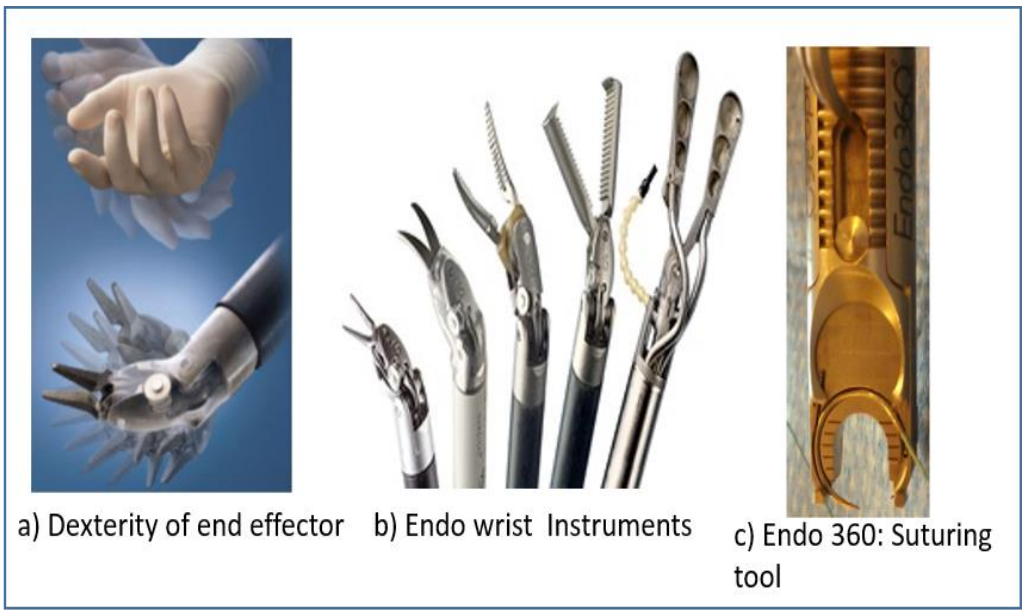

Figure 2.2: Different Types of End-Effector tools [36], [37]

2.3.2 TELE-OPERATIVE CONTROL

The robot in the healthcare industry used as a service robot and economic reasons may be the driving factor for its application. In healthcare, teleoperation plays an important role.

The Teleoperated system is such that it had a replica at the receivers end which mimics the function of the specialist side. It stands for the operating system from a distance. Human being controls teleoperated robots. The control signal is sent by a human that can be wired (through cables) or wireless. The need for the teleoperated system came from the urge to design and utilizes a device from a distance which can perform a controlled function. Tele-operation is different from telepresence. Telepresence refers to a group of technology which allows user sense to feel stimuli providing the presence of another individual. Telerobotics is the combination of these two fields, telepresence and teleoperation. A fully autonomous device is a robot. Teleoperator also called a telemanipulator if performs autonomous work then it's called a telerobot. A teleoperated robot consists of a central processing unit that sends the data from the input device (generally haptic devices) to the microcontroller through wifi or cable. Microcontroller wifi module connected to it that reads received data and then actuators are energized since the most commonly used actuators are motors. The microcontroller decides the direction of operation of the motor i.e clockwise or anti-clockwise.

Teleoperated robot systems have been developed for the operator to allow for various tasks via the remote control system. Teleoperation method, which is most frequently used in typical teleoperated robotic systems, and involves a master device that collects target task commands from an operator to a slave robot that carries out the commands. For example, Heikkila et al. proposed the functional design of a manufacturing robot cell [36]. Yamada et al. introduced the construction telerobot system with virtual reality [37]. Zhao et al. developed a construction telerobotic system that has wide applications in restoration work in stricken areas [38]. Kwon et al. developed a microsurgical telerobot system[39]. Geerinck et al. introduced the operability of an advanced demonstration platform incorporating reflexive teleoperated control concepts developed on a mobile robot

system [40]. The comparative study of different robotic solutions can be seen in Table 2.2.

Teleoperations finds it's applications in plenty of fields such as:

a. Medicine
b. Robotic Surgery
c. Space Exploration
d. Large Machinery management
e. Disaster Management
f. Elderly Care
g. Bomb Disposal
h. Remotely Operated Vehicle
i. Handling Radioactive Material

Other related healthcare benefits from robotics are Robotics in rehabilitation- Aims is to provide people with a tool that (slightly) compensates for their disabilities.

In Robotic Surgery, the surgeon directs the desired motion of the robot through an interface device where PSM control MTM. Through the visual interface, surgeons can have an inside view of the patient. The interfacing device replicates the movement of the surgeon's hand to robot motion. Through haptic interface force feedback was provided to make surgery more intuitive to the surgeon. An example includes the most widely used teleoperated robot i.e. DaVinci Robot.

Table 2.2: Comparative Study of different Robotic Solutions

Robotic Solution	Brief About the Robotic Solution	Specialty	Year	Category
PROBOT[9]	Is a floor robot which can be used for teaching advanced control technique	Prostatectomy	2004	Stand-alone device

ROBODOC (Integrated Surgical Supplies Ltd. from Sacramento, CA, USA) [41]	To create a robotic surgery system that would redefine precision in joint replacement procedure.	Hip replacement surgery	2006	Hands-on compliant control
FIPS Endoarm [42]	4 DoF, maintain an invariant point of constraint motion, FIST Endoarm was remotely controlled with a finger ring that was clipped to the surgeon's instruments.			Tele Robotic
Endoassist (Armstrong Healthcare Ltd.) [43]	A robotic camera holder, allows the surgeon to control its movement with the surgeon's head movement.			Tele Robotic
Gagner et al.	6 DoF prototyped robotic surgical assistant, controlled via a joystick by the surgeon in a remote room.	Laparoscopic surgery	1993	Tele Presence
da Vinci Surgical System (Intuitive Surgical Inc.)[44]–[46]	It is designed to facilitate complex surgery using the minimally invasive approach and is controlled by a surgeon from a console	Urological, Gynecological and gastronomical surgery [47], [48], Cardiac Surgery	1999	Tele Robotic

da Vinci Surgical System S model	Improved robotic arm movements, console display, and simpler setups	[49], [50], Abdominal surgery[51], [52]	2006	
da Vinci Si	Offers dual consoles for simultaneous operations of two individuals		2009	
ZEUS (Computer Motion Inc., Goleta, CA) [46]	Operates in master-slave mode, helps surgeon (master) to operate a console, which controls a robot (slave).	Cardiac surgery[53]	1994	Tele Robotic
Automated endoscope system for optimal positioning (AESOP) (Computer Motion, Santa Barbara, CA, USA) [28], [54]–[56]	The robotic system has an end effector that is adaptive to hold surgical instrument such as an endoscope	Urological, Laparoscopic surgery	1994	Voice Controlled/ Tele Robotic
SGRCCS [57]	A modified version of AESOP, to work on color tracking mechanism.		1999	Tele Robotic
Advanced robotic telemanipulator for minimally invasive surgery (ARTEMIS)[51], [58]	6 DoF. Voice-controlled, finger-ring joystick. It is having force-feedback.		1999	Tele Robotic

Laprotek (Brock-Rogers, Boston, USA)[59]	It provides 6 DoF and the system is moved by mechanical metal cables. Control of end effectors is realized by electronic data gloves.		2000	Tele Robotic

2.3.3 PRE-PROGRAMMED, SEMI–AUTONOMOUS CONTROL

In this, the extensive details of robot movement feed and saved to the system, which made the robot to move and articulate according to the parameters. Generally, the parameters are fetched from the image and processed further according to the requirement. The use of a dynamic system which is robust to the disturbance parameters.

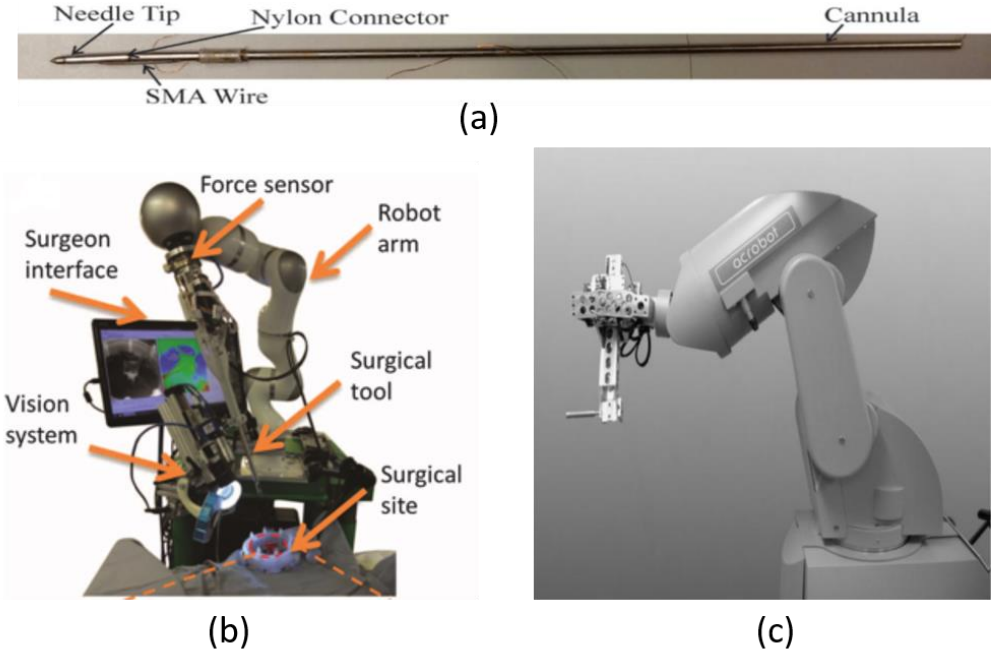

Figure 1.5**:** Pre-programmed or Semi-Autonomous Robot. (a) Self-Actuating Flexible Needle System. (b) STAR (c) Acrobot (Modified From Simon Leonard 2014, FO Maria Joseph 2015).

Examples as shown in Figure 1.5 include Smart tissue anastomosis robot (STAR), Self-Actuating Flexible Needle System, Acrobot, and many more in which the insertion point, cutting path, suturing points are pre-programmed and pre-define. The robot is guided with the help of visual feedback which makes the system real-time operated with minimal error.

2.4 SURGICAL SIMULATION

The simulation tool provides an added advantage to the surgeon to analyze the work environment of surgery and can rehearsal before performing complex surgery. Training of young surgeons in the simulation environment, prepare them to perform in the real world without any hesitation. Robotic simulator when integrating/fused/collaborate with Virtual Reality (VR) provides an eminent platform for treating human conscious and subconscious psychology which effect directly on physiological health. Some People who are afraid of few or something that always stays in their subconscious mind, which affects their psychology and different biological activity deeply due to which early age heart failure, disturbance in hormonal activity, instability in mind may occur. Therefore doctors take the help of the integration of a robotic simulator with virtual reality in which the patient asked to sit, stand, or lay down on the simulator wearing the VR glasses. This made the patient face its fear and help them to overcome it. During this activity, the different biological parameters are measure, updated on patient profile directly through IoT that help doctors as well patient to monitor the updated patient health, and can have a record of it for the future regime.

Table 2.3: Different Simulators for treatment of different diseases

Simulators	**Treatment of Diseases**
Sacral nerve stimulators [54]	Helps to treat chronic Pelvic Pain, constipation, interstitial cystitis, and different urinary disorder such as urge incontinence, non-obstructive urinary retention, overactive bladder, and fecal incontinence.
Artificial cardiac pacemakers[33]	Helps in the treatment of heart blockage, arrhythmia, Sinus Syndrome which causes irregular blood flow due to the dysfunctioning of the heart, which may lead to angina, syncope, dizziness, heart attack, or heart failure.
Deep brain stimulators [35,36]	Treatment of epilepsy, dystonia, brain essential tremors, Parkinson's disease, Tourette's syndrome, chronic pain, and obsessive-compulsive disorder.
Vagus nerve stimulators	Used to treat an inflammatory disorder of joint diseases, gastrointestinal tract, epilepsy, heart, and depression.
Spinal cord stimulators [32]	Helps to restore sensory, motor functioning, synapse, ischemic diseases and failed back surgery.
Transcutaneous electrical nerve stimulators [22,36]	Helps to treat pain like lower back pain, labor pain, musculoskeletal pain, neck pain, and used in dentistry.
Obesity Simulator	Help to treat Bariatric Patient

Table 2.3 describes the different simulators used to treat different diseases, which enable patients and doctors to monitor, record, and treat different real-time biological parameters.

Table 2.4: Different Suturing tools and their operations [60]

Technology	Operations	Parameters	Limitations
Linear Staplers [61], [62]	Stapling of six lines of titanium clips with cutting between third and fourth line	Different height of clips for the vascular and intestinal division Angulation of tip	Useful and safe for intestinal anastomosis, but not for the creation of neobladder owing to the lack of absorbable clips
Circular Staplers [63], [64]	End-to-end anastomosis by stapling the two sides of the bowel following purse-string suture	Different sizes of the device for different indications	• Mainly used in laparoscopic abdominal surgery • Theoretically useful in urology during the creation of a sigmoid neobladder
Endo Stitch™ (Medtronic Minimally Invasive Therapies, USA [65]	A straight needle with the centrally fixed suture is moved from one jaw to the other	• Flexible tip (SILS™ Stitch (Medtronic Minimally Invasive Therapies, USA)) • Motorized device (Autostitch – experimental)	• Very useful for continuous sutures (such as suturing the bowel or bladder) • Limited for fine sutures owing to stitching
Suture Assistant (Ethicon, USA) [65]–[67]	Straight needle for the single pass with a pretied knot	None	• Predominantly used for percutaneous pyeloplasty in urology • Continuous suture impossible
SEW-RIGHT® (LSI	Two built-in needles for interrupted sutures	None	Thick tissue is an issue for the jaws of the instrument

Solutions Inc., USA) [18,19]			
Ti-KNOT® (LSI Solutions Inc., USA)[68]	A knot-tying device using a titanium cylinder to lock the knot	Modified for cardiac surgery	• Not useful for urology owing to the titanium cylinder fixing the knot • Interrupted sutures
OverStitch® (Apollo Endosurgery Inc., USA) [69]	Spring-loaded curved suture with the suture fixed distal to the end	Developed for natural orifice transluminal endoscopic surgery	Might be useful for single-incision laparoscopic surgery
Endo360°® (EndoEvolution LLC, USA)[70]	A preloaded curved needle is pushed mechanically through tissue	Articulated tip	Mainly used for bariatric laparoscopic surgery
EndoSew® (Karl Storz GmbH and Co., Germany) [71]	Stitch and knotting mechanism	None	Laparoscopic transportation of sutured tissue difficult and clumsy

Table 2.4 illustrates the different suturing tools used in minimally invasive surgery and differentiate them with respect to their operations and tool specifications. This review enables us to select the appropriate end suturing tool for the Antebrachium Laceration modality.

2.5 PROBLEM STATEMENT

The present work involves the list of surgical robots as mentioned in the literature review. The maximum number of surgical robots consists of more than one arm in a robotic system. More number of arms consists of more number of

the actuator which enables the complex control system design. The surgeon also needs to go through a complex system of understanding to avoid any error. Even the most common repetitive task used in surgery having an “N” number of times needle tissue interaction is suturing, which inhabits the surgeon to ligate or approximate the tissue after surgery. To avoid large incision, heavy blood loss, human tremors, reduced time of operation, and precise suturing for the most common antebrachial laceration a robotic system is required.

The STAR Robot [70] developed has a huge dependence on the vision-based control without 3D sensing the control of STAR Robot has limitations. Tele-operated based surgery [54], [72], [73] relies on the surgeon's manipulability capability and prone to human errors. The manual filling is required for anastomosis suturing [74].

CHAPTER 3 GENERIC KINEMATIC AND DYNAMIC MODELING OF N- DOF ROBOT MANIPULATOR

In the current paradigm, there are vast changes in the standard of living. Therefore, to the easy life of humans the different robots has been introduced in different sectors of life such as healthcare robotics, cooking robot, cleaning robots, education robots, agriculture robot, etc [11], [15], [75]–[77]. This enables the huge domain to analyze the structure stability, motion, and control. The analysis of structural stability and control is only when the kinematics and dynamics of the system are known. Therefore, to compute the kinematics and dynamics of machinery the Generic Kinematic Model (GKM) and Generic Dynamic Model (GDM) are discussed. GKM and GDM help in computing kinematics and dynamics of the novel, novice, reconfigurable, and different n number of systems[78], [79]. This enables a rapid change in product design configurations, functionality, and applications.

In contrast to the application of robots in industries from a half-century ago, to automate dangerous, dirty, and recurring tasks, in the current scenario automation in healthcare and medicine change the entire environment of medication and task performed[76][80]. The robotics in surgery provide a huge impact on early recovery, less operating time, and more reliable outcomes in some cases. The basic task performed in any minor to major operation is approximating the tissues, which is commonly known as suturing. Suturing is an important, challenging, repetitive, and time-consuming task[62], [64]. To reduce operation time, blood loss, and achieve early recovery of the patient, accurate micro insertion the minimally invasive robot for suturing needs to be developed. Therefore, in this thesis, the novel Antebrachium laceration-suturing robot (ALSR) is discussed which is developed for antebrachium wound closure, which will reduce tissue trauma, human tremors, and aids healing. The

kinematic and dynamic model of ALSR has computed using GKM and GDM respectively.

3.1 MATHEMATICAL MODELLING:

The dynamic characteristics of a rigid body are determined to estimate the control specifications and performance estimation. The Euler Lagrange (EL) and Newton Euler (NE) formulation are the traditional algorithms used for computing mechanical system dynamics[81], [82]. In the Lagrange formulation, the derivation of the equation of motion considered the generalized coordinates independent of reference coordinate frames. The scalar quantity is used in the Lagrange coordinate system as it deals with the kinetic and potential energy of the system, which in turn eliminates the use of vectors and formulating by substituting one equation to another. Whereas in the Cartesian coordinate system the minimization of complex vectors takes place. Identifying the generalized coordinates of the system at the early stage of computation makes this method more prone to error[83], [84]. If wrong generalized coordinates are considered, the computed dynamics is not the dynamics of the system defined. The Euler Lagrange method is less efficient in computation with respect to Newton Euler in terms of multiplication, Addition, and Subtractions required to implement the algorithm[85]. Kane, Lagrange, and Wittenberg's algorithms were implemented algebraically. Each algorithm was analyzed according to their computation efficiency in calculating the dynamics of the 3R Puma robot[86].

John M. HollerBack compared and analyzed the recursive Lagrange formulation with the different algorithms such as Uicker/Kahn, Waters, Hollerbach (4x4), Hollerbach (3x3), Newton-Euler, Horn Raibert according to the dynamic formulation complexity with n^4 dependence in which n is taken as 6. He proved that the recursive Lagrangian formulation may be the most convenient efficient dynamics formulation until 1980[87]. The Featherstone

algorithm is a lower-order algorithm work efficiently to find out the inertia matrix, forward, and inverse dynamics of the manipulator[88]. The decoupled Natural Orthogonal Complement (DeNOC) has proven to be a numerically stable algorithm for computing forward and inverse dynamics of the system [63], [83]. On the computation of dynamics of the system, there are series of dynamic terms for each joint representation from which there inertia and gravity-dependent terms along with few least significant terms[89], [90]. These least significant terms do not contribute significantly to the dynamics of the system. These terms can be removed from the equation in order to increase the computation efficiency of the system and reduce time latency for control analysis[86], [91].

In this chapter, the kinematics and dynamics of the novel Antebrachium laceration suturing robot were computed with the help of the Generic Kinematic and Dynamic Model. The Recursive Newton Euler algorithm is selected for the computation of kinematics and Dynamics of the ALSR because of its numerical stability and computation efficiency as proven by the literature [83], [85]–[88], [92], [93]. To achieve the ALSR dynamics in the desired form of the dynamic equation having Inertia matrix, Coriolis, centripetal Matrix, and gravity vector the Generic separation algorithm (GSA) was developed and implemented using MATLAB Software.

3.2 GENERIC KINEMATIC MODEL FOR N-DOF:

The proposed model for generic kinematic modeling for an n-DOF configuration having n number of structural joints having either rotational and/ or translational joints [94]. For the n-DOF structure model, the generic representing of Denavit-Hartenberg (D-H) parameters are presented in Table 3.1, which shows the all-possible configurations of kinematic structures. Each joint can have six, possible positions of rotation and/ or translations. Either the Cartesian coordinate frame with x, y, z coordinates in a positive or negative

direction is used to represent the joint Vector $Z_{i-1.}$ To maintain the perpendicularity between the joint coordinate frames, there will be the five possible twist angle α_i which are $0, \pm 180, \pm 90$.

Table 3.1: D-H parameter of n-DOF Generic Kinematic model.

$\boldsymbol{i}$	$\boldsymbol{d_i}$	$\boldsymbol{\theta_i}$	$\boldsymbol{a_i}$	$\boldsymbol{\alpha_i}$
1	$R_1 d_{DH1} + T_1 d_1$	$R_1\theta_1 + T_1\theta_{DH1}$	a_1	$0, \pm 180, \pm 90$
2	$R_2 d_{DH2} + T_2 d_2$	$R_2\theta_2 + T_2\theta_{DH2}$	a_2	$0, \pm 180, \pm 90$
:	:	:	:	:
$\boldsymbol{n}$	$R_n d_{DHn} + T_n d_n$	$R_n\theta_n + T_n\theta_{DHn}$	a_n	$0, \pm 180, \pm 90$

R_i and T_i represents the rotational and translation joint respectively. R_i and T_i helps the generic D-H model to provide the variability to the selection of joint. The selection of joint in the n-DOF generic kinematic model is expressed in the following equations Eqn. (3.1) and Eqn. (3.2).

$$\text{When the joint is revolute then } R_i = 1 \text{ and } T_i = 0 \tag{3.1}$$

$$\text{When the joint is prismatic then } R_i = 0 \text{ and } T_i = 1 \tag{3.2}$$

The different configuration of the robot with constant DOF can be achieved by altering the modular parameter of each joint. The joint's modular parameter (K_{Si} and K_{Ci}) and can be expressed as below:

$$K_{Si} = \sin \alpha_i \tag{3.3}$$

$$K_{Ci} = \cos \alpha_i \tag{3.4}$$

The six possible position of the joint vector z_{i-1} provides the variability of modular joints. [95], [96] state that three can be 24 unique possible coordinate frames with x_{i-1} and y_{i-1} having four orientation on the selection of each joint

vector z_{i-1}. Figure 3.1 represents the possible position of the joint vector z_{i-1} for the joint i-1.

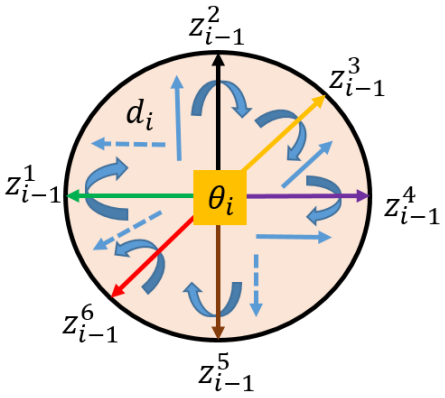

Figure 3.1: Possible position of joint Vector of joint i-1 [42]

The homogeneous transformation matrix is obtained by multiplication of all homogeneous matrices from base to end effector. For the n-DOF Generic Kinematic Model, the homogeneous transformation matrix can be represented as shown in Eqn. (3.5)

$$A_i^{i-1} = \begin{bmatrix} \cos(R_i\theta_i + T_i\theta_{DHi}) & -K_{Ci}\sin(R_i\theta_i + T_i\theta_{DHi}) & K_{Si}\sin(R_i\theta_i + T_i\theta_{DHi}) & a_i\cos(R_i\theta_i + T_i\theta_{DHi}) \\ \sin(R_i\theta_i + T_i\theta_{DHi}) & K_{Ci}\cos(R_i\theta_i + T_i\theta_{DHi}) & -K_{Si}\cos(R_i\theta_i + T_i\theta_{DHi}) & a_i\sin(R_i\theta_i + T_i\theta_{DHi}) \\ 0 & K_{Si} & K_{Ci} & R_i d_{DHi} + T_i d_i \\ 0 & 0 & 0 & 1 \end{bmatrix} \quad (3.5)$$

Where, $i = 1, 2, \ldots, n$

3.3 THE N-DOF GENERIC DYNAMICS MODEL BY NEWTON EULER:

The Newton Euler formation for dynamics modeling is based on newton's second law and d'Alembert Principle in which all the forces acting on a generic manipulator is been balanced. The set of equations developed on balancing the equations whose structure will provide a recursive solution to robot manipulator dynamics[97]. The recursive solution is subdivided into Forward Recursion

followed by backward Recursion. The forward Recursion provides the kinematic relationship of a moving coordinate frame, which infers the propagation of velocity and acceleration in consecutive links, followed by backward recursion for propagating forces and moments.

The generic augmented link is considered as Link i of the manipulator, which is connected between joint i and joint $i+1$. The kinematic chain of the manipulator is been computed with reference to the initial frame $\{0\}$. The frame of a link I can be seen in Figure 3.2 at the end of the generic joint i having frame $\{i\text{-}1\}$ and frame $\{i\}$. In Figure 2 the first two links of n-DOF GDM are illustrated with its possible different joint configurations.

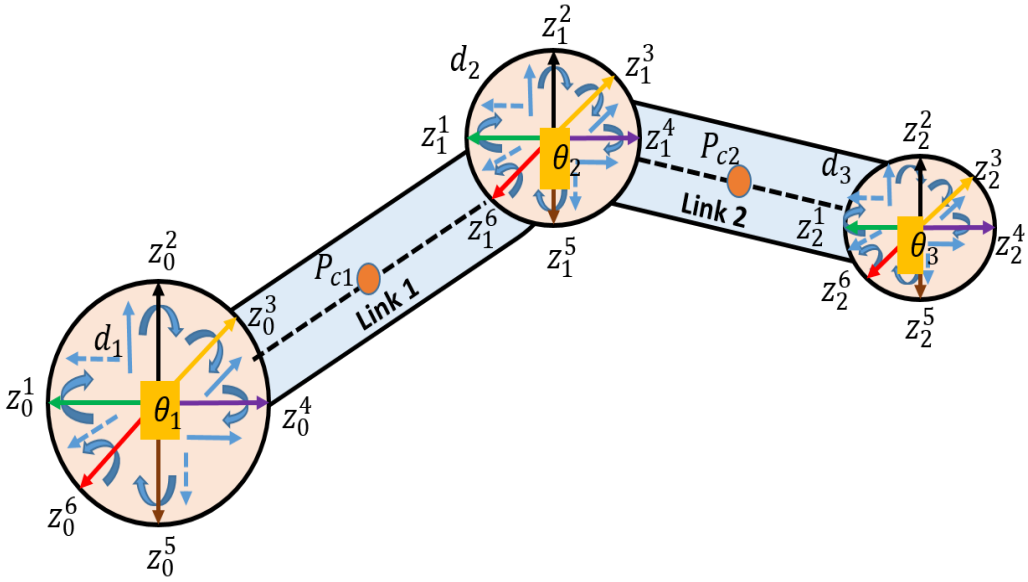

Figure 3.2: Representation for preceding two links of n-DOF GDM.

For the generic augmented link, the generic center of mass and moment of inertia has a direct relation with the dimensions of the link i of the manipulator. The generic center of mass coordinate and its respective moment of inertia can be represented by P_{ci} and I_i as shown in Eqn. (3.6) and (3.7) respectively.

$$P_{ci} = \begin{bmatrix} -\cos(\theta_{DHi})\frac{a_i}{2} \\ K_{Ci}\sin(\theta_{DHi})\frac{a_i}{2} - K_{Si}\frac{d_{DHi}}{2} \\ -K_{Si}\sin(\theta_{DHi})\frac{a_i}{2} - K_{Ci}\frac{d_{DHi}}{2} \end{bmatrix}, \qquad i = 1,2,\ldots,n \tag{3.6}$$

$$I_i = \begin{bmatrix} I_{xi} & 0 & 0 \\ 0 & I_{yi} & 0 \\ 0 & 0 & I_{zi} \end{bmatrix}, \qquad i = 1,2,\ldots,n \tag{3.7}$$

3.3.1 FORWARD COMPUTATION FOR VELOCITY AND ACCELERATION:

According to the D-H Parameters in Table 1 the joint coordinate frames are assigned can be seen in Figure 1. The upper $3X3$ submatrices of homogenous transformation matrices for each generic joint i represented as rotational matrices, as shown in Eqn. (3.8). The upper right $3X1$ submatrices of homogenous transformation matrices are position vector for each joint i, as shown in Eqn. (3.9).

$$R_i^{i-1} = \begin{bmatrix} \cos(R_i\theta_i + T_i\theta_{DHi}) & -K_{Ci}\sin(R_i\theta_i + T_i\theta_{DHi}) & K_{Si}\sin(R_i\theta_i + T_i\theta_{DHi}) \\ \sin(R_i\theta_i + T_i\theta_{DHi}) & K_{Ci}\cos(R_i\theta_i + T_i\theta_{DHi}) & -K_{Si}\cos(R_i\theta_i + T_i\theta_{DHi}) \\ 0 & K_{Si} & K_{Ci} \end{bmatrix}, \quad i = 1,2,\ldots,n \tag{3.8}$$

Transpose of all rotational matrices

$$(R_i^{i-1})^T$$
$$= \begin{bmatrix} \cos(R_i\theta_i + T_i\theta_{DHi}) & \sin(R_i\theta_i + T_i\theta_{DHi}) & 0 \\ -K_{Ci}\sin(R_i\theta_i + T_i\theta_{DHi}) & K_{Ci}\cos(R_i\theta_i + T_i\theta_{DHi}) & K_{Si} \\ K_{Si}\sin(R_i\theta_i + T_i\theta_{DHi}) & -K_{Si}\cos(R_i\theta_i + T_i\theta_{DHi}) & K_{Ci} \end{bmatrix}, \quad (3.9)$$
$$i = 1,2,\ldots,n$$

The generalized position vector of the manipulator.

$$P_i^{i-1} = \begin{bmatrix} a_i\cos(R_i\theta_i + T_i\theta_{DHi}) \\ a_i\sin(R_i\theta_i + T_i\theta_{DHi}) \\ R_i d_{DHi} + T_i d_i \end{bmatrix}, \qquad i = 1,2,\ldots,n \quad (3.10)$$

The linear and angular velocity for a generic augmented link can be presented as shown in Eqn. (3.11).

$$\dot{P}_i^{i-1} = \begin{bmatrix} 0 \\ 0 \\ \dot{d}_\iota \end{bmatrix}, \qquad \dot{\theta}_i^{i-1} = \begin{bmatrix} 0 \\ 0 \\ \dot{\theta}_\iota \end{bmatrix}, \qquad i = 1,2,\ldots,n \quad (3.11)$$

The linear and angular acceleration for a generic augmented link can be presented as shown in Eqn. (3.12)

$$\ddot{P}_i^{i-1} = \begin{bmatrix} 0 \\ 0 \\ \ddot{d}_\iota \end{bmatrix}, \quad \ddot{\theta}_i^{i-1} = \begin{bmatrix} 0 \\ 0 \\ \ddot{\theta}_\iota \end{bmatrix}, \qquad i = 1,2,\ldots,n \quad (3.12)$$

The angular velocity and angular acceleration for the Prismatic joint were given by the Eqn. (3.13) and (3.14) respectively.

$$\omega_i^i = R_{i-1}^i\,\omega_{i-1}^{i-1}, \qquad i = 1,2,\ldots,n \quad (3.13)$$

$$\dot{\omega}_i^i = R_{i-1}^i \, \dot{\omega}_{i-1}^{i-1}, \qquad i = 1,2,\ldots,n \tag{3.14}$$

The angular velocity and angular acceleration for the Revolute joint in a generic manipulator can be calculated from Eqn. (3.15) and Eqn. (3.16) respectively.

$$\omega_i^i = R_{i-1}^i [\, \omega_{i-1}^{i-1} + R_i(\dot{\theta}_i^{i-1})], \qquad i = 1,2,\ldots,n \tag{3.15}$$

$$\dot{\omega}_i^i = R_{i-1}^i \{\, \dot{\omega}_{i-1}^{i-1} + R_i \left[\ddot{\theta}_i^{i-1} + \omega_{i-1}^{i-1} \times \dot{\theta}_i^{i-1}\right]\}, \; i = 1,2,\ldots,n \tag{3.16}$$

The Linear velocity and Linear acceleration for Prismatic and Revolute joint can be calculated using the below mentioned generalized Eqn. (3.17) and (3.18) respectively

$$v_i^i = R_{i-1}^i \, v_{i-1}^{i-1} + R_i[\, \omega_i^i + R_{i-1}^i P_i^{i-1}] + R_i\{R_{i-1}^i[\dot{P}_i^{i-1} + \omega_{i-1}^{i-1} \times P_i^{i-1}]\}, \quad i = 1,2,\ldots,n \tag{3.17}$$

$$\begin{aligned} \dot{v}_i^i = R_{i-1}^i\{\, & \dot{v}_{i-1}^{i-1} + (v_i \times P_i^{i-1} + (\omega_{i-1}^{i-1} \times (\omega_{i-1}^{i-1} \times P_i^{i-1})) \\ & + R_i[\, 2(\omega_{i-1}^{i-1} \\ & \times (\dot{\theta}_i^{i-1} \times P_i^{i-1} + \ddot{\theta}_i^{i-1} \times P_i^{i-1} + \omega_i^{i-1} \times (\dot{\theta}_i^{i-1} \times P_i^{i-1})\big] \\ & + T_i\big[2\omega_{i-1}^{i-1} \times \dot{P}_i^{i-1} + \ddot{P}_i^{i-1}\big]\}, \qquad i = 1,2,\ldots,n \end{aligned} \tag{3.18}$$

In the below-mentioned Eqn. (3.19) the generic equation for the linear acceleration of the center of mass for n link.

$$\dot{v}c_i^i = \dot{v}_i^i + (v_i^i \times Pc_i^i) + (\omega_i^i \times (\omega_i^i \times Pc_i^i)), \qquad i = 1,2,\ldots,n \tag{3.19}$$

3.3.2 BACKWARD COMPUTATION FOR FORCE AND MOMENTS

The forward computation velocity and acceleration of each link are computed. The force and moment per link are computed starting from the end effector of the robot and ending at the base link. Taking into consideration at no load at the end effector the force and moment at the end effector link (n) considered to be zero can be seen in Eqn. (3.20).

$$F_n^n = 0 \text{ and } \eta_n^n = 0 \tag{3.20}$$

Therefore, taking velocity and acceleration into account the force and moment at each link can be computed using the following generalized equations for n DOF Eqn. (3.21) and Eqn. (3.22) respectively.

$$F_i^i = m_i^i \dot{v}c_i^i, \qquad i = 1,2,\ldots,n \tag{3.21}$$

$$N_i^i = I_i^i \dot{\omega}_i^i + \omega_i^i \times [I_i^i \omega_i^i], \qquad i = 1,2,\ldots,n \tag{3.22}$$

$$f_i^i = F_i^i + R_{i-1}^i f_{i+1}^{i+1} \tag{3.23}$$

$$\eta_i^i = R_{i+1}^i \eta_{i+1}^{i+1} + (R_i P_i^{i-1}) \times R_{i+1}^i f_{i+1}^{i+1} + (R_i P_i^{i-1} + R_i R_i^i) \times F_i^i + N_i^i \tag{3.24}$$

For the Prismatic joint, the force acting on the link is considered as the actuation torque as stated in Eqn. (3.25) while for revolute joint the torque acting on the link will be considered as the actuation torque stated in Eqn. (3.26).

$$\tau_i = (f_i^i)^T R_{i-1}^i \hat{Z}_0 \tag{3.25}$$

$$\tau_i = (n_i^i)^T R_{i-1}^i \hat{Z}_0 \tag{3.26}$$

The sequence of operations required to compute the dynamics of the system was represented in figure 3. The D-H parameters are the initial parameters required for the computation of the dynamics of a system. From the D-H parameters, the Homogeneous Transformation, Position, and Rotation matrices were computed. While implementing symbolic math function considering $\dot{\theta}_i^{i-1}$as angular velocity and $\dot{P}_i^{i-1}$as linear velocity and their respective derivatives represents their angular acceleration and linear acceleration. Implementing the forward computation algorithm on each joint with respect to its nature either revolute or prismatic their angular velocity, angular acceleration, linear velocity, and linear acceleration were achieved. Whereas in backward computation algorithm the total external torque and forces acting on each joint which in return provides the torque acting on each joint of the manipulator.

The generalized dynamic equation of the n- DOF system is represented as mentioned in Eqn. (3.27).

$$M(q)\ddot{q} + N(q,\dot{q})\dot{q} + G(q) = \tau \qquad (3.27)$$

Whereas the Generalized system Torque Vector (n x 1 dimension) is expressed as τ, M matrix represents the mass parameters of the manipulator also named as Inertia Matrix with n x n dimension. $M(q)$ is a The positive symmetric property of $M(q)$ matrix ensures the correct computation of the dynamics, N matrix represents the Centrifugal and Coriolis Forces (n x 1 dimension), G is the Gravitational Force Vector represents the dynamic terms associated with gravity having n x 1 dimension. Joint Angular Velocity Vector$(\dot{q})$ and Joint Position Vector (q) was the function of time as per the desired joint trajectory as an input. The implementation of the GDM algorithm is done using the Symbolic algebra in Matlab Software.

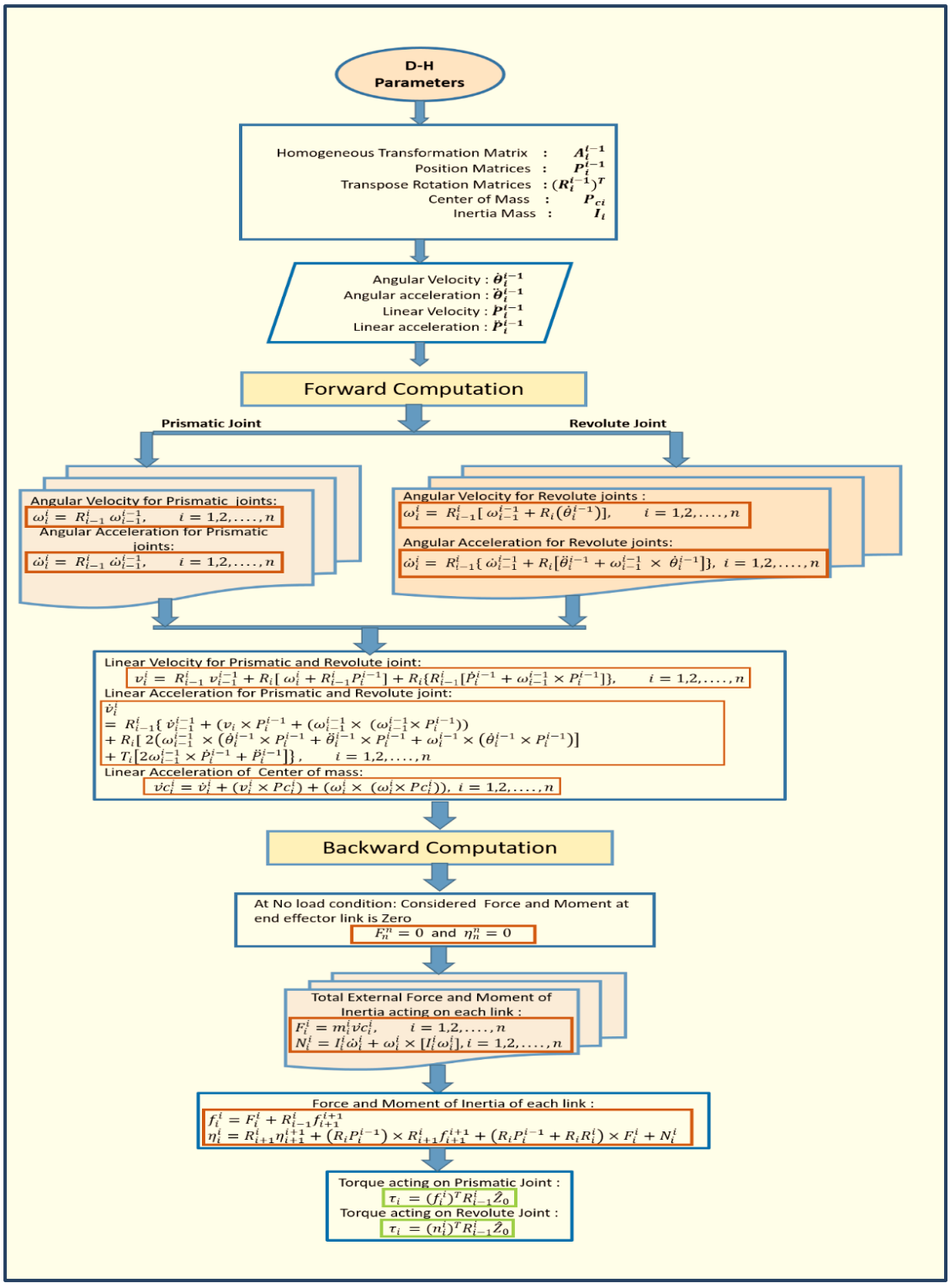

Figure 3.3: Flow chart of dynamic calculation

3.4 GENERIC SEPARATION ALGORITHM (GSA):

The resultant of the GDM algorithm provides the torque acting on each joint of the n-DOF manipulator in an unstructured form. To achieve the dynamics of the system in the form of Eqn. (3.27) the Generic Separation Algorithm (GSA) is used. GSA discards the least significant terms of dynamics acting on each joint and decreases the computation load from the system for fast computation.

The result of the Recursive Newton Euler Algorithm is the n number of equations representing forces and/or torque for n link of the system. The force /torque equation of each link consists of four elements. The inertia matrix is the first element of the system, which defines the mass property of the link. The second element is the Coriolis vector, the third element is the centripetal Matrix that describes the centripetal force/torque acting on the link. The fourth element is the gravity vector, which describes the gravitation force acting on the link.

To segregate the elements of the dynamic equation from the respective torque and force element of each link. The torque for revolute joint and force acting on the prismatic joint is iterated through the Generic Separation Algorithm (GSA). The GSA is based on the elimination of unwanted terms and collecting and simplifying the terms associated with the coefficients of $\ddot{\theta}_i, \dot{\theta}_i, \theta_i$.

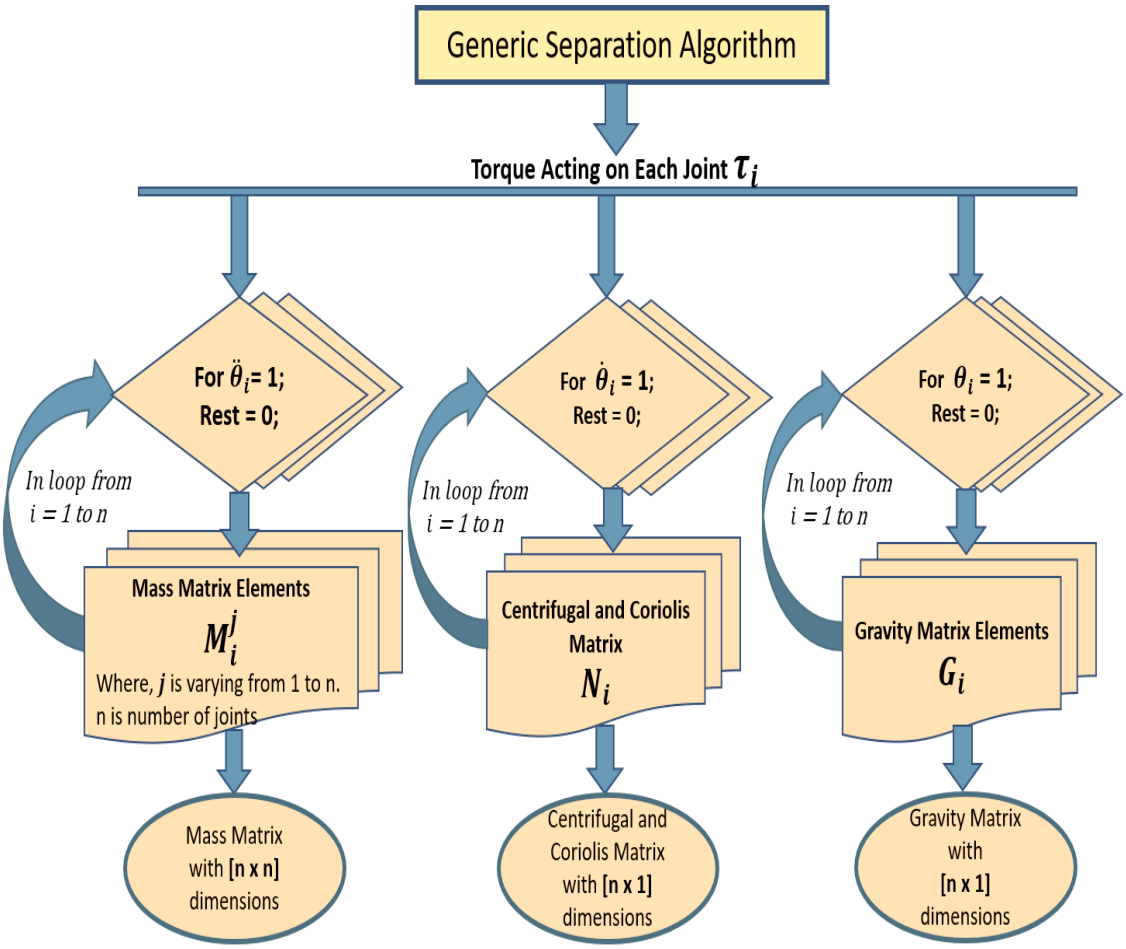

Figure 3.4: The flow chart representation of the Generic Separation Algorithm

3.5 MODEL EVALUATION:

For the verification of the GKM and GDM, the dynamics of the two-link manipulator is used with three different configurations. The three different configurations of the two-link robot are as follows with their initial parameters: The dynamic analysis of the two-link different robot configuration was computed and verified from the literature. The MATLAB simulation software was used for the dynamic computation and the MSC ADAMS software was used for motion and joint torque analysis of different robot configurations.

- **Case 1:** Two link robot with both revolute joint (2R)

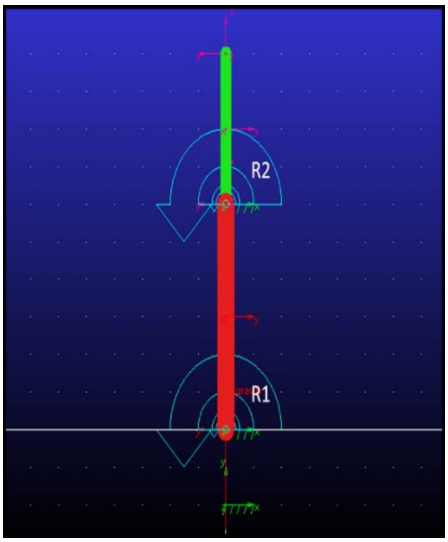

Figure 3.5: Structural Representation of two-link 2R configuration robot.

The initial parameters considered for the Generalized Kinematic model (GKM) and DKM for the 2R robot are as shown in Table 3.2.

Table 3.2: D-H Parameters for 2R Planar

Parameters for 2R planar	R_i	T_i	K_{Ci}	K_{Si}	d_{DH2}	θ_{DH1} (°)	a_i	α_i
Joint 1	1	0	1	0	0	θ_1	L_1	0
Joint 2	1	0	1	0	0	θ_2	L_1	0

Dynamic Equation of a two-link 2R configuration robot computed using the DKM algorithm is given in Eqn. (3.28)[98].

$$\begin{bmatrix} m_1 l_{c1}^2 + m_2(l_1^2 + l_{c2}^2 + 2l_1 l_{c2}\cos(\theta_2)) + I_1 + I_2 & m_2(l_{c2}^2 + l_1 l_{c2}\cos(\theta_2)) + I_2 \\ m_2(l_{c2}^2 + l_1 l_{c2}\cos(\theta_2)) + I_2 & m_2 l_{c2}^2 + I_2 \end{bmatrix} \begin{bmatrix} \ddot{q}_1 \\ \ddot{q}_2 \end{bmatrix} - m_2 l_1 l_{c2}\sin(\theta_2) \begin{bmatrix} 2\dot{q}_1\dot{q}_2 + \dot{q}_2^2 \\ -\dot{q}_1 \end{bmatrix} + \begin{bmatrix} (l_{c1}m_1 + l_1 m_2)\cos(\theta_1)\, g + l_{c2}m_2\cos(\theta_1 + \theta_2)\, g \\ l_{c2}m_2\cos(\theta_1 + \theta_2)\, g \end{bmatrix} \tag{3.28}$$

- **Case 2:** a two-link robot with one revolute and another prismatic joint (RT)

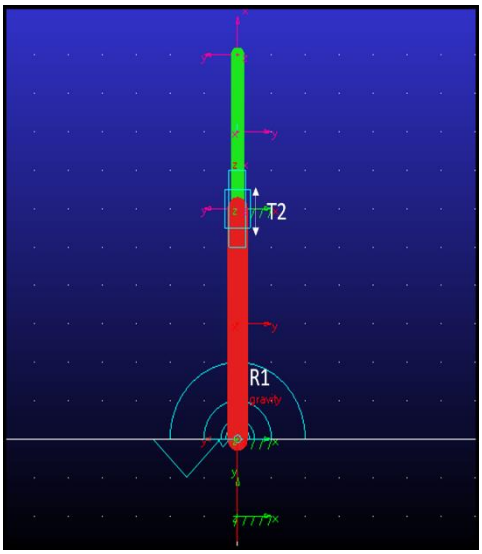

Figure 3.6: Structural Representation of a two-link RT configuration robot.

The Initial parameters required for implementing n-GKM and n-DKM for RT robot are as shown in Table 3.3.

Table 3.3: D-H Parameters for RT Planar robot manipulator

Parameters for RT planar	R_i	T_i	K_{Ci}	K_{Si}	d_{DH2}	θ_{DHi} (º)	a_i	α_i
Joint 1	1	0	1	0	0	θ_1	0	90
Joint 2	0	1	1	0	d_2	0	0	0

The computed dynamic Equation of a two-link RT configuration robot is as stated in Eqn. (3.29).

$$\begin{bmatrix} M_{RT11} & 0 \\ 0 & m_2\ddot{d}_2 \end{bmatrix}\begin{bmatrix} \ddot{q}_1 \\ \ddot{q}_2 \end{bmatrix} + \begin{bmatrix} 0 \\ 0 \end{bmatrix}\begin{bmatrix} \dot{q}_1\dot{q}_2 \\ \dot{q}_1\dot{q}_2 \end{bmatrix} + \begin{bmatrix} 0.25(l_1m_1 + l_2m_2)\cos(\theta_1)\, g \\ 0 \end{bmatrix} \quad (3.29)$$

$$M_{RT11} = l_1l_2m_1\alpha_1 + 0.25l_2^2m_2\alpha_1 + I_{Z2}\alpha_1 + l_2^2m_2\alpha_1 + 0.25l_2^2m_2\alpha_1 + I_{Z1}\alpha_1 \quad (3.30)$$

- **Case 3:** Two link robot with both prismatic joints (TT)

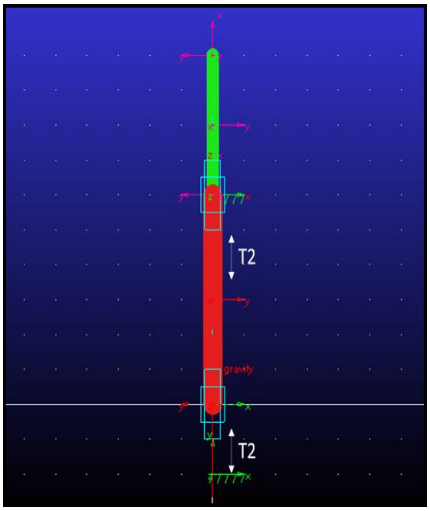

Figure 3.7: Structural Representation of a two-link TT configuration robot.

Initial parameters required for implementing n-GKM and n-DKM for TT robot are as shown in Table 3.4.

Table 3.4: D-H Parameters for TT Planar robot manipulator

Parameters for TT planar	R_i	T_i	K_{Ci}	K_{Si}	d_{DH2}	θ_{DH1} (º)	a_i	α_i
Joint 1	0	1	1	0	d_1	0	0	0
Joint 2	0	1	1	0	d_2	0	0	0

The computed generic dynamics of the 2 DOF having both prismatic joints (TT) configuration is stated in Eqn. (3.31)[98].

$$\begin{bmatrix} m_2\ddot{d}_1 + m_1\ddot{d}_1 & 0 \\ 0 & 0 \end{bmatrix} \begin{bmatrix} \ddot{q}_1 \\ \ddot{q}_2 \end{bmatrix} + \begin{bmatrix} 0 \\ 0 \end{bmatrix} \begin{bmatrix} \dot{q}_1\dot{q}_2 \\ \dot{q}_1\dot{q}_2 \end{bmatrix} + \begin{bmatrix} 0 \\ .5l_2m_2\cos(\theta_2)\, g \end{bmatrix} \tag{3.31}$$

3.6 SUMMARY:

The contribution of this chapter is to enables the researchers to develop and model the n- DOF robot manipulator, which is having n number of applications in different domains like in industrial, healthcare, transportation, medical sciences, etc. This chapter illustrates the generalized kinematic modeling and dynamic modeling of the n-DOF manipulator named GKM and DKM respectively. The mentioned technique to identify the kinematics and dynamics of the system can be used to obtain parameters of modular robots. The use of modularity and reconfigurable robots in their respective domain will increase the effective utilization of robots and leads to the higher efficiency of time utilization. The novel generic separation algorithm (GSA) is used to automatically separate the dynamic parameters of the n-DOF manipulator. GSA provides an ease to the researcher to control each joint of the n-DOF manipulator with its type prismatic and/or rotational. The n-GKM and n-DKM have been evaluated by comparing the results of the proposed model with the standardized Euler Lagrange technique for 2R, RT, and TT cases.

CHAPTER 4 KINEMATIC AND DYNAMIC MODELING OF ANTEBRACHIUM LACERATION SUTURING ROBOT

In recent decades, robotic researches have become great attention and has N number of applications in every field of research such as industrial, medical, agriculture, and so forth [98]. In industrial applications, robots are used for packaging, segregating, assembling, etc. Agriculture used for picking, collecting, and segregating fruits, vegetables, flowers, etc. In medical research is used as assistive robots, surgical robots, etc.[99] For every application, the requirement of robot configuration differs. Therefore, Robotic manipulators were developed with various types of joints such as rectangular, cylindrical, spherical, revolute, and horizontal joints to perform different tasks.

The most commonly used robot in industrial and medical applications is Selective Compliance Assembly Robot Arm (SCARA) although the first robot was invented by Japan more than half-decade still it is an indispensable element in the automation industries. Speed, reliability, small workspace, and cost-effectiveness make this robot widely used all over the world. Figure 4.1 shows the RRPR robot manipulator manufactured by Rexroth is considered an object of interest, which is a four-axis horizontal joined articulated arm configuration. The first two joints of the robot are revolute to establish the horizontal position of the robot. The third joint is the prismatic joint which defines the vertical position of the end tool. Finally, the last joint will provide the tool orientation. Therefore it has RRPR Configuration with the cylindrical workspace [100].

The integration of the smart instruments with the RRPR manipulator provides an edge to the application of RRPR in the field of Healthcare solutions.

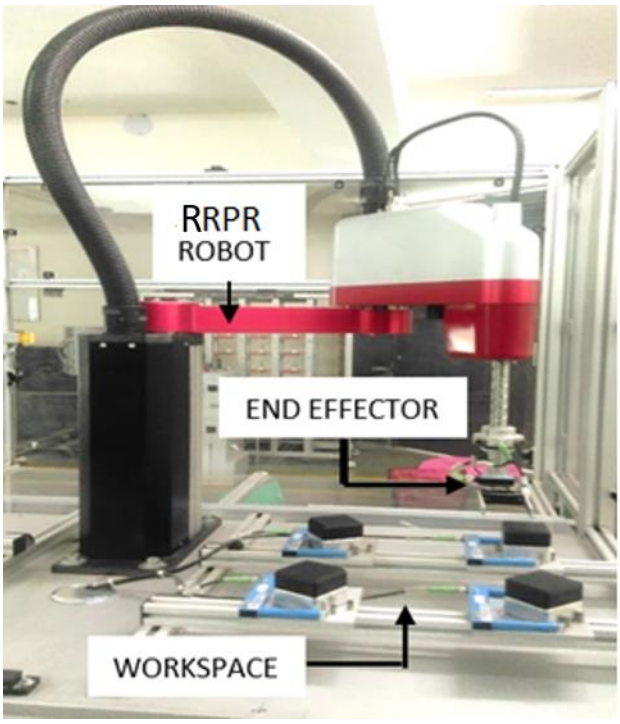

Figure 4.1. RRPR Robot Manipulator (Center of Excellence Laboratory, U.P.E.S., Dehradun,India)

This chapter is to illustrate, analyze, and evaluate the kinematic and dynamic modeling of the Antebrachium Laceration Suturing Robot (ALSR) using the GKM, DKM, and GSA techniques as mentioned in chapter 3.

4.1 KINEMATIC MODELING OF ANTEBRACHIUM LACERATION SUTURING ROBOT (ALSR)

The wide range of medical healthcare is equipped with robots in the current paradigm. The surgical robots play a crucial role in the healthcare domain. The increasing interest of robots in different surgical applications like orthopedic surgery, bariatric surgery, Cosmetic surgery, Ocular surgery, etc.[101], [102]. The surgical manipulator is widely used in various surgical applications like cutting, suturing, catering, etc. The impact of surgical robots in the healthcare domain is increasing day by day for the betterment of human beings. To develop

a robust and efficient system for surgical applications the estimation of Kinematics and Dynamics of the system is required. The surgical robot taken into consideration consists of RRPR (Two Revolute one Prismatic and one Revolute Joint) serial configuration with a suturing tool as an end effector. The RRPR Manipulators are widely used in various assembly applications like Cutting, Selecting, Segregating, Pick and Place, etc. It has a horizontal jointed articulated arm configuration manipulator. The end tool of the robot can be modified to perform various surgical tasks such as a holding camera and smart tools like endostitch, endosew, etc [77].

In the research, the RRPR robotic arm has been integrated with the smart instrument designed for actuated suturing. The integration of RRPR with the smart suturing instrument for the application of Antebrachium laceration suturing is named as Antebrachium Laceration Suturing Robot (ALSR). The CAD model of the ALSR can be seen in Figure 4.2. The proposed surgical manipulator is chosen specifically for the suturing task and is assumed to have ex-vivo antebrachium laceration [103], [104].

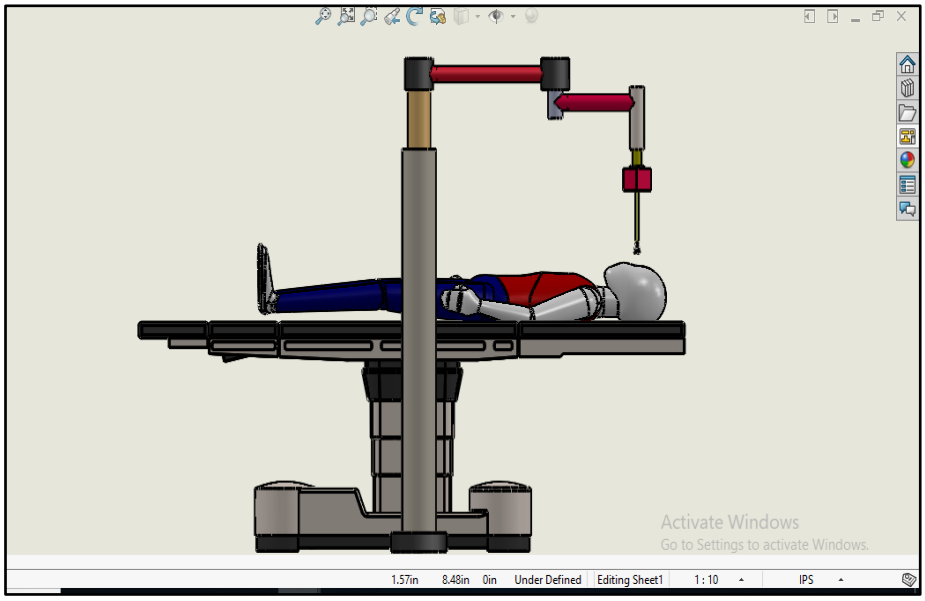

Figure 4.2: CAD model of the Antebrachium Laceration Suturing Robot (ALSR)

The main component of the ALSR consists of 4 degree of freedom (DOF) Serial manipulator with an actuated suturing tool and a Vision camera. The tool has two actuators, one to drive the jaws of the suturing tool by the static pin located at 22 mm pitch axis land one to perform shuttling of needle between the jaws.

4.1.1 FORWARD KINEMATICS

The frame assignment and joint angles of ALSR were assigned as per the Denavit Hartenberg (D-H) conventions. Figure 4.3 represented the coordinate frame arrangements and joint angles of the ALSR.

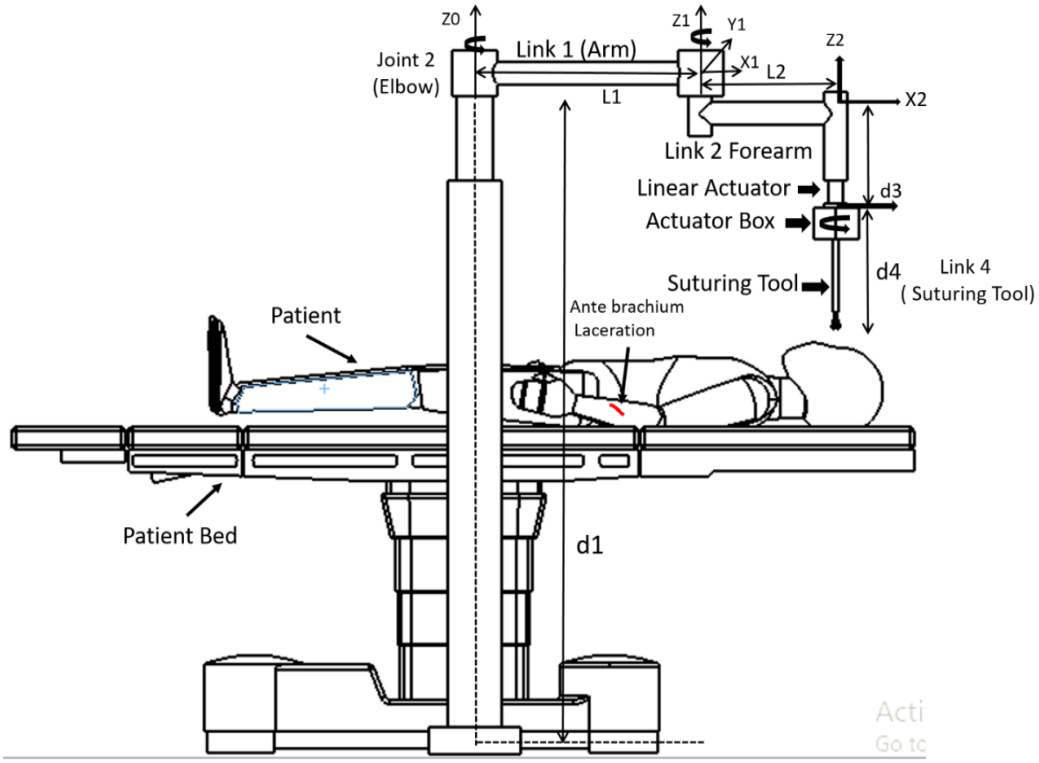

Figure 4.3: Frame assignment of the Antebrachium Laceration Suturing Robot (ALSR)

To identify the dynamics and kinematics of the manipulator the mass, link length and moment of inertia parameter are required. Therefore, Table 4.1 illustrates the parameters taken into consideration during the modeling of the manipulator in simulation.

Table 4.1: ALSR Robot Parameters and Their Value

Parameters	***Value***
Mass of Link 1 (m_1)	3.1 Kg
Mass of Link 2 (m_2)	.85 kg
Mass of Link 3 (m_3)	.56 kg
Mass of Link 4 (m_4)	.24 kg

Link1 Length (l_1)	.5 meter
Link1 Length (l_2)	.2 meter
Link 1 Offset (d_1)	1.9 meter
Link 3 Offset (d_3)	.24 meter
Link 4 Offset (d_4)	1.3meter
Moment of Inertia for link 1 (I_1)	.5728 Kg.m^2
Moment of Inertia for link 2 (I_2)	.2130 Kg.m^2
Moment of Inertia for link 3 (I_3)	1.64 Kg.m^2
Moment of Inertia for link 4 (I_4)	.567 Kg.m^2
Acceleration Due To Gravity (g)	9.8 m/sec^2

The Denavit-Hartenberg (D-H) parameter of the ALSR robot are defined in Table 4.2

Table 4.2: D-H Parameter of the ALSR Manipulator

Parameters for RT planar	R_i	T_i	K_{Ci}	K_{Si}	d_{DHi}	θ_{DHi} (°)	a_i	α_i
Joint 1	1	0	1	0	l_{12}	θ_1	l_1	0
Joint 2	1	0	1	0	0	θ_2	l_2	0
Joint 3	0	1	-1	0	d_3	0	0	180
Joint 4	1	0	1	0	l_4	θ_4	0	0

The A_i represents the generalized Transformation Matrices of link i can be seen from Eqn. (4.1) to Eqn. (4.3).

$$Ai = Rot_{z,\theta i} Trans_{z,di} Trans_{x,ai} Rot_{x,\alpha i} \quad (4.1)$$

$$A_i = \begin{bmatrix} Cos\theta_i & -Sin\theta_i & 0 & 0 \\ Sin\theta_i & Cos\theta_i & 0 & 0 \\ 0 & 0 & 1 & 0 \\ 0 & 0 & 0 & 1 \end{bmatrix} \begin{bmatrix} 1 & 0 & 0 & 0 \\ 0 & 1 & 0 & 0 \\ 0 & 0 & 1 & d_1 \\ 0 & 0 & 0 & 1 \end{bmatrix} \begin{bmatrix} 1 & 0 & 0 & a_i \\ 0 & 1 & 0 & 0 \\ 0 & 0 & 1 & 0 \\ 0 & 0 & 0 & 1 \end{bmatrix} \begin{bmatrix} 1 & 0 & 0 & 0 \\ 0 & Cos\alpha_i & -Sin\alpha_i & 0 \\ 0 & Sin\alpha_i & Cos\alpha_i & 0 \\ 0 & 0 & 0 & 1 \end{bmatrix} \quad (4.2)$$

$$A_i = \begin{bmatrix} Cos\theta_i & -Sin\theta_i Cos\alpha_i & Sin\theta_i Sin\alpha_i & a_i Cos\theta_i \\ Sin\theta_i & Cos\theta_i Cos\alpha_i & -Cos\theta_i Sin\alpha_i & a_i Sin\theta_i \\ 0 & Sin\alpha_i & Cos\alpha_i & d_i \\ 0 & 0 & 0 & 1 \end{bmatrix} \quad (4.3)$$

The joint parameters as given in the D-H table and the transformation matrix defined as A-matrix for each joint have defined as follows from Eqn. (4.4) to Eqn. (4.7).

$$A_1 = \begin{bmatrix} Cos\theta_1 & -Sin\theta_1 & 0 & l_1 Cos\theta_1 \\ Sin\theta_1 & Cos\theta_1 & 0 & l_1 Cos\theta_1 \\ 0 & 0 & 1 & l_{12} \\ 0 & 0 & 0 & 1 \end{bmatrix} \quad (4.4)$$

$$A_2 = \begin{bmatrix} Cos\theta_2 & -Sin\theta_2 & 0 & l_2 Cos\theta_2 \\ Sin\theta_2 & Cos\theta_2 & 0 & l_2 Sin\theta_2 \\ 0 & 0 & 1 & 0 \\ 0 & 0 & 0 & 1 \end{bmatrix} \quad (4.5)$$

$$A_3 = \begin{bmatrix} 1 & 0 & 0 & 0 \\ 0 & -1 & 0 & 0 \\ 0 & 0 & -1 & d_3 \\ 0 & 0 & 0 & 1 \end{bmatrix} \quad (4.6)$$

$$A_4 = \begin{bmatrix} Cos\theta_4 & -Sin\theta_4 & 0 & 0 \\ Sin\theta_4 & Cos\theta_4 & 0 & 0 \\ 0 & 0 & 1 & l_4 \\ 0 & 0 & 0 & 1 \end{bmatrix} \quad (4.7)$$

The Forward Kinematic Equation of the manipulator can be written as stated in Eqn. (4.8).

$$T_0^4 = A_1 ... A_4 = \begin{bmatrix} Cos(\theta_1+\theta_2-\theta_4) & Sin(\theta_1+\theta_2-\theta_4) & 0 & l_1Cos(\theta_1)+l_2Cos(\theta_1+\theta_2) \\ Sin(\theta_1+\theta_2-\theta_4) & -Cos(\theta_1+\theta_2-\theta_4) & 0 & l_1Sin(\theta_1)+l_2Sin(\theta_1+\theta_2) \\ 0 & 0 & -1 & l_{12}+d_3-l_4 \\ 0 & 0 & 0 & 1 \end{bmatrix} \quad (4.8)$$

On comparing the above Eqn. (4.8) with Eqn. (4.9)

$$T_0^4 = \begin{bmatrix} r_{11} & r_{12} & r_{13} & d_x \\ r_{21} & r_{22} & r_{23} & d_y \\ r_{31} & r_{32} & r_{33} & d_z \\ 0 & 0 & 0 & 1 \end{bmatrix} \quad (4.9)$$

Where the arbitrary parameters are used in Eqn. (4.9) were illustrated in below from Eqn. (4.10) to Eqn. (4.17).

$$r_{11} = Cos(\theta_1+\theta_2-\theta_4) \quad (4.10)$$

$$r_{12} = r_{21} = Sin(\theta_1+\theta_2-\theta_4) \quad (4.11)$$

$$r_{22} = -Cos(\theta_1+\theta_2-\theta_4) \quad (4.12)$$

$$r_{13} = r_{31} = r_{32} = r_{23} = 0 \quad (4.13)$$

$$r_{33} = -1 \quad (4.14)$$

$$d_x = l_1Cos(\theta_1)+l_2Cos(\theta_1+\theta_2) \quad (4.15)$$

$$d_y = l_1Sin(\theta_1)+l_2Sin(\theta_1+\theta_2) \quad (4.16)$$

$$d_z = l_{12}+d_3-l_4 \quad (4.17)$$

d_x, d_y, d_z represents the end-effector position and can be called a d matrix with a 3x1 matrix dimension and similarly R as a rotation matrix with a 3x3 dimension.

The varying joint angles help in determining the respective suture tool position and orientation.

4.1.2 INVERSE KINEMATICS

Inverse Kinematics provides the joint angles of the ALSR from the coordinates of the suture tool position. To compute joint angles of the ALSR the transformation matrix Eqn. (4.18) from Forward kinematics were compared with Eqn. (4.19). The Inverse Kinematics was given by the set of solution of the equations as follows

$$\begin{bmatrix} Cos(\theta_1+\theta_2-\theta_4) & Sin(\theta_1+\theta_2-\theta_4) & 0 & l_1Cos(\theta_1)+l_2Cos(\theta_1+\theta_2) \\ Sin(\theta_1+\theta_2-\theta_4) & -Cos(\theta_1+\theta_2-\theta_4) & 0 & l_1Sin(\theta_1)+l_2Sin(\theta_1+\theta_2) \\ 0 & 0 & -1 & l_{12}+d_3-l_4 \\ 0 & 0 & 0 & 1 \end{bmatrix} = \begin{bmatrix} R & d \\ 0 & 1 \end{bmatrix} \tag{4.18}$$

Since four DOF of ALSR matrix will not have a definite solution unless R is in the form as stated in Eqn. (4.19)

$$\begin{bmatrix} Cos\beta & Sin\beta & 0 \\ Sin\beta & -Cos\beta & 0 \\ 0 & 0 & -1 \end{bmatrix} \tag{4.19}$$

In this case, $\theta_1+\theta_2-\theta_4$ can be determined by Eqn. (4.20) and respective Eqn. (4.21) defined θ_2.

$$\theta_1+\theta_2-\theta_4=\beta=A\tan(r_{12},r_{11}) \tag{4.20}$$

$$\theta_2=A\tan(\pm\sqrt{1-r^2},r) \tag{4.21}$$

Where the arbitrary constant r^2 is stated n Eqn. (4.22) and Eqn. (4.23) illustrate the computation of θ_1.

$$r^2=\frac{d_x^2+d_y^2-l_1^2-l_2^2}{2l_1l_2} \tag{4.22}$$

$$\theta_1=A\tan(d_x,d_y)-A\tan(l_1+l_2C_2,l_2S_2) \tag{4.23}$$

The tool roll angle θ_4 from Eqn. (4.20) can be defined as stated in Eqn. (4.24) and Eqn. (4.25).

$$\theta_4 = \theta_1 + \theta_2 - \beta \tag{4.24}$$

$$\theta_4 = \theta_1 + \theta_2 - A\tan(r_{12}, r_{11}) \tag{4.25}$$

The prismatic joint variable d_3 is associated with a sliding tool up and down with a tool roll axis. The vertical component of tool motion is uncoupled from the horizontal components. Finally, the prismatic joint d_3 has given as stated in Eqn. (4.26).

$$d_3 = d_z + l_4 \tag{4.26}$$

4.2 ANTEBRACHIUM LACERATION SUTURING ROBOT DYNAMIC FORMULATION

There is n number of methods to formulate the dynamics of the system such as Euler Lagrange, Recursive Lagrange, Newton Euler, Bond Graph, Featherstone, Wittenberg algorithms, etc. [87], [94]. From which Newton Euler and Euler Lagrange are commonly used algorithms. Newton Euler is considered to be more efficient with respect to Euler Lagrange because less number of addition, multiplication, and athematic operations are used.[105] Therefore, the computation of the surgical manipulator dynamic equation the Newton Euler formulation is chosen. The generalized dynamic expression for N degree of freedom (DOF) robot manipulator without disturbances (τdis) can be seen in Eqn. (4.27).[106]–[109]

In this section, the dynamic model of the ALSR is discussed. The Newton Euler and Euler Lagrange are the two common methods used for finding the dynamic equation. The dynamic equation of the ALSR is derived from the Newton Euler Method. The generalized dynamic expression for N degree of freedom robot manipulator can be expressed as below in Eqn. (4.27).

$$M(q)\ddot{q} + N(q,\dot{q})\dot{q} + G(q) = \tau \tag{4.27}$$

Where Generalized Force Vector (n x 1 dimension) is expressed as τ, M is Inertia Matrix with the dimension of n x n. $M(q)$ is a positive symmetric matrix, N is Centrifugal and Coriolis Forces (n x 1 dimension),G is a Gravitational Force Vector, $\dot{q}$ is Joint Angular Velocity Vector and q is Joint Position Vector.

The Inertia Matrix of the ALSR 4 DOF is as stated in Eqn. (4.28).

$$M(q) = \begin{bmatrix} p_1 + p_2 Cos(\theta_2) & p_3 + 0.5 p_2 Cos(\theta_2) & 0 & -p_5 \\ p_3 + 0.5 p_2 Cos(\theta_2) & p_3 & 0 & -p_5 \\ 0 & 0 & p_4 & 0 \\ -p_5 & -p_5 & 0 & -p_5 \end{bmatrix} \tag{4.28}$$

And Coriolis ($N(q)$) Matrix is calculated as the following Eqn. (4.29)

$$N(q) = \begin{bmatrix} -p_2 Sin(\theta_2)\dot{\theta}_2 & -0.5 p_2 Sin(\theta_2)\dot{\theta}_2 & 0 & 0 \\ 0.5 p_2 Sin(\theta_2)\dot{\theta}_1 & 0 & 0 & 0 \\ 0 & 0 & 0 & 0 \\ 0 & 0 & 0 & 0 \end{bmatrix} \tag{4.29}$$

Gravity Matrix (G) can be written as Eqn. (4.30)

$$G(q) = \begin{bmatrix} 0 \\ 0 \\ -p_4 g \\ 0 \end{bmatrix} \tag{4.30}$$

The ALSR dynamic parameters as mentioned in Eqn. (4.28) to Eqn. (4.30) can be seen in Appendix A. The ALSR manipulator Jacobian, With respect to the robot base frame, is as mentioned in Eqn. (4.31).

$$J(q)=\begin{bmatrix} -l_1 Sin(\theta_1)-l_2 Sin(\theta_1+\theta_2) & -l_2 Cos(\theta_1+\theta_2) & 0 & 0 \\ l_1 Cos(\theta_1)+l_2 Cos(\theta_1+\theta_2) & l_2 Cos(\theta_1+\theta_2) & 0 & 0 \\ 0 & 0 & -1 & 0 \\ 1 & 1 & 0 & 1 \end{bmatrix} \tag{4.31}$$

4.3 SUMMARY

The mathematical modeling of ALSR is the primary aim of this chapter which includes the kinematic and dynamic equations of ALSR. The kinematic equations of ALSR depict the relationship between the joint angles of ALSR to the Suture tool end position by the use of forward and inverse kinematics. The dynamic equation of ALSR was computed using GDM and GSA technique illustrated in Chapter 3. This chapter also covers the Jacobian transformation which helps in mapping the suturing tool velocity to the joint velocities of ALSR.

CHAPTER 5 SKIN LACERATION DETECTION

In the biomedical imaging domain, the majority of image segmentation includes skin segmentation. The common difficulty faced by the researcher is to identify the skin segmentation as the skin texture varies from person to person. This produced ambiguous results for a set parameter threshold values. Interactive segmentation techniques have been used before to trace the part of the desired object from its background[110]–[112]. In the skin segmentation technique, the researchers frequently used the bounding box as an identifier around the desired object [113]. The ultimate goal of the researcher is to segment the desired object from its background with minimal efforts[114]–[116].

The chapter focuses on the technique where the researcher marks on the object of interest with respect to the background in order to seed segmentation known as marking based segmentation technique (MBST)[117], [118]. This approach requires less accurate input provided by the researcher to estimate the required region of interest (ROI). The bounding box based segmentation technique (BBST) for segmentation allows the researcher to draw a bounding box over the ROI[113], [119]. BBST approach is simpler but has less control over the output parameters whereas MBST results are relatively having more control and refined results.

The marking based segmentation technique has been used by many researchers explicitly or conceptually[120]–[122]. MBST technique works outwards to the marked segment to attain the desired ROI. This method is useful to select the desired complex boundaries ROI. Thin and long objects are considered to be complex boundary objects because it is difficult for the researcher to mark the desired object pixels. This article illustrates the new method of interactive segmentation in which the researcher can mark the pixel of the desired object also termed as seeding to segment the image. The Euclidean distance Metric and Geodesic distance metric were the two different MBST techniques that were

implemented and compared in this article. Before implementing a segmentation algorithm some color-based preprocessing is required on the test image to achieve an indistinct color model irrespective of ambient lighting condition[123]. The chapter illustrates the segmentation of ex-vivo skin laceration termed as the Skin Laceration Detection System.

5.1 REVIEW OF IMAGE SEGMENTATION IN MEDICAL DIAGNOSIS

In medical diagnosis, the medical image segmentation is frequently used in various domains of medical research such as Microbiology, Pathology, Preoperative planning of different Surgeries, Radiology, Dermatology, etc[77]. The popular image segmentation use to analyze the health condition of patients are X-Rays, CT scan, MRI, etc. In Dermatology, a large amount of skin segmentation is required to detect minor cases like allergy, pimples to extreme cases like cancer and eczema. Skin lesion detection is the basic requirement for complex surgeries. Ex-vivo skin laceration detection the first step before any surgery. To detect the boundary of laceration the different segmentation techniques were used by the researchers such as K-means algorithm, Graph cut[117], [124], multiple thresholding [116], [125], adaptive GMMRF[126], Euclidean distance metric[127], [128], Geodesic distance metric algorithm[117], [129], etc. The boundary of skin lesions may vary with the inner surface. The results of ex-vivo skin lesion segmentation may vary with varying luminescence[115], [123].

5.2 SKIN LACERATION DETECTION TECHNIQUE

The laceration detection algorithm includes four major steps that include image acquisition, image preprocessing, feature extraction, and recognition. The skin phantom is used to detect the laceration using the proposed MBST. The test image for laceration detection can be seen in Figure 5.1.

Figure 5.1: Skin Phantom

5.2.1 IMAGE ACQUISITION

The test image can be captured in two ways: Real-Time and manual mode. In Real-Time Mode the test image will be captured using a digital camera and simultaneously the test image will pass on to further steps. In manual mode, the pre-existing image from storage in jpg format is feed to the system algorithm.

5.2.2 IMAGE PRE-PROCESSING

In this step, the essential modulation in the captured test image is done to feed the required correct information to the system algorithm. This includes resizing, Colour space correction, etc. of the test image. Resizing of the test image is used to maintain the uniformity in the size of the input test image. The colour space correction includes conversion of Input RGB image into other colour spaces such as Grey Colour space, HSV Colour space, etc.[116], [130]. In this proposed laceration detection algorithm, the RGB Colour Space has converted into HSV Colour Space. HSV includes two channels in which H represents the chrominance channel, S represents colour and luminance channel whereas V

represents the texture feature of an input image. The following are the equations of colour space conversion from RGB to HSV.

$$H = \cos^{-1}\left\{\frac{0.5[(R-G)+(R-B)\}}{[(R-G)^2+(R-B)(G-B)]^{0.5}}\right\} \tag{5.1}$$

$$S = 1 - \frac{3}{(R+B+G)}[\min\,(R+G+B) \tag{5.2}$$

$$V = \frac{1}{3}(R+G+B) \tag{5.3}$$

HSV colour space is robust to varying camera direction and illuminance. Figure 5.2 represents the HSV Converted test image.

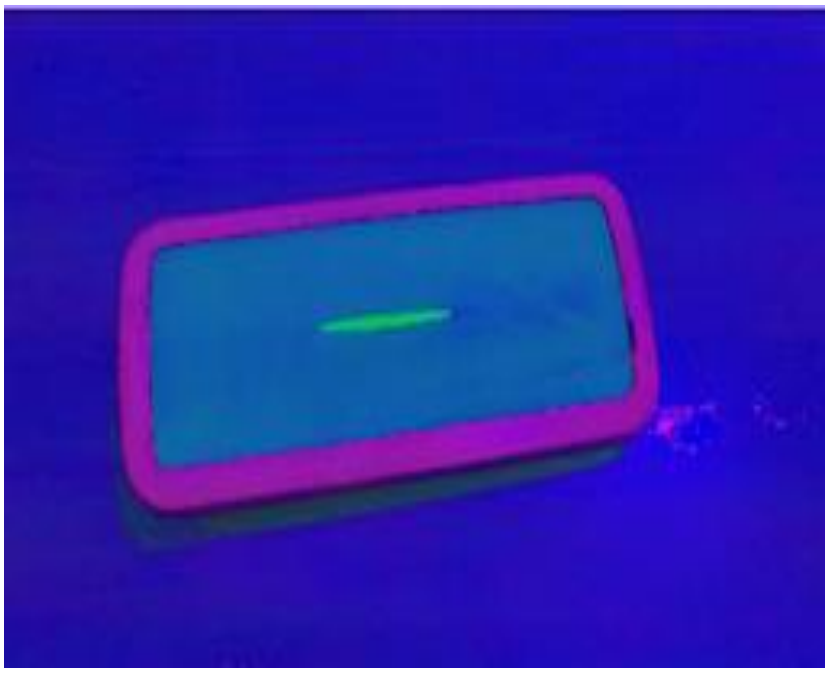

Figure 5.2: HSV Image of Skin Phantom

5.2.3 FEATURE EXTRACTION

Feature extraction plays a major role in image segmentation. There is n number of ways to extract the desired features from the image. The 8 color features and 5 texture features were extracted from the HSV color space of the desired object. The HSV color features include mean, standard deviation, skewness, Kurtosis, and so on. In texture features include energy, entropy, contrast, correlation, Homogeneity[127].

In the proposed laceration detection system, the interactive selection of the color space of ROI is given by the researcher. As per the interactive selection made by the researcher, the above-mentioned color and texture feature from the converted HSV image is stored as a featured database which is therefore used as the desired feature by the algorithm. Figure 5.3 represents the desired feature of a skin laceration detection system. Similarly, the test image features were computed by the feature extraction technique.

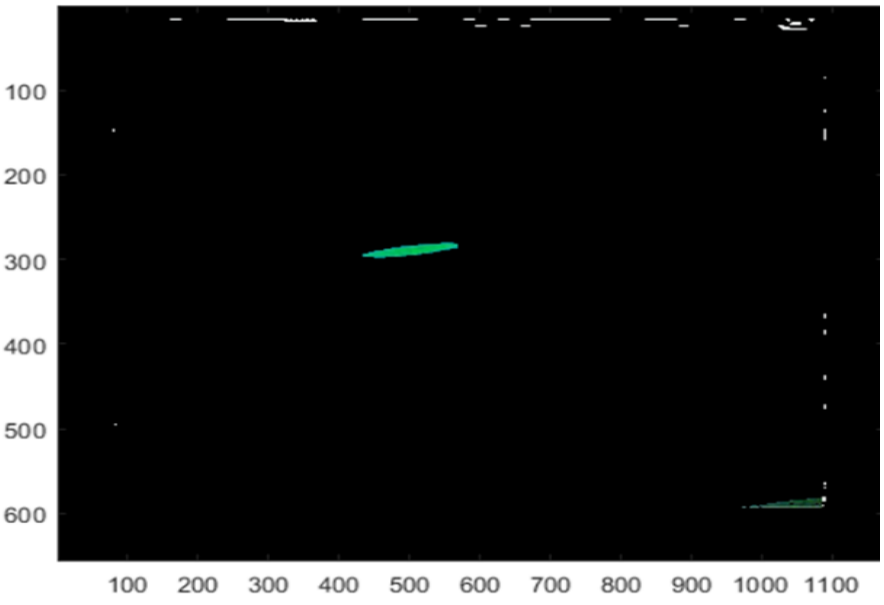

Figure 5.3: Interactive selection of desired HSV color space

Then the test image features were compared with the featured database of ROI through two different algorithms such as Euclidean Distance metric and Geodesic distance metric.

5.3 GEODESIC SEGMENTATION

Geodesic segmentation is robust enough to segment thin and long structures irrespective of its boundary length. The formulation of the Geodesic distance metric for the unary region term is given as in Eqn. (5.4). $M_l(x_i)$ represents the global colour model, $G_l(x_i)$ is geodesic distance formulated by using the relative desired object/background geodesic distance with respect to researcher input marker as stated in Eqn. (5.5).

$$R_l(x_i) = s_l(x_i) + M_l(x_i) + G_l(x_i) \tag{5.4}$$

$$G_l(x_i) = \frac{D_l(x_i)}{D_F(x_i) + D_B(x_i)} \tag{5.5}$$

Where ∂_l represents the set of seeds with label$l \epsilon \{F\}$. In this method, the conjugate$l$ is considered as the set of seeds with the label $\bar{l} \epsilon \{B\}$.

$$s_l(x_i) = \begin{cases} \infty & if\ x_i \epsilon \partial_{\bar{l}} \\ 0 & otherwise \end{cases} \tag{5.6}$$

With the help of Fast Gauss Transform the desired object/background colour model $P_l(C)$was computed and stated in Eqn. (5.7)

$$M_l(x_i) = P_l(C(x_i)) \tag{5.7}$$

The computed boundary term can be stated as in Eqn. (5.8).

$$B(x_0, x_1) = \frac{1}{1 + \left\| C(x_i) - C(x_j) \right\|^2} \tag{5.8}$$

Where, $C(x) \epsilon [0,255]$.

5.4 EUCLIDEAN DISTANCE SEGMENTATION

Euclidean distance segmentation requires the accurate distance of pixels to achieve précised results. The metric coefficient defines Euclidean distance which depends on pixel information. Euclidean distance has insensitivity towards the minor deformations. Let $P_i P_j$ are the pixels of image where i,j = 1,2,3,……,MN. The e_i represents the coordinate system of image space. The metric coefficient g_{ij} of an image can be determined by Eqn. (5.9).

$$g_{ij} = < e_i, e_j > \sqrt{< e_i, e_i >} \sqrt{< e_j, e_j >}. \cos \theta_{ij} \tag{5.9}$$

where <,> represents the scalar product, θ_{ij} is the angle between e_i and e_j. When base vectors are of the same length then g_{ij} depends upon θ_{ij}. Then the Euclidean distance of two image spaces x, y will be computed as stated in Eqn. (5.10).

$$d_E^2(x, y) = \sum_{i,j=1}^{MN} g_{ij}(x^i - y^i)(x^j - y^j) = (x - y)^\tau G(x - y) \tag{5.10}$$

The Euclidean distance segmentation is robust and more accurate segmentation technique for medical imaging where the results depend upon the Euclidean distance computation. The segmented image pixels and the number of pixels

retained in rows and columns were stored. The total number of pixels in the image can be written as stated below in Eqn. (5.11)

$$p = R * C \tag{5.11}$$

Where p represents the Total number of Pixels which is equivalent to the product of pixels in Rows (R) and Number of pixels in Columns(C) of the image.

Figure 5.4 represents the flow chart for the skin laceration detection system, which provides information about the steps required to be followed for the detection of skin laceration. The process of conversion of test image into the desired segmented image as discussed above is pictorially represented in the flow chart for easy understanding of the algorithm for researchers. The performance of the algorithm is evaluated on the bases of the number of information pixels

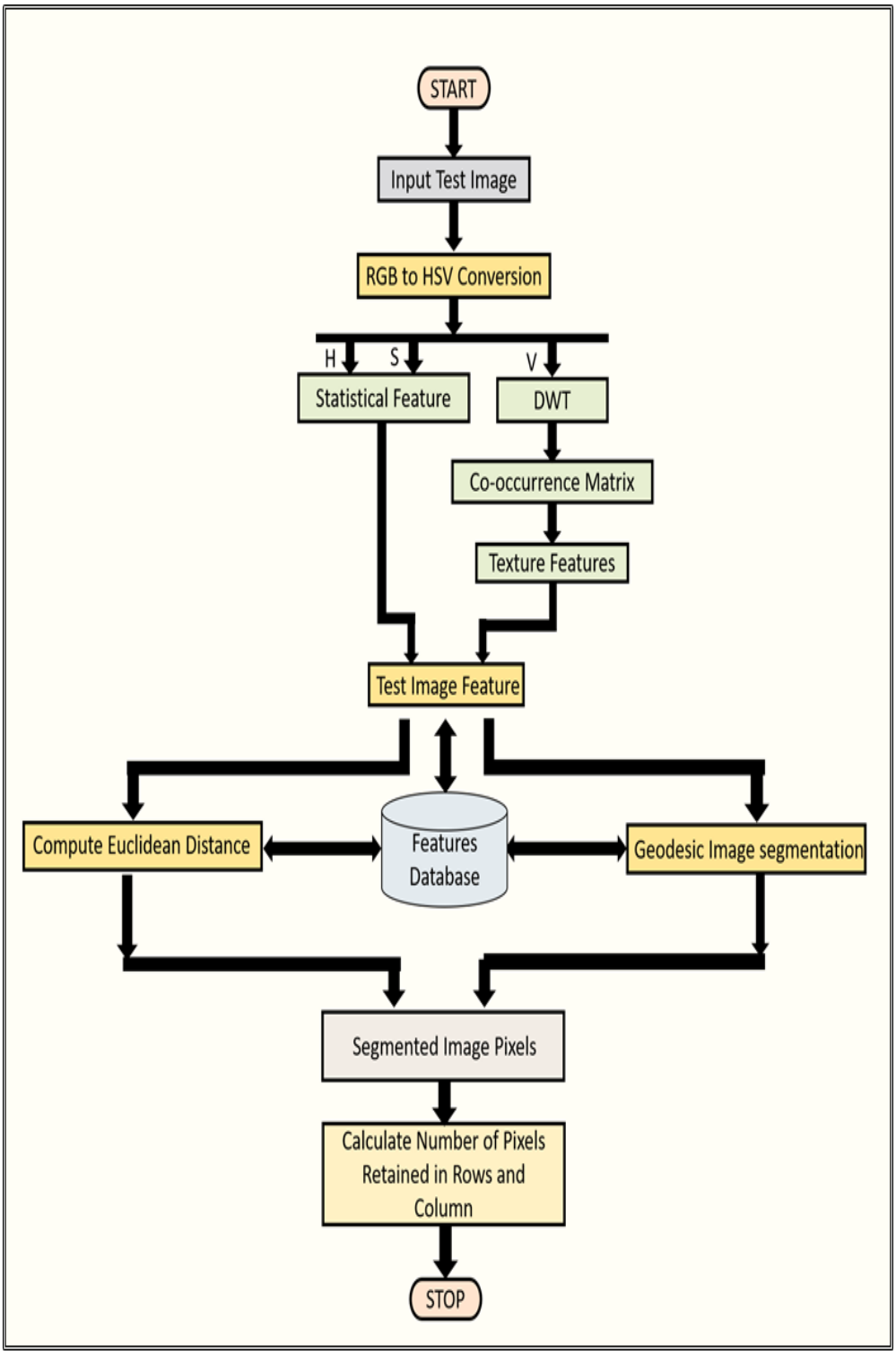

Figure 5.4: Flow chart for Skin laceration detection system.

5.5 RESULT

The Skin laceration detection system was provided with the skin phantom test image. The results of the Euclidean distance metric algorithm with varying tolerance is shown in Figure 5.5. The detected ROI of skin laceration can be seen with the highlighted blue colour grown region. The 0.2 tolerance value of the Euclidean distance metric algorithm shows poor results as compared with 0.05, 0.1 and 0.15 tolerance results. Similarly, The results of the Geodesic distance metric algorithm with varying tolerance is shown in Figure 5.6. The variation in tolerance exhibits the variation in the number of pixels used for identification of skin laceration in Euclidean Distance Metric algorithm as well as in Geodesic distance metric algorithm.

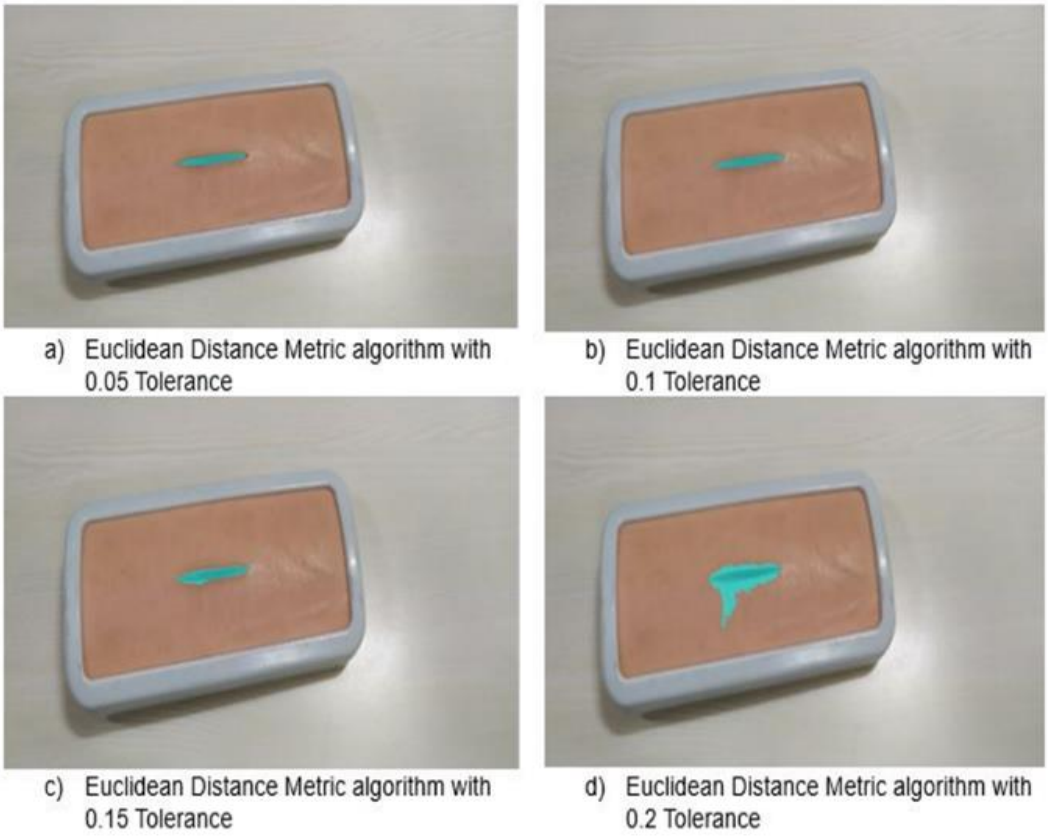

Figure 5.5: Laceration segmentation of Phantom using Euclidean Distance Metric algorithm with varying Tolerance.

The 0.2 tolerance value of the Geodesic distance metric algorithm and

Euclidean distance metric algorithm shows poor results as edges are spilled off and incorrect pixels were taken in consideration as compared with 0.05, 0.1 and 0.15 tolerance results. The edge of Geodesic is oval in nature where as in Euclidean segmentation edges are sharp in nature. The best skin laceration segmentation results can be seen using the Euclidean distance metric algorithm with 0.05 tolerance value with higher pixel information along with sharp edges laceration segmentation. The number of pixels of the segmented ROI provides an accurate measure for the efficiency of the algorithm. The total pixel of an image can compute as the multiplication of the number of pixels in rows to the number of pixels in columns.

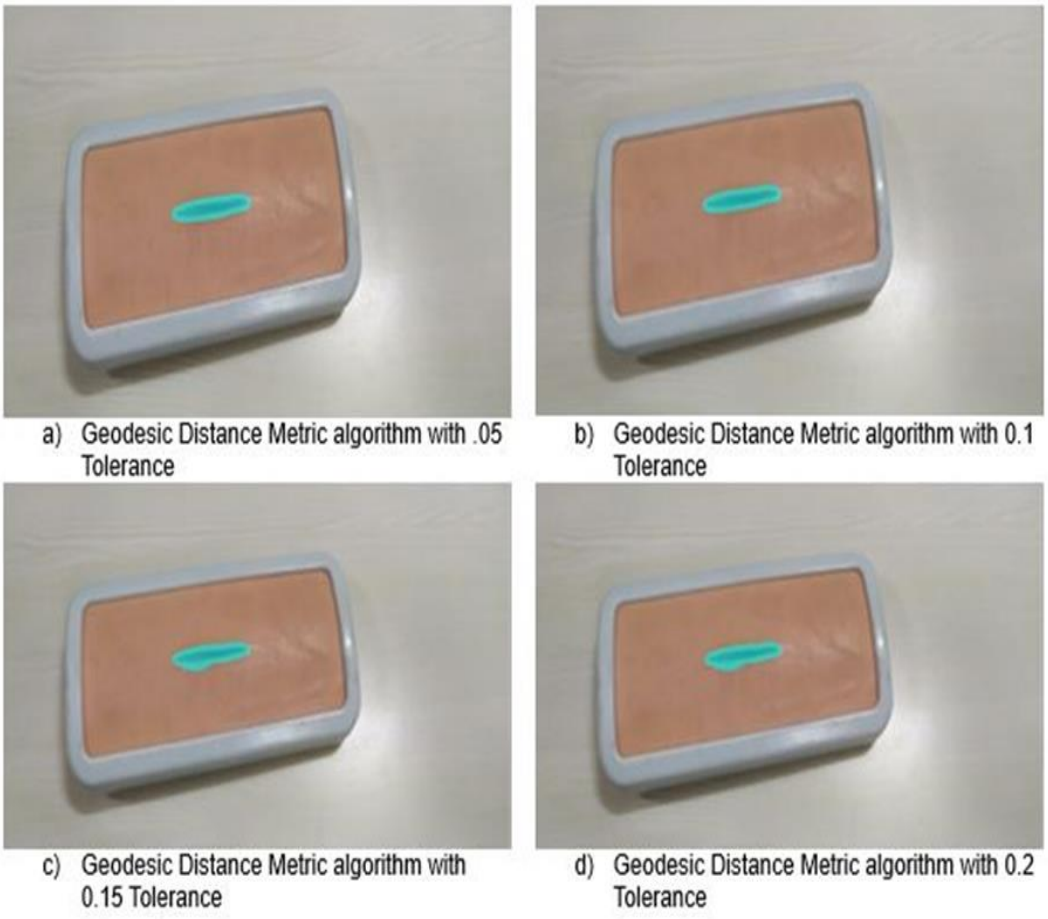

Figure 5.6: Laceration segmentation of Phantom using Geodesic Distance Metric algorithm with varying Tolerance.

Efficiency calibration of the algorithm can be computed with the help of information pixels. On applying different tolerance to the segmentation algorithms the number of pixels representing in rows and columns of the segmented ROI can be seen in Table 5.1.

Table 5.1: Comparison table for Euclidean distance matric with respect to Geodesic Distance Metric

Distance Metric	Tolerance	Rows	column
Euclidean	0.05	1047	1648
Euclidean	0.1	1059	1679
Euclidean	0.15	1051	1660
Euclidean	0.2	1047	1671
Geodesic	0.05	1051	1660
Geodesic	0.1	1043	1644
Geodesic	0.15	1051	1652
Geodesic	0.2	1043	1664

The total number of pixels representing the ROI of the skin laceration on applying different algorithms Euclidean and Geodesic distance metric concerning varying tolerance were projected using Figure 5.7.

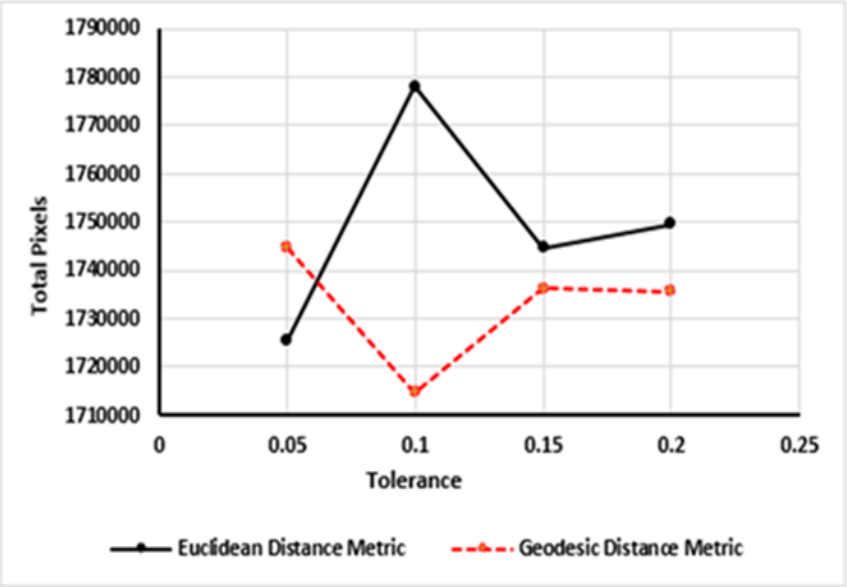

Figure 5.7: Comparative analysis of Total pixels required for each Euclidean and Geodesic Distance metric algorithm for laceration detection.

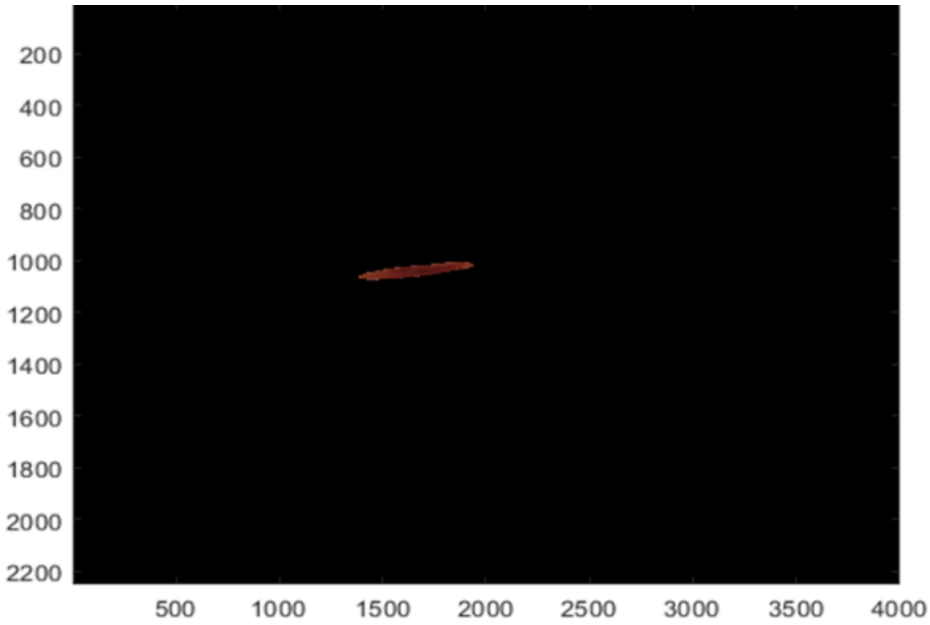

Figure 5.8: Segmentation of Skin laceration

On Appling the best segmentation technique after exploring the Geodesic and Euclidean distance Metric with the optimal tolerance providing maximum pixel information is Eucledian Distance Metric Algorithm with 0.1 Tolerance value.

The segmented ROI of skin laceration with its pixels can be seen in Figure 5.8. The information of pixels from the segmented image is used by the robotic arm to perform trajectory tracking control.

5.6 SUMMARY

This chapter illustrates the proposed skin laceration detection system. The skin segmentation technique is based on interactive skin segmentation which helps in effective and efficient skin segmentation. The Euclidean distance segmentation algorithm and Geodesic segmentation algorithm were implemented on our test skin Phantom image. The results of both algorithms are compared with each other with varying tolerance. The experiment results show that Euclidean distance Segmentation produced good results as compared to Geodesic Segmentation. From the best-segmented image, the suture points were computed in XYZ coordinate and were considered as the desired trajectory of the ALSR.

CHAPTER 6 TRAJECTORY TRACKING CONTROL

The chapter illustrates the task comprises a skin laceration trajectory or path and the robot is expected to maneuver or follow that required trajectory [3–5]. Different control schemes are used to follow that required trajectory because there exists the nonlinearity, uncertainty, external disturbances, strong coupling, and time varied of the robotic system. There are Linear and nonlinear control schemes such as PD (Proportional-Derivative) Control, PID (Proportional Integration Differentiation) Control, CTC (Computed Torque Control), Adaptive control Fuzzy Control and so on [6–10]. This chapter focuses on trajectory tracking control of ALSR to track skin laceration to perform suturing. The four cases for the PD-CTC controller are taken into consideration with different gain values the best from which is compared with the tuned PD and PID control in order to achieve the desired joint trajectory. The CTC control technique is used to produce tracking control with minimum error[136]–[138]. The common techniques used for disturbance rejection are such as Adaptive control, Robust Control, active Kalman filtering, Sliding mode control, etc. for the different robotic applications. The emerging technique used for disturbance compensation is known as disturbance observer. The disturbance observer is popular because of considering the disturbance model acting on each joint of the robot and estimating the unknown parameters of the system such as torque and forces. In the independent joint control, the disturbance observer considers the varying load [139], dynamic uncertainties[140], friction force [141], [142], unmodeled dynamics as the lumped disturbance term [143]. By the use of linear matrix inequality (LMI) the disturbance observer is designed for the slow varying disturbances. The SCARA robot configuration and Phantom Omni was taken into consideration for the validation of results [144]. For the rapid time-varying disturbance like friction, the nonlinear disturbance observer technique was discussed by W.Chen [145] A Nonlinear disturbance observer using feedforward compensation technique without computing acceleration measurements which is useful for computing sensorless torque control and fault

detection. Further Nikoobin et.al. modified Chen's Method for the generalized nonlinear disturbance observer applicable for n DOF robot manipulator having revolute joints [146]. The A Mohammadi [147] provides a nonlinear disturbance observer generalized solution for all serial manipulator irrespective of its joint configuration.

6.1 CONTROL: PD, PID AND COMPUTED TORQUE CONTROLLER ANALYSIS

The most widely used nonlinear and powerful controller used for almost all schemes for robot control in robot manipulators is Computed Torque Control (CTC)[148]. It has a special application on the different nonlinear systems based on feedback linearization by the use of nonlinear feedback law it would able to compute the required torque in the arm. It performs significantly well when all dynamic and physical parameter of the system is known. The CTC like control appears in Robust, Adaptive, and Learning Control. Figure 6.1 provides the block diagram for PD-CTC Controller, which illustrates that it's a feedback control system. The notation representing in the block diagram $\ddot{q}_d, \dot{q}_d$ and q_d are desired acceleration, desired velocity, and the desired position respectively were provided as the input to the system and acquires actual position (q_a) and velocity($\dot{q}_a$) as an output.

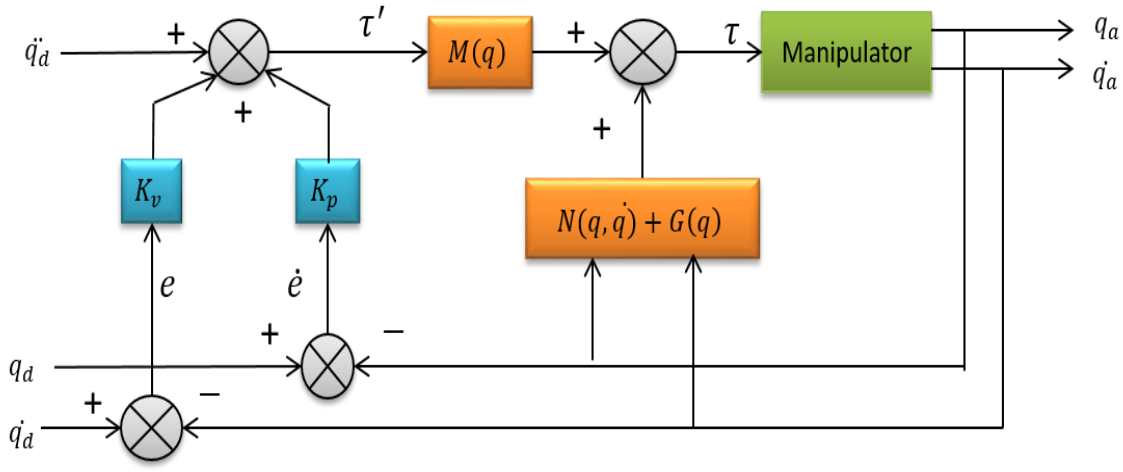

Figure 6.1: Block Diagram of PD–Computed Torque Control (PD-CTC)

Originally this algorithm is called as feedback Linearization Controller. It has assumed that the desired trajectory of the manipulator is $q_d(t)$ and $q_a(t)$ is the actual trajectory of the manipulator. The Tracking error can be defined as $e(t)$ in Eqn. (6.1), i.e. displacement error

$$e(t) = q_d(t) - q_a(t) \tag{6.1}$$

The derivative of displacement error $e(t)$, would be able to achieve velocity error denoted as $\dot{e}(t)$ stated in Eqn. (6.2).

$$\dot{e}(t) = \dot{q_d}(t) - \dot{q_a}(t) \tag{6.2}$$

Similarly, on taking the derivative of velocity error from Eqn. (6.2) able to achieve acceleration error represented as $\ddot{e}(t)$ stated in Eqn.(6.3)

$$\ddot{e}(t) = \ddot{q_d}(t) - \ddot{q_a}(t) \tag{6.3}$$

Rewriting Eqn. (4.27) with reference to actual angle denoted as q_a. The resultant is represented in Eqn.(6.4)

$$M(q)\ddot{q_a} + N(q,\dot{q})\dot{q}_a + G(q) = \tau \tag{6.4}$$

If an alternative linear state space equation in the form $\dot{x} = Ax + BU$ can be, defined as Eqn. (6.5).

$$\dot{x} = \begin{bmatrix} 0 & I \\ 0 & 0 \end{bmatrix} x + \begin{bmatrix} 0 \\ I \end{bmatrix} U \tag{6.5}$$

The Brunousky canonical form state that $U = -M^{-1}(q).N(q,\dot{q}) + M^{-1}(q).\tau$ with the help of Eqn. (6.5) and Eqn. (6.4) the Brunousky canonical form can be seen in Eqn. (6.6) written in terms of state $= [e^T\ \dot{e}^T]^T$. The U is represented as Eqn. (6.7)

$$\frac{d}{dx}\begin{bmatrix} e \\ \dot{e} \end{bmatrix} = \begin{bmatrix} 0 & I \\ 0 & 0 \end{bmatrix} . \begin{bmatrix} e \\ \dot{e} \end{bmatrix} + \begin{bmatrix} 0 \\ I \end{bmatrix} U \tag{6.6}$$

With

$$U = \ddot{q}_a + M^{-1}(q).\{N(q,\dot{q}) - \tau\} \tag{6.7}$$

Taking the inverse of the Eqn. (6.7), the computed torque for the required arm as stated in Eqn. (6.8)

$$\tau = M(q)(\ddot{q_d} - U) + N(q,\dot{q}) \tag{6.8}$$

On selecting the proportional–plus-derivative (PD) feedback for control input U (t) results in PD computed torque control that guarantees the tracking of the desired trajectory as mentioned in Eqn. (6.9).

$$\tau = M(q)\left(\ddot{q_d} + K_v\dot{e} + K_p e\right) + N(q,\dot{q}) \tag{6.9}$$

Then Eqn. (6.11) shows the resulting linear error dynamics from Eqn. (6.9) and Eqn. (6.10).

$$\tau' = \ddot{q} \tag{6.10}$$

$$\ddot{q} = \ddot{q}_d + K_d\dot{e} + K_p e \tag{6.11}$$

Or with $\ddot{e} = \ddot{q}_d - \ddot{q}_a$

$$\ddot{e} + K_d\dot{e} + K_p e = 0 \tag{6.12}$$

Where K_d and K_p are the Velocity and Position gain.

For the critical damping performance of each joint, the Eqn. (6.13) states the relationship between K_d and K_p.

$$K_d = 2\sqrt{K_p} \tag{6.13}$$

The computed torque control is used to linearize the error dynamics using nonlinear feedback, which provides better tracking performance in comparison with linear controllers. The computational cost is more as compared to linear

controllers and inaccuracies in the dynamic model and other parameters limit the performance of the manipulator.

6.2 COMPARATIVE RESULTS OF PD AND PID CONTROLLER WITH REFERENCE TO CTC CONTROLLER AND ITS CASES

The computed torque controller (CTC) control was implemented for step responses. The simulation is implemented using the MATLAB/ Simulink Software. In this chapter, the simulation results of the ALSR with 4 DOF are discussed moving the robot from its home to the final position taking consideration of different K_d and K_p values.

6.3 PERFORMANCE ESTIMATION

As stated in refer [15,16]; the performance estimation of the controller is estimated by its trajectory tracking. In the PD-CTC controller, the proportional and derivative gain directly affects the performance of the controller. The Performance of the PD-CTC controller is computed by tuning gains using trial and error. The CTC cases were considered with the different gain coefficient of the controller and their respective responses with respect to steady-state error and Root mean square error that can be seen in Table 6.1.

In PD-CTC controller two-gain coefficient have considered i.e. Proportional Gain (K_p) and Derivative gain (K_d). The proportional gain is directly proportional to the error. Therefore, if there is an increase in error we should increase the Kp value in the same proportion. To make a robot move in the desired trajectory the large value of Kp should be kept which will make the robot follow the desired trajectory or tries to reduce the error. The lower value of Kp makes the system sluggish, the reaction is slow to lead the heading change and it can happen it never reaches the desired values. Higher Kp made the system to respond rapidly and smoothly to reach the desired values. Too higher Kp will provide high control command even for smaller errors which leads to the system overshoot. Increasing Kp even after too higher a value makes the system oscillating. As per the dynamics of the system, it may cause unnecessary

vibrations to the system. The Derivative gain is the rate of change of error, which implies an increase in Kd will make the system respond faster. Right value Kd reduced overshoot caused by increased Kp and system smooth and faster.

Considering the above tuning conditions of Kp and Kd the below mention cases are considered for PD-CTC Tuning. In Table 6.1, the case of PD-CTC with their respective Root mean square error and Steady-state error at each joint is calibrated. The gains for the operations were manually tuned until the motion controller with observer gave desired performance. The trajectory tracking responses of each case can be seen in Figure 6.2 which shows the great contrast caused by taking different Kp and Kd values as mentioned below from case 1 to case 4. From the Figure 6.2 clearly depicts the case 1 is showing better trajectory tracking than other cases.

- **Case 1:** Kd =60, Kp =360

As the value of Kp is higher and respectively the value of Kd is less than Kp but relatively higher than in other cases. The selected values of Kp and Kd made the system to respond faster and follow the smoother trajectory to reach the desired angle without any overshoot.

- **Case 2:** Kd =2, Kp =10

The value of Kp and Kd are lower with respect to case 1 but the value of Kp is higher than Kd similar to case 1. The lower value of Kp and Kd made the system sluggish in response with respect to case 1.

- **Case 3:** Kd =10, Kp =10

In case 3, the value of Kp and Kd is equal. The large value of Kd will provide excessive force to the system to attain the desired trajectory. This excessive force by derivative gain will make the system to cause overshoot.

- **Case 4:** Kd =10, Kp =2

In case 4, the value of Kp is much lower than the Kd. The lower value of Kp made the system extremely sluggish in response, which in turn system does not reach its desired trajectory in the system simulation time frame of 50 seconds.

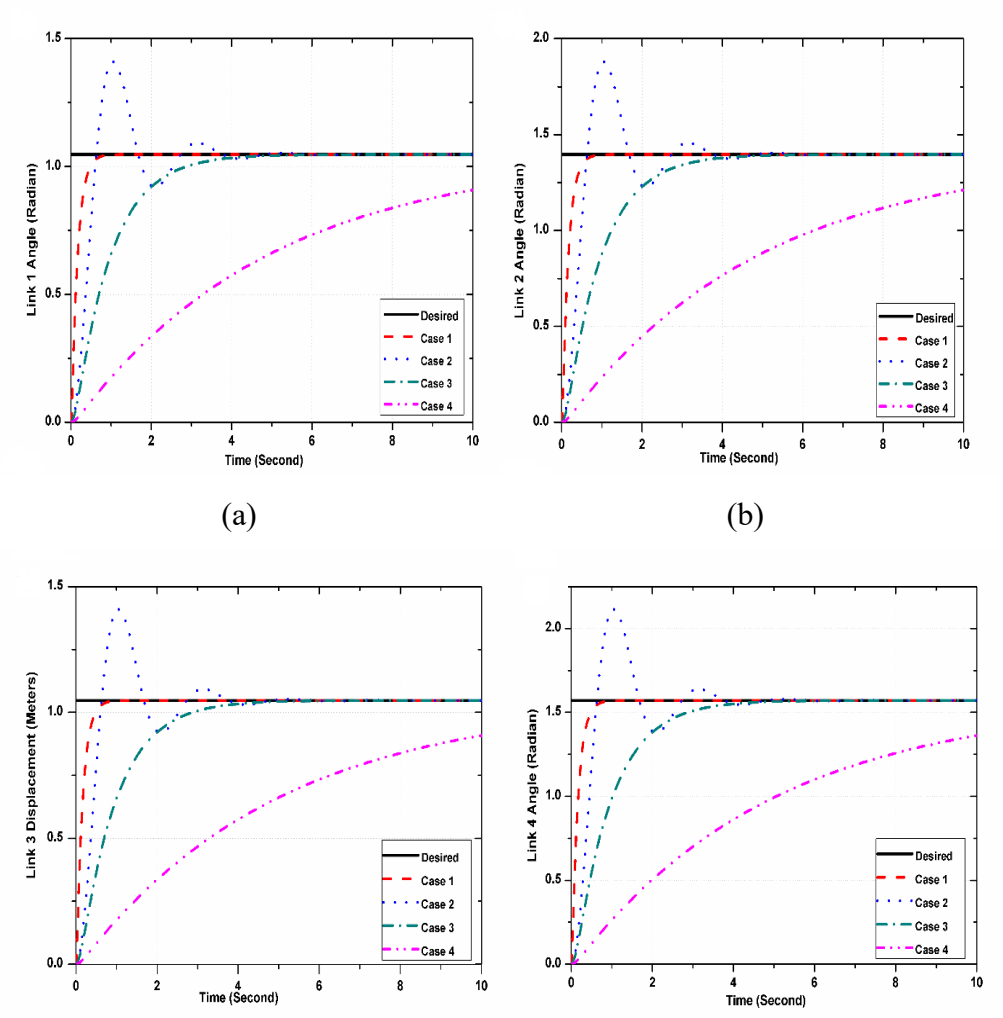

Figure 6.2: Computed Torque Control (CTC) at different cases and Desired Input Step Trajectory for (a) Link 1 Joint Angle, (b) Link 2 Joint Angle, (c) Link 3 Joint Displacement, and (d) Link 4 Joint Angle.

Table 6.1: Comparison table of Computed Torque Control (CTC) of different cases followed with their respective Steady State Error (SS Error) and Root Mean Square Error (RMS Error)

Case	Kp 1	Kd 1	Kp 2	Kd 2	Kp 3	Kd 3	Kp 4	Kd 4	SS Error 1	SS Error2	SS Error3	SS Error 4	RMS Error
Case 1	10	2	10	2	10	2	10	2	8.326 e^-06	1.110e ^-05	8.326e ^-06	1.249 e^-05	0.195 9
Case 2	36 0	60	36 0	60	36 0	60	36 0	60	1.49e ^-05	1.986e ^-05	1.49e^ -05	2.234 e^-05	0.100 3

Case 3	10	10	10	10	10	10	10	10	1.529e^-05	2.039e^-05	1.529e^-05	2.294e^-05	0.2456
Case 4	2	10	2	10	2	10	2	10	1.388e^-01	1.851e^-01	1.851e^-01	1.388e^-01	0.1704

From the above analysis illustrated in Table 6.1 based on SS and RMS Error the case 1 is considered as the best tuned PD-CTC controller with Kp and Kd valued as 360 and 60 respectively. The best case of PD-CTC controller case 1 is compared with the tuned PD and PID controller [8,17]. The trajectory tracking of the PD-CTC, PD, and PID controller for step trajectory can be seen in Figure 6.3. According to Figure 6.3, the CTC, PD, and PID controller, the CTC controller tracks the step input trajectory more precisely with the least RMS error of 0.1003. This shows accurate trajectory tracking of CTC controller with respect to individual PD and PID controller. Therefore, the CTC control with best case 1 is opted for further disturbance observer based control.

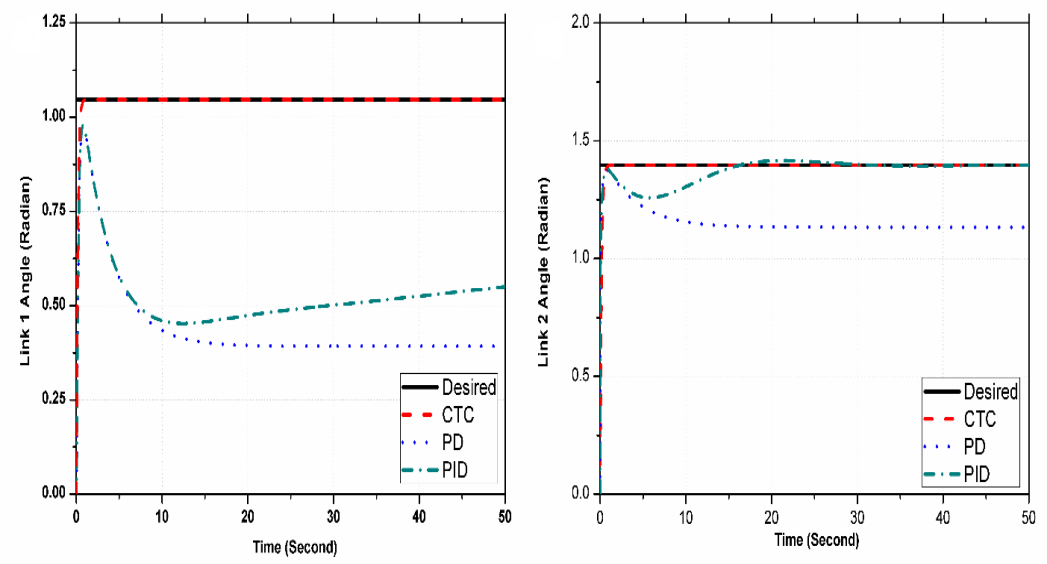

(a) (b)

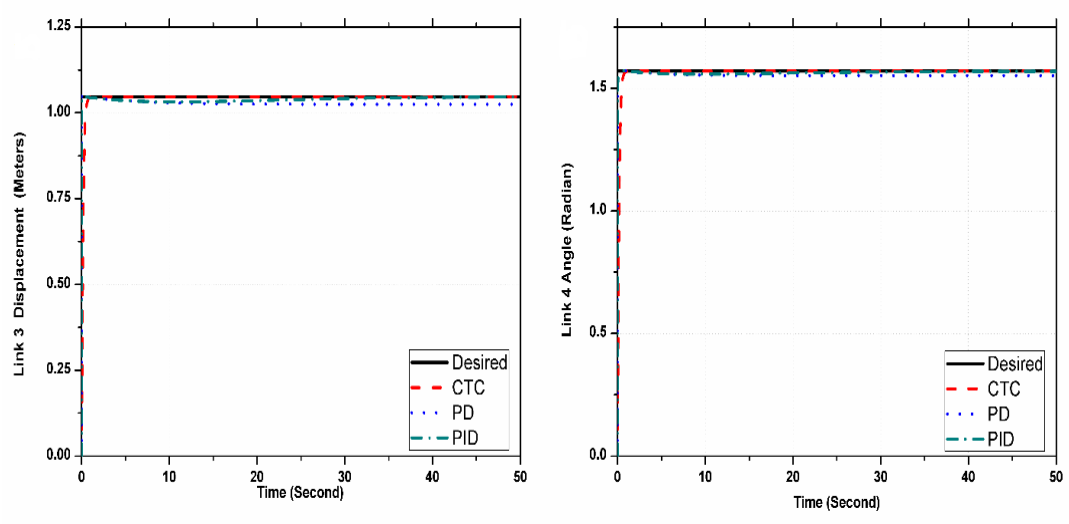

(c) (d)

Figure 6.3: Computed Torque Control (CTC), Proportional-Derivative Control (PD), Proportional Integrated Derivative Control (PID) and Desired Input Step Trajectory for (a) Link 1 Joint Angle, (b) Link 2 Joint Angle, (c) Link 3 Joint Displacement and (d) Link 4 Joint Angle.

For PD, PID, and CTC the Kp and Kd values of each joint of the robot are mentioned in Table 6.2. The gain values of the controller for each joint are taken as constant in PD and PD- CTC whereas in PID control implementation the gain values of each joint of the manipulator are well-tuned.

Table 6.2: Different control techniques: CTC, PD and PID with their respective gains.

Control Technique	Kp1	Ki1	Kd1	Kp2	Ki2	Kd2	Kp3	Ki3	Kd3	Kp4	Ki4	Kd4
CTC	10	0	2	10	0	2	10	0	2	10	0	2
PD	360	0	60	360	0	60	360	0	60	360	0	60
PID	300	.0056 1	4	200	0.22061 18	4	36	0.05833 9	6	30	0.05833	4

Table 6.3: Root Mean Square (RMS) Error of system and Steady State (SS) Error at each joint of the system at different control techniques.

Control Technique	SS Error1	SS Error2	SS Error3	SS Error4	RMS error
CTC	1.49e^-05	1.986e^-05	1.49e^-05	2.234e^-05	0.1003
PD	0.6549	0.2639	0.02222	0	0.3534
PID	4.971e^-01	2.291e^-04	5.504e^-04	7.090e^-01	0.2486

On comparison of well-tuned PD and PID Controller with the best case of CTC control technique, their respective Steady-state error and Root mean square error can be seen in Table 6.3. The steady-state error for each joint of the robot manipulator as mentioned in Table 6.3 illustrates that the CTC controller performs well to minimize the error in joint trajectory tracking. The steady-state error of each joint in CTC control is reduced to e^-05 with Root Mean Square Error of 0.1003. The RMS error of CTC is 71.61% less than the PD controller and 59.65% less than PID controller. The performance of CTC controller for trajectory tracking is best with respect to PD and PID control taking steady-state and root mean square error as an estimation function.

6.4 DISTURBANCE MODELLING FOR ALSR

As compared to the task performances of the surgical manipulator need to undergo various interactions between patient body parts and robot end tool. The robot will receive different interaction forces on interacting with different body parts due to the difference in stiffness coefficient. The interaction forces while interacting with the patient is assumed to be external disturbances represented by τ_{extdis} . The internal disturbance of the manipulator represented by τ_{indis} is considered to be caused by system uncertainty and noises. Therefore a controller needs to design who will have the knowledge of each state of the system and able to compensate for the effect of disturbances [136]–[138].

The mathematical modeling of internal and external disturbances affecting the system dynamics was illustrated in Eqn. (6.16) and Eqn. (6.17) respectively. Therefore the dynamic equation of the system becomes as stated in Eqn. (6.14) which includes internal and external disturbances.

$$M(q)\ddot{q} + N(q,\dot{q})\dot{q} + G(q) = \tau_{i/p} + \tau_{dis} \tag{6.14}$$

Where the Generalized Input Force Vector (n x 1 dimension) is expressed as $\tau_{i/p}$, The Inertia Matrix of a surgical manipulator is represented by M with the dimension of n x n. $M(q)$ is a positive symmetric matrix, N is Centrifugal and Coriolis Forces (n x 1 dimension), G is a Gravitational Force Vector, $\dot{q}$ is Joint Angular Velocity Vector and q is Joint Position Vector. τdis is stated as the total disturbance acting on each joint of the manipulator. The total disturbance is the algebraic sum of internal disturbances caused by model uncertainty and external disturbances caused by friction forces are stated in Eqn. (6.15) [107]

$$\tau_{\text{dis}} = \tau_{\text{indis}} + \tau_{\text{extdis}} \tag{6.15}$$

The internal and external disturbances in the system were modeled as mentioned in Eqn. (6.16) and Eqn. (6.17). [150]

$$\tau_{indis} = \Delta M(q)\ddot{q} + \Delta N(q,\dot{q})\dot{q} + \Delta G(q) + v \tag{6.16}$$

Where, $\Delta M(q)\ddot{q}, \Delta N(q,\dot{q})\dot{q}\ and\ \Delta G(q)$ are the representation of variation in system modeling from the actual system to the nominal system also known as parameter uncertainties. The system noises due to measurement and process are represented as v.

The modeling of external disturbances for the ith joint of the manipulator, i=1, 2, 3, 4 is stated below in Eqn. (6.17). Where f_{ri} is the coefficient of friction, which includes coulomb, static and viscous friction. The parameters used for simulation are chosen as $f_{r1} = 1.43, f_{r2} = 1.6, f_{r3} = 1.4, f_{r4} = 1.2$ and t as a simulation time of the system.

$$\tau_{iextdis} = f_{ri} * sgn(2 * t + 1) \quad (6.17)$$

6.5 DISTURBANCE OBSERVER BASED CONTROL SCHEME OF THE ALSR

The purpose of implementing the Disturbance Observer (DOB) control scheme on the surgical manipulator is to optimize the effect of both internal and external disturbances. From the literature reviewed, the system is assumed accurate and with the help of sensors, external disturbances are measured [137], [151]–[153]. The robust and effective control scheme implement to compensate the disturbances is disturbance observer-based computed torque control. To estimate the states of the system when the measurements are not available the disturbance observer is the most effective technique for the same as proven by the literature[146], [150], [154]–[158]. In the proposed suturing system, the measurement devices are considered through which the joint position of the manipulator is achieved.

The desired task space trajectory is feed to the system through inverse kinematics such that the desired angle for each joint is computed. The error between desired and actual joint angles/ joint displacement is passed through a control block diagram that provides the control torque represented as τc. Disturbance observer in order to compensate for the disturbance and achieve accurate trajectory tracking computed the estimates of disturbance stated in Eqn. (6.19)[106].

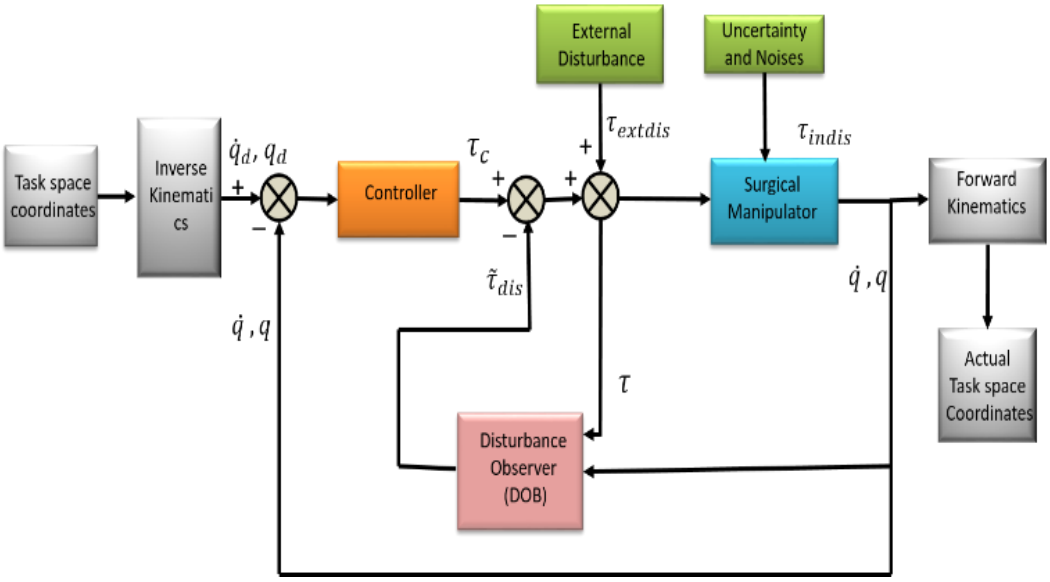

Figure 6.4: Block Diagram of the disturbance observer scheme for the surgical robot

The nonlinear control law for a surgical robot is stated in Eqn. (6.18)[108].

$$\tau_{i/p} = M(q)(\ddot{q}_d) + N(q,\dot{q})\dot{q} + G(q) - \tilde{\tau}_{dis} + k_d\dot{e} + k_p e \qquad (6.18)$$

On solving Eqn. (6.14) with Eqn. (6.18) , the following equation will be obtained

$$M(q)\left[\ \ddot{e} + k_d\dot{e} + k_p e\ \right] = 0 \qquad (6.19)$$

Let's assume $\ddot{e} + k_d\dot{e} + k_p e = \tilde{\tau}_{dis}$. From the above equation, it states that $M(q)\tilde{\tau}_{dis} = 0$.The mass matrix of the system cannot be zero hence it states that $\tilde{\boldsymbol{\tau}}_{\boldsymbol{dis}} = 0$.

$$\tau_{i/p} = \widehat{M}(q)\left(\ddot{q}_d + k_d\dot{e} + k_p e\right) + \widehat{N}(q,\dot{q})\dot{q} + \hat{G}(q) - \tilde{\tau}_{dis} \qquad (6.20)$$

Where the estimates of $M(q)$,τ_{dis}, $N(q,\dot{q})$ and $G(q)$ are represented as $\widehat{M}(q), \tilde{\tau}_{dis}, \widehat{N}(q,\dot{q})$ and $\hat{G}(q)$. The $\tilde{\tau}_{dis}$ is represented as a disturbance estimator with n x 1 matrix dimension. The $\tilde{\tau}_{dis}$ is equivalent to the product of

the gain constant (k_3) and joint velocity ($\dot{q}$) with the algebraic sum of Z which is an arbitrary vector taken into consideration can be seen in the below Eqn. (6.21)

$$\tilde{\tau}_{dis} = k_3\dot{q} + Z \tag{6.21}$$

On taking the derivative of $\tilde{\boldsymbol{\tau}}_{\boldsymbol{dis}}$ stated in the above Eqn. (6.21) will become as

$$\dot{\tilde{\tau}}_{dis} = k_3\ddot{q} + \dot{Z} \tag{6.22}$$

On replacing $\ddot{\boldsymbol{q}}$ value from Eqn. (6.22)

$$\dot{\tilde{\tau}}_{dis} = k_3M^{-1}(\tau + \tilde{\tau}_{dis} - N - G) + \dot{Z} \tag{6.23}$$

On rearranging the values of Eqn. (6.23)

$$\dot{Z} = -k_3M^{-1}(\tau + \tilde{\tau}_{dis} - N - G) - \tilde{\tau}_{dis} \tag{6.24}$$

On replacing the value of $\tilde{\tau}_{dis}$ from Eqn. (6.24)(6.25)

$$\dot{Z} = -k_3M^{-1}(\tau + \tilde{\tau}_{dis} - N - G) - k_3\dot{q} \tag{6.25}$$

Equation (6.25) is the final expression of the disturbance estimator of the proposed disturbance observer. The error causing in each joint of the manipulator due to internal and external disturbances provides the accumulative error at the end-effector position. Similarly, to reduce the error in the position of the surgical tool to locate the targeted position the error at each joint gets reduced using the proposed disturbance observer control technique with successive operations. This observer requires only the measurement of joint velocity. The tuning of the gain parameter of the DOB $k_p, k_d, and\ k_3$ brings the significant difference in system settling time and steady-state errors.

6.6 SIMULATION STUDY OF DISTURBANCE OBSERVER

The mathematical modeling of the surgical manipulator and control system is implemented in Matlab/Simulink package shown in Figure 6.5. While modeling the system the external disturbances and internal disturbances were taken into consideration. The reference trajectory is the trajectory of laceration on the patient. The reference trajectory is given to the manipulator defined in Cartesian space. Through inverse kinematics, the joint space trajectory is feed to the system to achieve accurate and robust trajectory tracking. The results of the manipulator with and without disturbance observer are compared in presence of disturbance torque, as modeled in Eqn. (6.14).

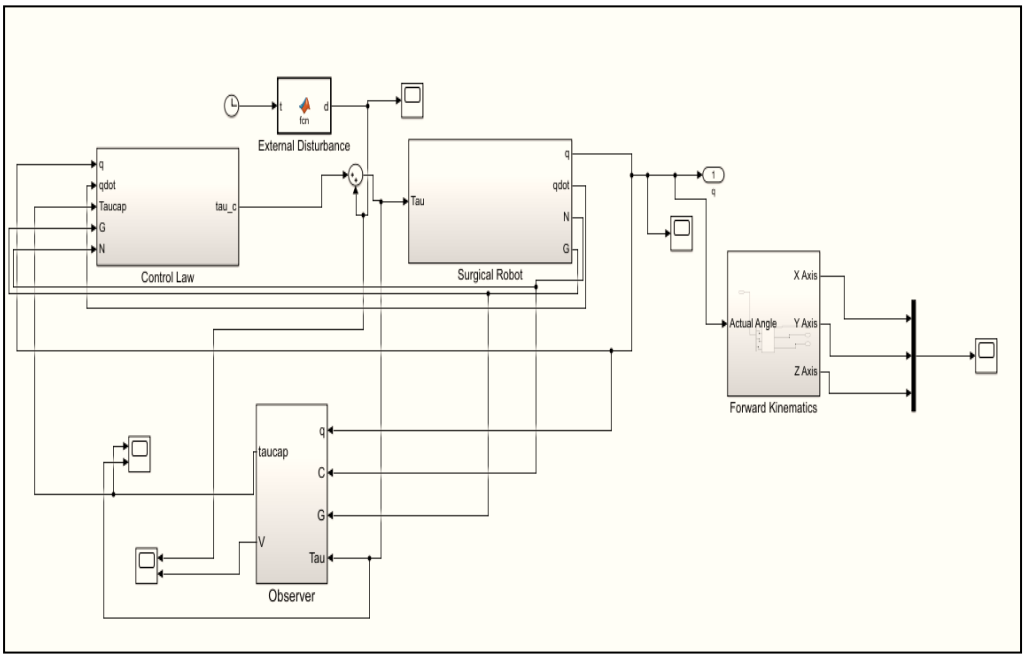

Figure 6.5: Modelling of disturbance observer assisted surgical manipulator

The gain values of the DOB control used during simulation are Kp = 180I, Kd= 36I, and K3= 10I.

In Figure 6.6 the results of DOB, without DOB and desired trajectory of the joint angle of link1, link 2, and link 4 and length of displacement of link 3 in case of the prismatic joint are compared. The difference between the desired position and the actual joint position is the position tracking error of the surgical

manipulator while tracking the laceration for the suturing task. The position tracking error with and without observer can be seen in Figure 6.7. This depicts the use of DOB for compensating the disturbances.

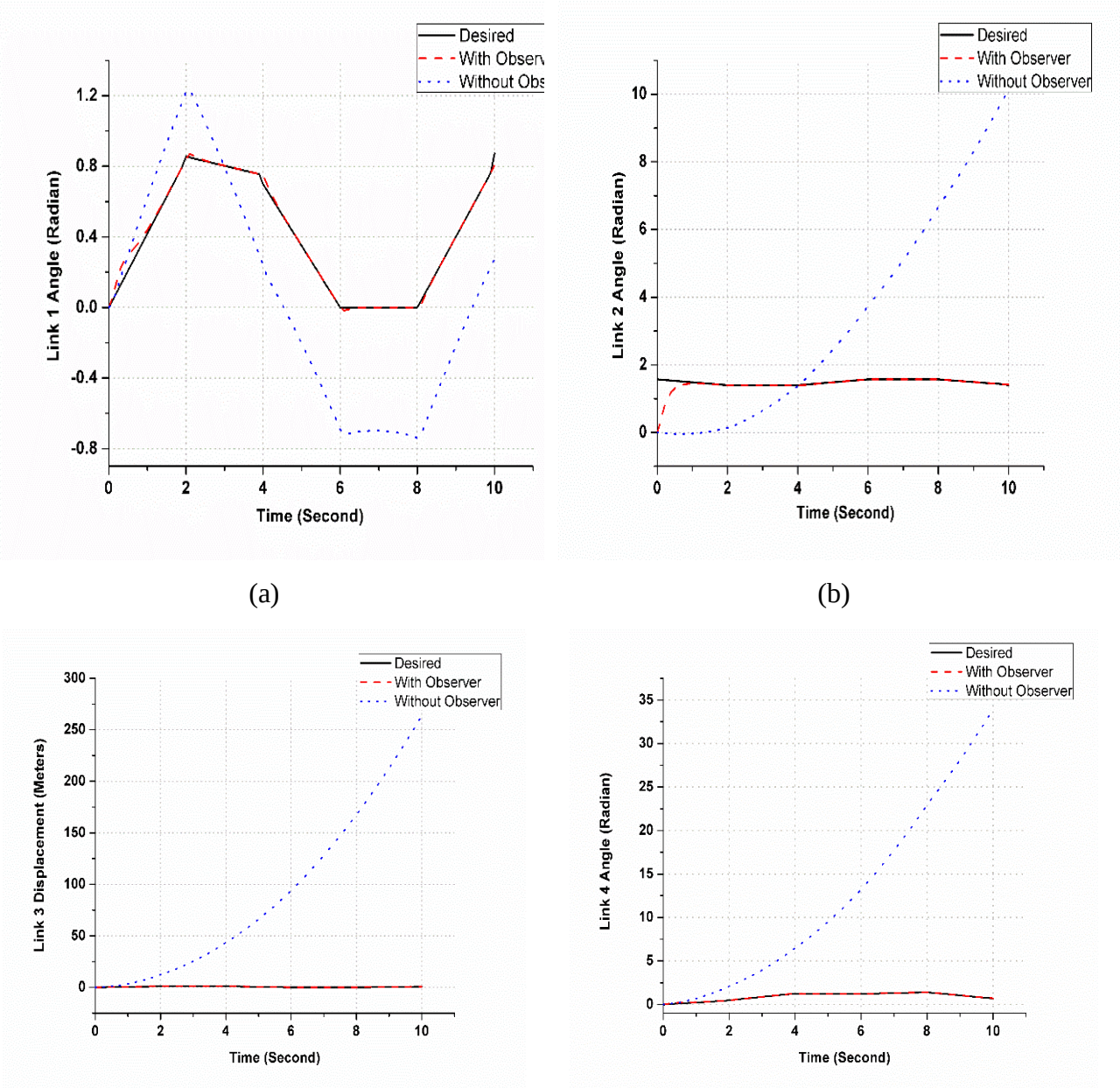

Figure 6.6: Time Trajectory position tracking of each link of the manipulator (a), (b), (c) and (d) with and without Observer.

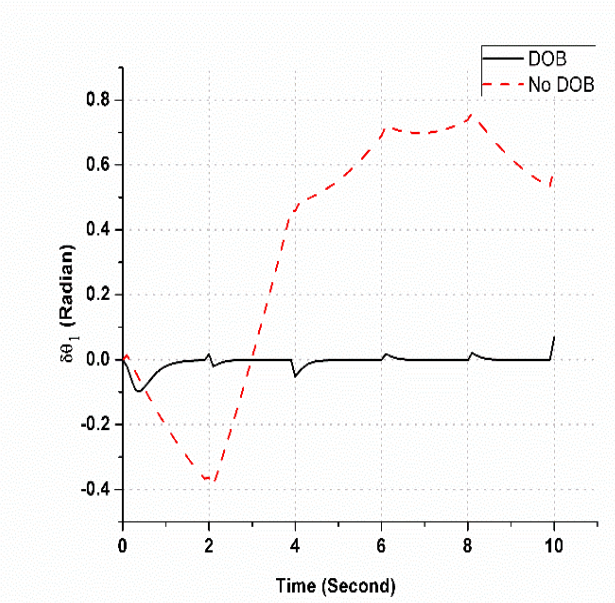

(a)

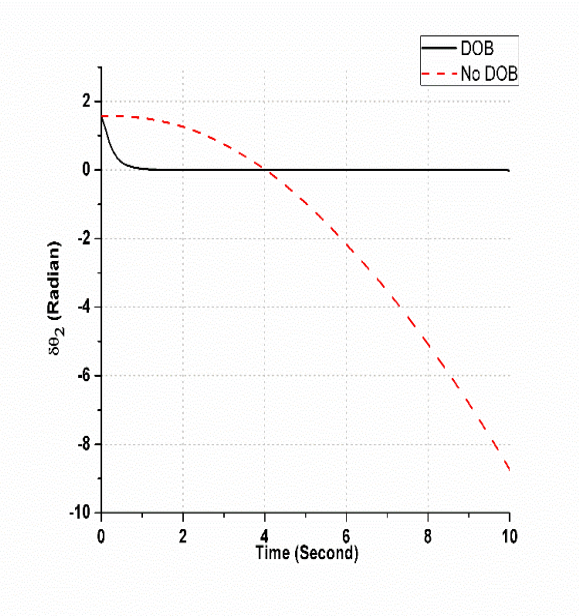

(b)

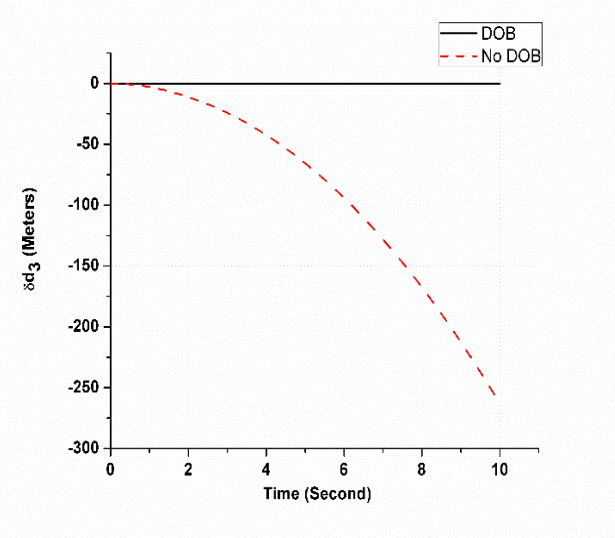

(c)

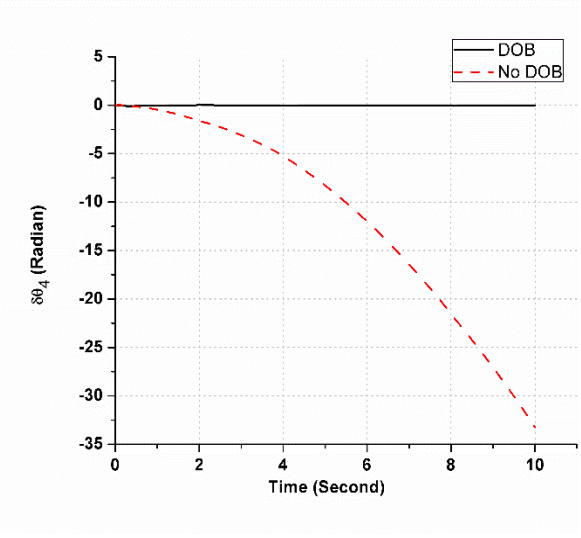

(d)

Figure 6.7: Position tracking error profile for link 1 (a), link 2 (b), link 3(c), and link 4 (d) in laceration tracking.

The joint disturbance tracking using disturbance observer in each joint of the surgical manipulator can be seen in Figure 6.8. This shows the system would able to optimize the disturbance both internally and externally by tracing the required laceration trajectory. Figure 6.9 shows the error joint disturbance torque/force at each joint of the surgical manipulator for tracing the trajectory.

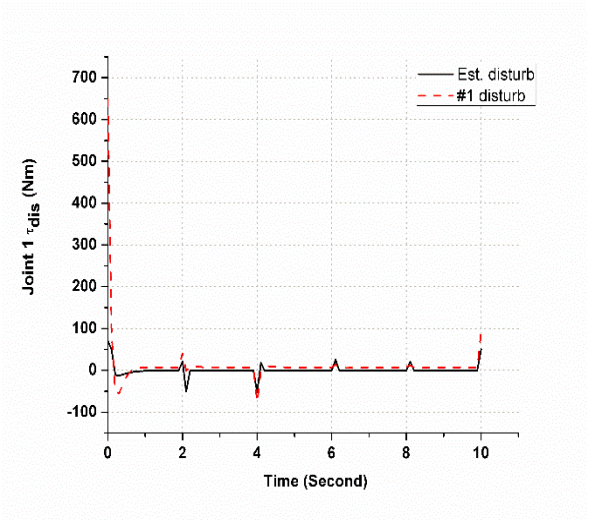

(a)

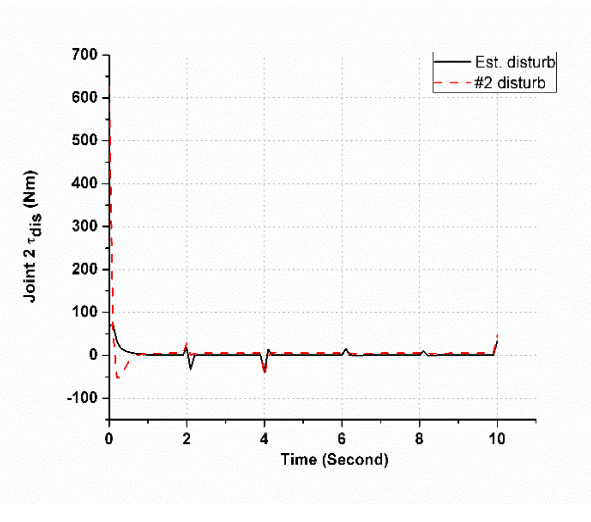

(b)

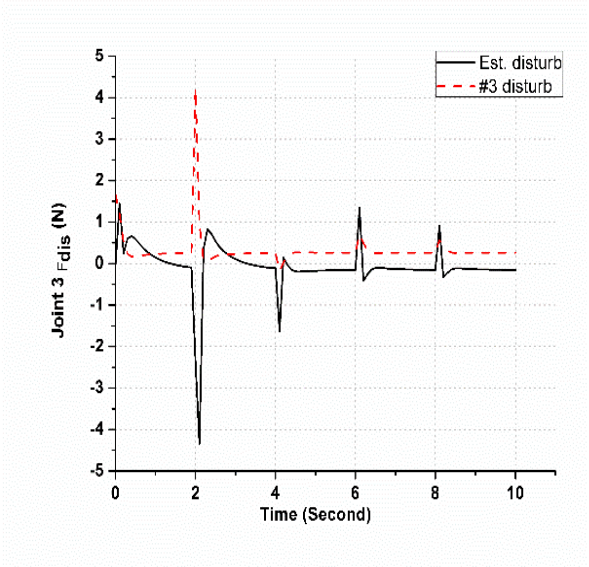

(c)

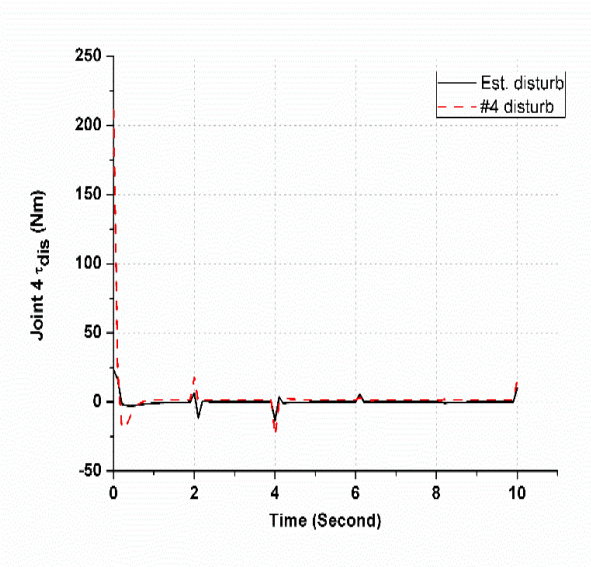

(d)

Figure 6.8: Joint disturbance tracking profile for each joint of the surgical manipulator

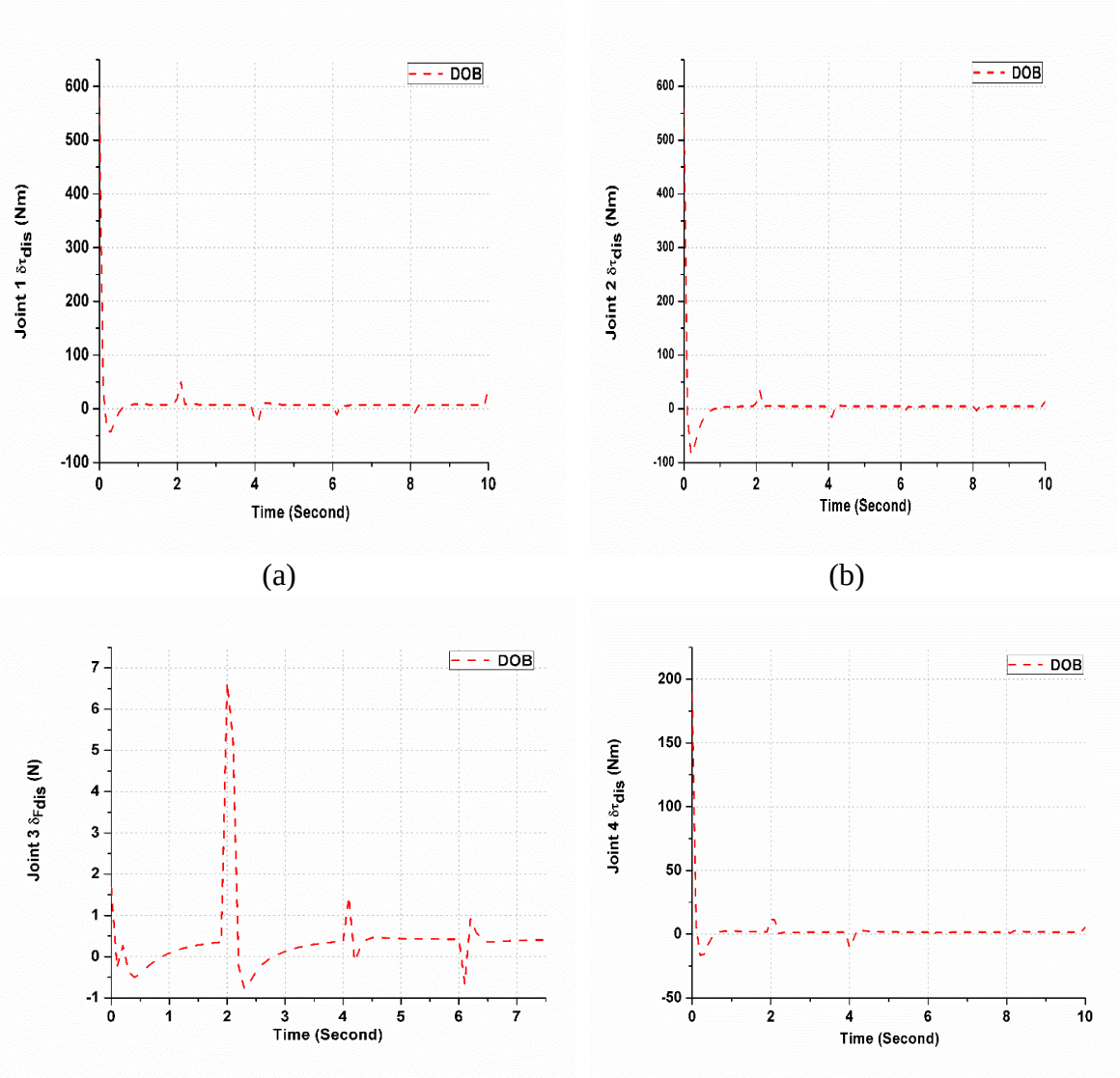

Figure 6.9: Disturbance tracking error in each joint of a surgical manipulator

In the task-space coordinates, the performance of the DOB controller with respect to without the DOB controller can be seen in Figure 6.10. The trajectory of laceration on the patient is tracked effectively and adapting disturbances by disturbance observer control. This task of the surgical robot considered in the system is to track the desired trajectory and compensate for the disturbance caused by internal and external factors to achieve the precise motion of the manipulator for suturing tasks.

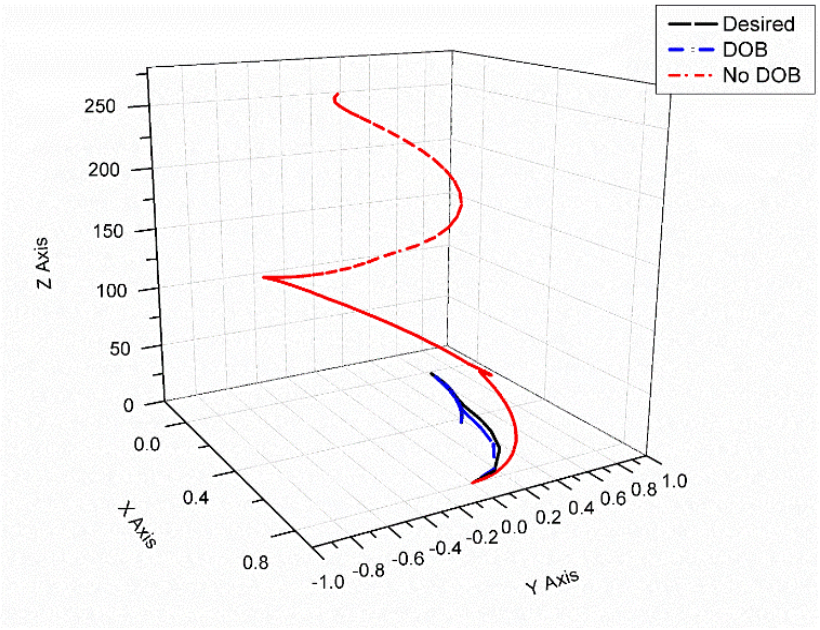

Figure 6.10: Task space coordinate (XYZ) of the end effector during laceration tracking operation.

The performance estimation of the controller can be through the root mean square (RMS) error for the position and disturbance tracking. The below-mentioned Eqn. (6.26) and Eqn. (6.27) is used for the estimation of RMS error.

$$q_{rms\_error} = \sqrt{\sum_{i=1}^{n} \frac{(q_d - q_i)^2}{n}} \tag{6.26}$$

$$\tau_{dis\_rms\_error} = \sqrt{\sum_{i=1}^{n} \frac{(\tau_d - \tau_i)^2}{n}} \tag{6.27}$$

Table 6.4: Illustrate the RMS value of position tracking error and disturbance tracking error while performing the surgical task by the manipulator

RMS error	**Joint 1**	**Joint 2**	**Joint 3**	**Joint 4**
Position Tracking	0.06902	0.01774	0.05902	0.007978

Disturbance Tracking	5.559	3.355	1.403	1.197

It is observed that uncertainties, external disturbances, and dynamic changes in the system are well adapted by the disturbance observer control. The simulation results are intuitive and point out the effectiveness and use of control for a surgical robot. The laceration tracking performance of the controller extended the work to an autonomous surgical robot. The accurate and robust tracking performance of control enables the surgical robot to do n number of tasks performed during surgery.

6.7 CO SIMULATION ANALYSIS AND RESULTS

Building up a new robot model, analyzing, and verification of the model should be taken care of before constructing up in the real world. The simulation is more popular because of the low cost of the computer, which helps analyze feasibility studies, the presentation with animation, layout evaluation, and offline programming. Therefore, the simulation tool like MATLAB, ADAMS, Vrep, and ROS, and so on can be used to simulate robot to analysis robot motion [159]. During the surgical simulation for preoperative planning of maneuvering the robot to operate the patient, the joint control of the robot for trajectory tracking is required. To visualize the motion of the robot in a 3D environment the co-simulation technique is very popular.

In the research, collaborative simulation is used to visualize the system performance in real-time. The collaborative simulation is popularly known as Co-simulation. To validate the system performance of a virtual prototype of any machinery, the Co-simulation technique is used. This technique reduces the dependency on dynamic system modeling for analyzing various dynamic parameters like force, torque, velocity, position, etc. In the research, the DOB-assisted CTC control system design has been validated using co-simulation MSC ADAMS and MATLAB Software platform. The DOB-assisted CTC

controller is designed and implemented to control the joint position of ALSR to reach the desired position in order to perform the suturing task.

For co-simulation, initially the ALSR prototype model has been developed in the SOLIDWORKS Software platform. The dynamic model parameters of the ALSR were obtained from the CAD model designed. The designed CAD model was imported into the MSC ADAMS Software platform. The necessary markers and state variables were defined to create the input and output variables. Input variables consist of joint torques and forces whereas output variables were joint position and velocity while performing Antebrachium laceration suturing by ALSR. The placed marker helps in extracting the simulation data. The ALSR is considered to be a bedside robot manipulator with the suturing tool. The skin properties as mentioned in Table 6.5 were applied to the virtual human lying on the operation theater bed.

Table 6.5: Generalised Antebrachium Skin Properties

Antebrachium Skin Parameters	**Value**
Elastic Modulus	10 Skin Elastic modulus (MPa)
Density	1100 (kg/mm3)
Poisson's ratio	0.3

The Adams/control plant Export is used to Create a control_plant.m file that can be invoked in MATLAB for the co-simulation environment. The coordinates points of skin laceration have been invoked from the Image processing as described in chapter 5 to MATLAB/SIMULINK software platform. Through inverse kinematics, the joints motion of ALSR was computed. The ALSR control equations were developed in MATLAB Platform to provide input to adams_sub block. The interaction between ADAMS and MATLAB/SIMULINK software platform were established with the help of adams_sub block as shown in Figure 6.11.

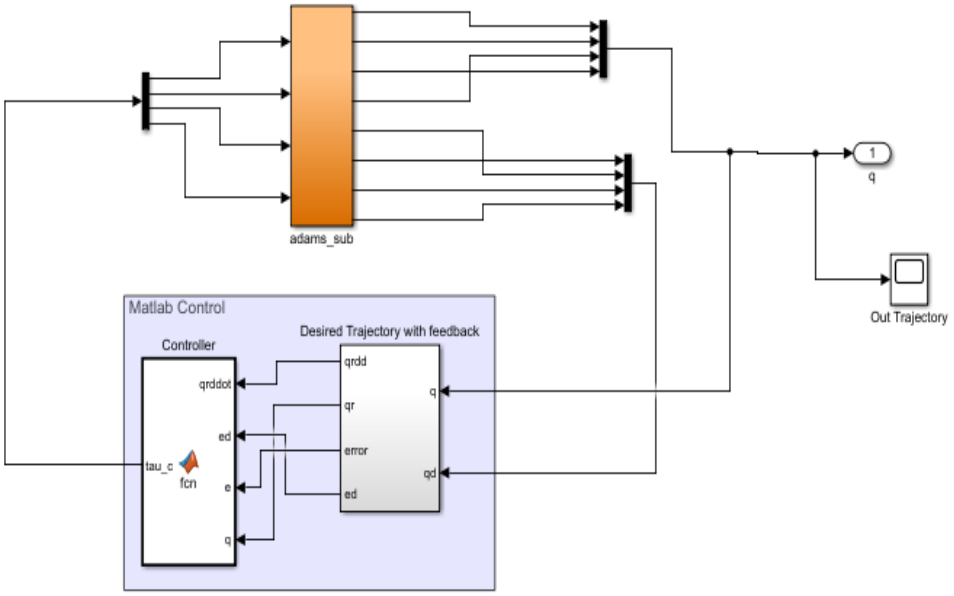

Figure 6.11: Co-simulation experiment of ALSR in Matlab/ADAMS interface

The MSC ADAMS interface projected while performing interactive ADAMS/MATLAB co-simulation can be seen in Figure 6.12. The upper left corner of Figure 6.12 represents the zoom view of needle tissue interaction while performing the suturing task.

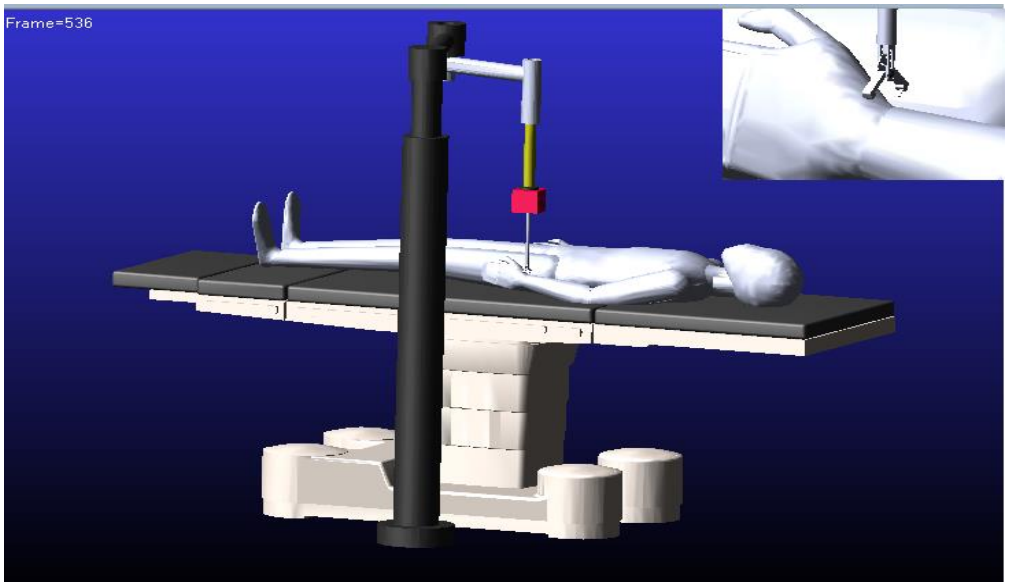

Figure 6.12: Co-simulation experiment of ALSR invoking ADAMS platform through MATLAB shows the suturing operation

The task-specific joint angle movements were computed. The joint angle movements of ALSR were given to the desired trajectory for the DOB assisted control. DOB assisted CTC control was implemented in order to perform joint position tracking to fulfill the suturing task. Figure 6.13 shows the accurate tracking of the desired joint position by the DOB-assisted CTC control.

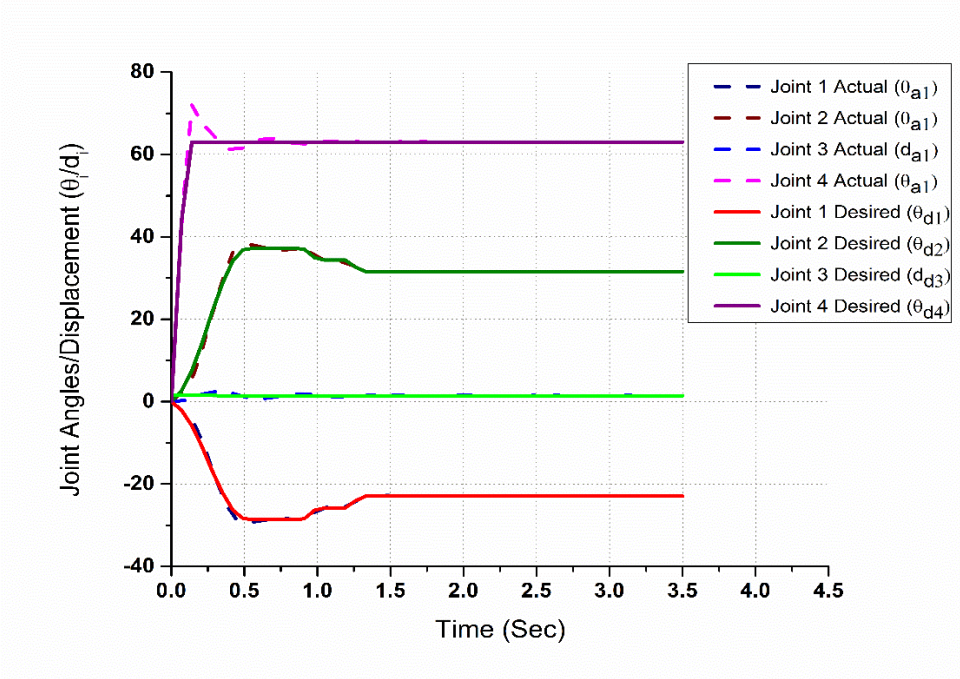

Figure 6.13: Suturing task-specific joint angle position tracing by ALSR

The hardware construction of the ALSR prototype model has been developed and can be seen in Figure 6.14. At each revolute joint the digital encoder to attached to calibrate the joint position. Joint 1 and joint 2 of the ALSR provide the maximum and minimum reach position of ALSR in the X-axis and Y-axis. Joint 3 is a linearly actuated joint that helps to reach out to the position of the phantom in the Z-axis. The orientation of the tool is positioned using the revolute joint 4. The actuator box attached to joint 4 consists of a camera to detect the skin phantom and actuators to provide the end-effector needle motion to perform suturing. The hardware in-loop is used to perform Antebrachium laceration suturing.

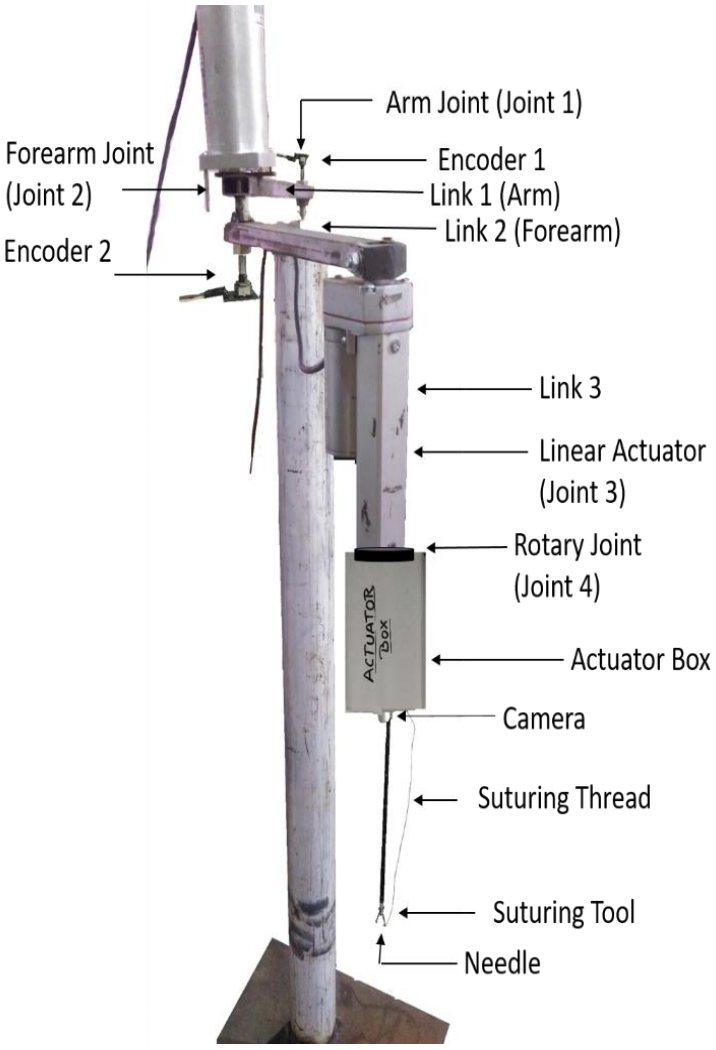

Figure 6.14: Hardware model of ALSR

The skin phantom is used as a dummy model to perform the complex suturing task. The skin phantom depicts the ex-vivo Antebrachium laceration. The complex suturing task was performed by the end effector of ALSR can be seen in Figure 6.15. The length of cut on skin phantom is 5 cm and the points of insertion were computed through an interactive image segmentation technique. The shuttling of the needle has taken a primary task to perform suturing.

Figure 6.15: Sutured skin phantom

The estimated contact force at the end effector were calibrated using a strain gauge experiment on Scientech kit can be seen in Figure 6.16. The calibration of the strain gauge is done by excluding the weight of the phantom. The estimated change in weight is used to calibrate the force acting on the end effector while performing the suturing task. The calibrated force acting on the end effector can be seen in Figure 6.17.

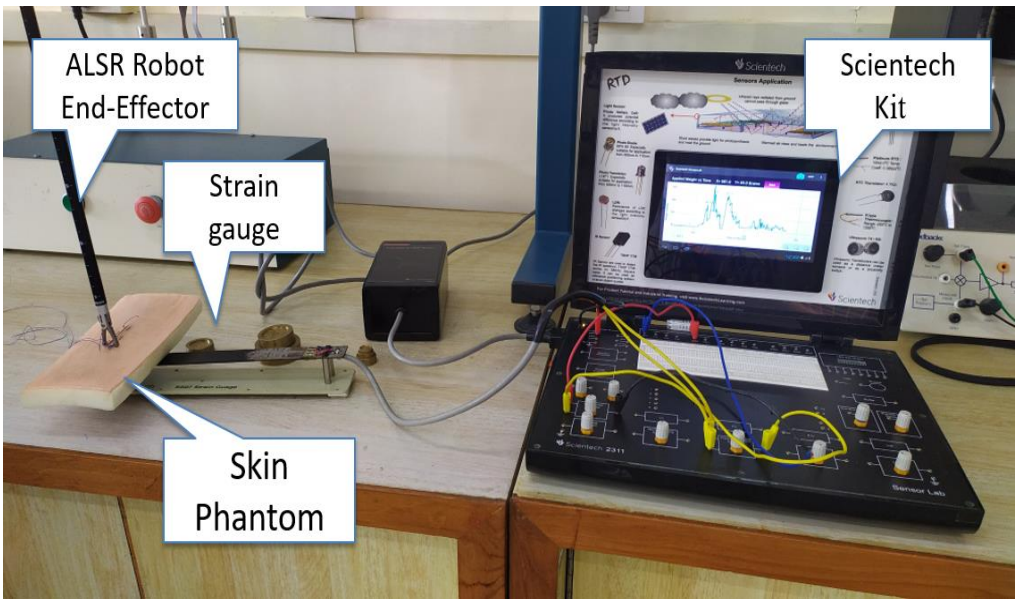

Figure 6.16: Interaction force estimation setup

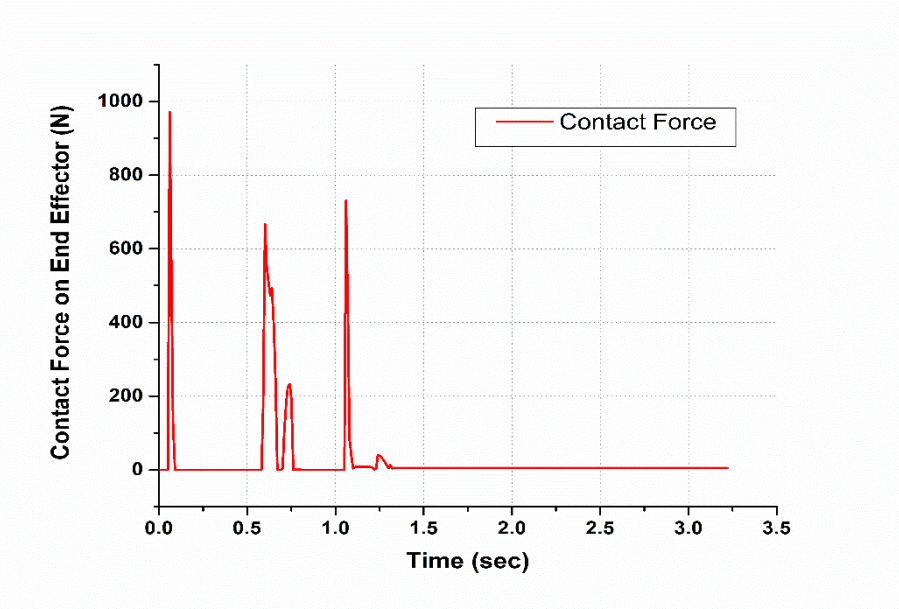

Figure 6.17: Contact force on end effector

The needle displacement in the workspace were monitored and represented in Figure 6.18. The needle shuttling and depth of needle penetration were estimated by co-simulation modeling and validated on hardware.

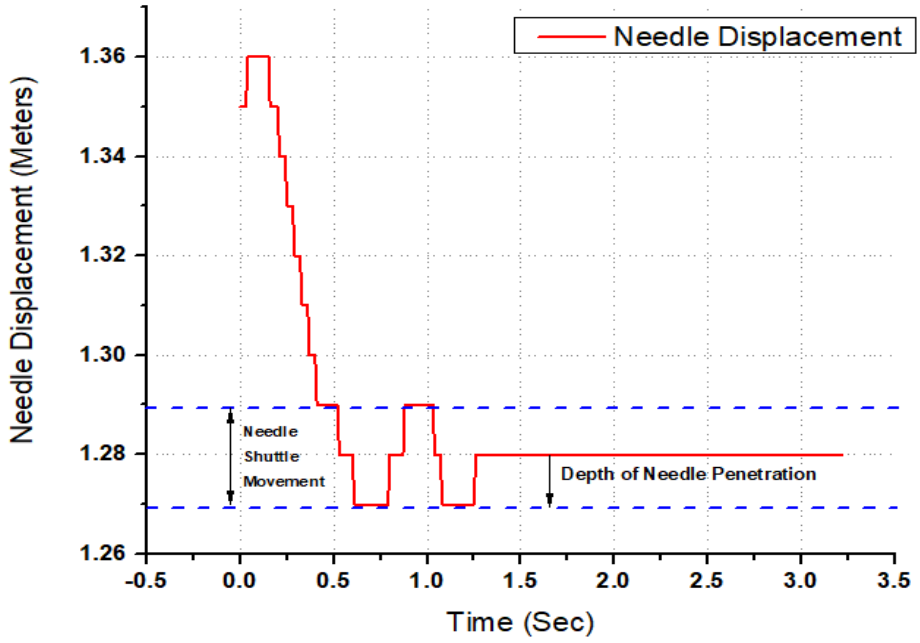

Figure 6.18: ALSR suture needle displacement in the workspace

6.8 SAFETY ASPECTS

The factor of safety plays a crucial role in the healthcare domain. To ensure safe human-robot interaction, the different factors play a key role. In skin laceration detection, the interactive image segmentation technique has been used to ensure correct segmentation and waypoints extraction. While performing suturing task some tangible and nontangible interrupts can occurs. Tangible interrupts can be an undesirable presence of any physical object or person in the robot workspace where emergence stop has been introduced in the system. Whereas nontangible interrupts include the robot's internal disturbance and environmental factors. These interrupts directly affect the torque acting at the joints of the robot. To ensure the safety of the proposed ALSR system, the disturbance acting on the system needs to be compensated. Therefore, the Disturbance observer-based control (DOB) has been used in the system. The internal and external disturbances acted on the ALSR were modelled. DOB estimates the state of the system to achieve the desired trajectory tracking by compensating disturbances. This makes the system more robust to disturbances and ensure safe human robot interaction.

6.9 SUMMARY

The chapter presented the comparative study of CTC control with different gain values and tunned PD and PID controller with the best gain valued CTC controller. To compensate for the disturbances, the nonlinear disturbance observer is used to stabilized the trajectory tracking of ALSR. The application of this scheme is to test the RRPR surgical robotic manipulator with the end tool as a suturing tool. The computation of external disturbances affecting the system for the surgical task. The laceration tracking operation was done successfully in order to assist the surgeon to perform the suturing task. The obtained results illustrate the feasibility of the DOB control in the suturing application.

CHAPTER 7 CONCLUSION AND FUTURE SCOPE

The research work focuses on the design and analysis of a novel robot the Antebracium Laceration Suturing Robot (ALSR). The design of ALSR is developed in Solidworks software. The kinematic and dynamic mathematical modeling of ALSR is illustrated in chapter 4. The implementation of mathematical modeling is performed in the simulation platforms. The kinematic modeling is computed by the analytical method using D-H notations. The dynamic modeling of the robot is computed using Newton Euler Method. In order to test the system modeling, which is a surgical robot the need for high performance, precise, robust, and speedy control, therefore, the three feedback loop controllers i.e., CTC, PD and PID. The CTC control technique is illustrated and implemented with different Proportional Gain (Kp) and Derivative Gain (Kd) using the trial and error method. The best-suited CTC with its gain values is further compared with best-tuned gains of PD and PID controller in order to have a performance comparison of the different implemented controllers. The research proves that CTC with the optimized value of Kp and Kd is successfully proven to be having the least amount of RMS error 0.1003.

The nonlinear disturbance observer to stabilized trajectory tracking for surgical robotic application. The computation of external disturbances affecting the system for the surgical task. The laceration tracking operation was done successfully in order to assist the surgeon to perform the suturing task. The obtained results illustrate the feasibility of the DOB control in the application surgical task. The virtual simulation of robot is done through the MSC ADAMS software in order to validate the estimate the performance of trajectory tracking control.

7.1 CONTRIBUTION

1. The derivation of the generic mathematical modeling technique is illustrated in chapter 1. This helps in the development of mathematical modeling of the novel model by any novice researcher. The generic

mathematical modeling techniques include GKM, GDM, and GSA which can be used for obtaining Kinematic and Dynamic Equations of n-DOF serial manipulator.

2. The Significant contribution of this research is to design the novel Antebrachium laceration suturing robot for the application of Ex-vivo suturing. This will reduce operating time, less blood loss, early recovery, no human tremors, and can perform precise micromotion.
3. An insight into the significance and challenges in the skin laceration segmentation. The interactive selection of ROI is used for accurate skin segmentation. To estimate the precise task space coordinate of Antebrachium laceration, the different skin segmentation techniques were compared at different tolerance values the best of which is used for coordinate extraction.
4. To compensate, the joint disturbances caused due to internal and external factors the proposed disturbance observer is developed. This dynamic observer accurately estimates the joints torque of ALSR. This can also be used as a sensor less joint estimation.
5. The Simulation environment helps in analyzing the feasibility test at a low cost. The virtual simulation allows the testing of control algorithms. Dynamic Virtual Simulation of ALSR helps in estimating the joint torque, needle tissue interaction forces, etc of ALSR while performing suturing operation.

7.2 FUTURE WORK

The skin phantom is taken as the object of interest which is static in nature. The dynamic model or living model can be used for further studies. This research is focused on ex-vivo antebrachium laceration. To enhance the scope of this research the in-vivo flexible arm manipulator can be used with the spherical workspace. The use of the RRPR manipulator as a base robot is applicable for cylindrical workspace. The design of a model can further be improved for advanced applications. The advanced learning based control technique can be

implemented for skin segmentation and tracking of skin laceration. The skin phantom laceration is considered in a straight line. The complex and irregular shaped laceration can also be considered for further studies.

REFERENCES

[1] B. Dunkin, G. L. Adrales, K. Apelgren, and J. D. Mellinger, “Surgical simulation: A current review,” *Surg. Endosc. Other Interv. Tech.*, vol. 21, no. 3, pp. 357–366, 2007, doi: 10.1007/s00464-006-9072-0.

[2] F. Nageotte, P. Zanne, C. Doignon, and M. de Mathelin, “Stitching planning in laparoscopic surgery: Towards robot-assisted suturing,” *Int. J. Rob. Res.*, vol. 28, no. 10, pp. 1303–1321, 2009, doi: 10.1177/0278364909101786.

[3] M. A. Liss and E. M. Mcdougall, “Robotic surgical simulation,” *Cancer J.*, vol. 19, no. 2, pp. 124–129, 2013.

[4] H. W. R. Schreuder, R. Wolswijk, R. P. Zweemer, M. P. Schijven, and R. H. M. Verheijen, “Training and learning robotic surgery, time for a more structured approach: A systematic review,” *BJOG An Int. J. Obstet. Gynaecol.*, vol. 119, no. 2, pp. 137–149, 2012, doi: 10.1111/j.1471-0528.2011.03139.x.

[5] S. Kumar, P. Singhal, and V. N. Krovi, “Computer-Vision-Based Decision Support in Surgical Robotics,” *IEEE Des. Test*, vol. 32, no. 5, pp. 89–97, Oct. 2015, doi: 10.1109/MDAT.2015.2465135.

[6] M. Baumann, S. Léonard, E. A. Croft, and J. J. Little, “Path planning for improved visibility using a probabilistic road map,” *IEEE Trans. Robot.*, vol. 26, pp. 195–200, 2010, doi: 10.1109/TRO.2009.2035745.

[7] W. S. Newman, D. Chow, W. Newman, and S. Member, “Improved Knot-Tying Methods for Autonomous Robot Surgery Improved Knot-Tying Methods for Autonomous Robot Surgery,” in *IEEE International Conference on Automation Science and Engineering (CASE)*, 2013, no. August 2013, pp. 467–471, doi: 10.1109/CoASE.2013.6653955.

[8] R. A. Beasley, “Medical Robots : Current Systems and Research Directions,” *J. Robot.*, vol. 2012, pp. 14–32, 2012, doi: 10.1155/2012/401613.

[9] D. Araiza-illan, D. Western, A. G. Pipe, and K. Eder, “Systematic and Realistic Testing in Simulation of Control Code for Robots in Collaborative Human-Robot Interactions,” *Towar. Auton. Robot. Syst.*, vol. 9716, pp. 20–31, 2016.

[10] S. Guo, Q. Chen, N. Xiao, and Y. Wang, “A Fuzzy PID Control Algorithm for The Interventional Surgical Robot with Guide Wire Feedback Force,” in *International Conference on Mechatronics and Automation*, 2016, pp. 426–430.

[11] Varnita Verma, Roushan Kumar, and Vivek Kaundal, “Implementation of Ladder Logic for

Control of Pipeline Inspection Robot Using PLC," in *Advances in Intelligent Systems and Computing*, 2017, vol. 479, pp. 965–971, doi: 10.1007/978-981-10-1708-7_113.

[12] T. Miguel, S. Salgueiro, and E. Committee, "Robot assisted needle interventions for brain surgery Tiago Miguel Sousa Salgueiro Thesis to obtain the Master of Science Degree in Biomedical Engineering," 2014.

[13] X. Jin *et al.*, "Human movement training with a cable driven ARm EXoskeleton (CAREX) Supraspinal mobility control in people with multiple sclerosis View project Perturbation-based Balance Training View project Human Movement Training with a Cable Driven ARm EXoskeleton (CAREX)," 2014, doi: 10.1109/TNSRE.2014.2329018.

[14] A. Gupta, A. K. Mondal, and M. K. Gupta, "Kinematic, Dynamic Analysis and Control of 3 DOF Upper-limb Robotic Exoskeleton," *J. Eur. des Systèmes Autom.*, vol. 52, no. 3, pp. 297–304, Aug. 2019, doi: 10.18280/jesa.520311.

[15] A. Okamura, M. Mataric, and H. Christensen, "Medical and Health-Care Robotics," *IEEE Robot. Autom. Mag.*, vol. 17, no. 3, pp. 26–37, Sep. 2010, doi: 10.1109/MRA.2010.937861.

[16] T. Autonomous, "The Autonomous Mobile Robot SENARIO: A Sensor-Aided Intelligent Navigation system for Powered wheelchairs," *IEEE Robot. Autom. Mag.*, vol. 4, no. 4, pp. 60–70, 1997.

[17] G. Bourhis and Y. Agostini, "The Vahm Robotized Wheelchair : System Architecture and Human-Machine Interaction," *J. Intell. Robot. Syst.*, vol. 22, pp. 39–50, 1998.

[18] H. A. Yanco, "Wheelesley: A robotic wheelchair system: Indoor navigation and user interface," in *Assistive Technology and Artificial Intelligence*, Berlin/Heidelberg: Springer-Verlag, 1998, pp. 256–268.

[19] A. Lankenau and T. Rofer, "Mobile robot self-localization in large-scale environments," in *Proceedings 2002 IEEE International Conference on Robotics and Automation (Cat. No.02CH37292)*, 2002, vol. 2, no. May, pp. 1359–1364, doi: 10.1109/ROBOT.2002.1014732.

[20] S. P. Levine *et al.*, "The NavChair Assistive Wheelchair Navigation System," *IEEE Trans. Rehabil. Eng.*, vol. 7, no. 4, pp. 443–451, 1999.

[21] T. Iwase, R. Zhang, and Y. Kuno, "Robotic Wheelchair Moving with the Caregiver," in *2006 SICE-ICASE International Joint Conference*, 2006, pp. 238–243, doi: 10.1109/SICE.2006.315614.

[22] L. Y. Deng, C.-L. Hsu, T.-C. Lin, J.-S. Tuan, and S.-M. Chang, "EOG-based Human–Computer Interface system development," *Expert Syst. Appl.*, vol. 37, no. 4, pp. 3337–3343, Apr. 2010, doi: 10.1016/J.ESWA.2009.10.017.

[23] R. Barea, L. Boquete, M. Mazo, and E. López, "Wheelchair Guidance Strategies Using EOG,"

J. Intell. Robot. Syst., vol. 34, no. 3, pp. 279–299, 2002, doi: 10.1023/A:1016359503796.

[24] M. Razali, Y. Kobayashi, and Y. Kuno, “Development of Smart Wheelchair System for a User with Severe Motor Impairment,” *Procedia Eng.*, vol. 41, pp. 538–546, 2012, doi: 10.1016/j.proeng.2012.07.209.

[25] A. Halawani, H. Li, and A. Anani, “Active vision for controlling an electric wheelchair,” *Intell. Serv. Robot.*, vol. 5, no. 2, pp. 89–98, 2012, doi: 10.1007/s11370-011-0098-3.

[26] A. C. Lopes, G. Pires, and U. Nunes, “Assisted navigation for a brain-actuated intelligent wheelchair,” *Rob. Auton. Syst.*, vol. 61, no. 3, pp. 245–258, 2013, doi: 10.1016/j.robot.2012.11.002.

[27] X. Perrin, R. Chavarriaga, F. Colas, R. Siegwart, and R. Millán, “Brain-coupled interaction for semi-autonomous navigation of an assistive robot,” *Rob. Auton. Syst.*, vol. 58, no. 12, pp. 1246–1255, 2010, doi: 10.1016/j.robot.2010.05.010.

[28] H. M. Le, T. N. Do, and S. J. Phee, “A survey on actuators-driven surgical robots,” *Sensors Actuators A Phys.*, vol. 247, pp. 323–354, Aug. 2016, doi: 10.1016/j.sna.2016.06.010.

[29] T. Mukai, S. Hirano, H. Nakashima, Y. Sakaida, and S. Guo, “Realization and Safety Measures of Patient Transfer by Nursing-Care Assistant Robot RIBA with Tactile Sensors,” *J. Robot. Mechatronics*, vol. 23, no. 3, pp. 360–369, 2011.

[30] K. P. Zeungnam *et al.*, “Robotic smart house to assist people with movement disabilities,” *Auton. Robots*, vol. 22, no. 2, pp. 183–198, 2007, doi: 10.1007/s10514-006-9012-9.

[31] J. Jung, J. Do, Y. Kim, K. Suh, D. Kim, and Z. Z. Bien, “Advanced Robotic Residence for the Elderly / the Handicapped : Realization and User Evaluation,” in *Intelligent Service Robotics*, 2005, pp. 492–495.

[32] P. Taylor, R. Bostelman, and J. Albus, “Robotic Patient Transfer and Rehabilitation Device for Patient Care Facilities or the Home Patient Care Facilities or the Home,” *Adv. Robot.*, vol. 22, no. 12, pp. 1287–1307, 2008, doi: 10.1163/156855308X344837.

[33] R. Bostelman and J. Albus, “A Multipurpose Robotic Wheelchair and Rehabilitation Device for the Home,” in *Intelligent Robots and Systems*, 2007, pp. 3348–3353.

[34] R. Bostelman and J. Albus, “Robotic Patient Lift and Transfer,” in *Service Robot Applications2*, 2008, pp. 1–22.

[35] R. Bostelman and J. Albus, “Sensor experiments to facilitate robot use in assistive environments,” in *Proceedings of the 1st ACM international conference on PErvasive Technologies Related to Assistive Environments - PETRA ’08*, 2008, p. 1, doi: 10.1145/1389586.1389596.

[36] T. Heikkilä, M. Järviluoma, and T. Juntunen, “Holonic control for manufacturing systems: Functional design of a manufacturing robot cell,” *Integr. Comput. Aided. Eng.*, vol. 4, no. 3, pp. 202–218, Jan. 1997, doi: 10.3233/ica-1997-4305.

[37] H. Yamada, T. Xinxing, N. Tao, Z. Dingxuan, and A. A. Yusof, “Tele-operation Construction Robot Control System with Virtual Reality,” *IFAC Proc. Vol.*, vol. 42, no. 16, pp. 639–644, 2009, doi: 10.3182/20090909-4-JP-2010.00108.

[38] D. Zhao, H. Yamada, T. Muto, H. Huang, W. Gong, and Y. Xia, “6 DOF Presentaion of Realistic Motion in Operating a Construction Tele-Robot System,” *Proc. JFPS Int. Symp. Fluid Power*, vol. 2002, no. 5–2, pp. 507–512, 2002, doi: 10.5739/isfp.2002.507.

[39] D. Kwon, K. Y. Woo, S. K. Song, S. Kim, and H. S. Cho, “Microsurgical Telerobot System a,” in *Intelligent Robots and Systems*, 1998, no. October, pp. 945–950.

[40] T. Geerinck, E. Colon, S. A. Berrabah, K. Cauwerts, and H. Sahli, “Tele-robot with shared autonomy: Distributed navigation development framework,” *Integr. Comput. Aided. Eng.*, vol. 13, no. 4, pp. 329–345, Sep. 2006, doi: 10.3233/ICA-2006-13403.

[41] R. H. Taylor *et al.*, “Computer-integrated revision total hip replacement surgery : concept and preliminary results,” *Med. Image Anal.*, vol. 3, no. 3, pp. 301–319, 1999.

[42] A. Arezzo, F. Ulmer, O. Weiss, M. O. Schurr, M. Hamad, and G. F. Buess, “Experimental trial on solo surgery for minimally invasive therapy,” *Surg. Endosc.*, vol. 14, no. 10, pp. 955–959, Oct. 2000, doi: 10.1007/s004640000106.

[43] Y. Yavuz, B. Ystgaard, E. Skogvoll, and R. Mårvik, “A Comparative Experimental Study Evaluating the Performance of Surgical Robots Aesop and Endosista,” *Surg. Laparosc. Endosc. Percutan. Tech.*, vol. 10, no. 3, pp. 163–167, 2000.

[44] S. Sen, A. Garg, D. V. Gealy, S. McKinley, Y. Jen, and K. Goldberg, “Automating multi-throw multilateral surgical suturing with a mechanical needle guide and sequential convex optimization,” in *2016 IEEE International Conference on Robotics and Automation (ICRA)*, May 2016, vol. 2016-June, pp. 4178–4185, doi: 10.1109/ICRA.2016.7487611.

[45] R. Autorino *et al.*, “Current Status and Future Directions of Robotic Single-Site Surgery: A Systematic Review,” *Eur. Urol.*, vol. 63, no. 2, pp. 266–280, Feb. 2013, doi: 10.1016/j.eururo.2012.08.028.

[46] G. T. Sung and I. S. Gill, “Robotic laparoscopic surgery: A comparison of the da Vinci and Zeus systems,” *Urology*, 2001, doi: 10.1016/S0090-4295(01)01423-6.

[47] J. E. Anderson, D. C. Chang, J. K. Parsons, and M. A. Talamini, “The First National Examination of Outcomes and Trends in Robotic Surgery in the United States,” *J. Am. Coll. Surg.*, vol. 215, no. 1, pp. 107–114, 2012, doi: 10.1016/j.jamcollsurg.2012.02.005.

[48] N. E. W. Engla and N. D. Journal, “New technology and health care costs—the case of robot-assisted surgery,” *N. Engl. J. Med.*, vol. 363, no. 8, pp. 701–704, 2010.

[49] V. Falk, A. Diegler, T. Walther, R. Autschbach, and F. W. Mohr, “Developments in robotic cardiac surgery,” *Coron. artery Surg.*, pp. 378–387, 2000.

[50] U. Kappert *et al.*, “Robotic-Enhanced Dresden Technique for Minimally Invasive Bilateral Internal Mammary Artery Grafting,” *Heart Surg. Forum*, vol. 3, no. 4, pp. 319–321, 2000.

[51] M. O. Schurr, G. Buess, B. Neisius, and U. Voges, “New technology Robotics and telemanipulation technologies for endoscopic surgery A review of the ARTEMIS project,” *Surg. Endosc. Ultrasound Other Interv. Tech.*, vol. 14, pp. 375–381, 2000, doi: 10.1007/s004640020067.

[52] G. B. Cadi *et al.*, “Evaluation of telesurgical (robotic) NISSEN fundoplication,” *Surg. Endosc. Ultrasound Other Interv. Tech.*, vol. 15, pp. 918–923, 2001, doi: 10.1007/s004640000217.

[53] B. Kiaii *et al.*, “Robot-Assisted Computer Enhanced Closed-Chest Coronary Surgery : Preliminary Experience Using a Harmonic Scalpel ® and ZEUS ™,” *Hear. Surg. Forum.*, vol. 3, no. 3, pp. 194–197, 2000.

[54] J. Rosen, J. D. Brown, L. Chang, M. N. Sinanan, and B. Hannaford, “Generalized Approach for Modeling Minimally Invasive Surgery as a Stochastic Process Using a Discrete Markov Model,” *IEEE Trans. Biomed. Eng.*, vol. 53, no. 3, pp. 399–413, Mar. 2006, doi: 10.1109/TBME.2005.869771.

[55] L. K. Jacobs, V. Shayani, and J. M. Sackier, “Determination of the learning curve of the AESOP robot,” *Surg Endosc*, vol. 11, pp. 54–55, 1997.

[56] M. E. Allaf *et al.*, “Laparoscopic visual field,” *Surg. Endosc.*, vol. 12, no. 12, pp. 1415–1418, Dec. 1998, doi: 10.1007/s004649900871.

[57] K. Omote, H. Feussner, A. Ungeheuer, K. Arbter, G. Wei, and J. Ru, “Self-Guided Robotic Camera Control for Laparoscopic Surgery Compared with human camera control,” *Am. J. Surg.*, vol. 177, no. 4, pp. 321–324, 1999.

[58] M. O. Schurr, A. Arezzo, and G. F. Buess, “Robotics and systems technology for advanced endoscopic procedures : experiences in general surgery q,” *Eur. J. Cardio-Thoracic Surg.*, vol. 16, no. Supplement_2), pp. S97–S105, 1999.

[59] D. H. Birkett, “Electromechanical instruments for endoscopic surgery,” *Minim. Invasive Ther. Allied Technol.*, vol. 10, no. 6, pp. 271–274, 2001, doi: 10.1080/136457001753337302.

[60] D. T. Jens J. Rassweiler, “The Advances in Laparoscopic Surgery in Urology,” *Nat. Rev.*, vol. 52, no. 2, pp. 95–105, 2016, doi: 10.1038/nrurol.2016.70.

[61] S. Palmisano, M. Giuricin, P. Makovac, B. Casagranda, and G. Piccinni, “Totally hand-sewn anastomosis using barbed suture device during laparoscopic gastric bypass in obese . A feasibility study and preliminary results,” *Int. J. Surg.*, vol. 12, pp. 1385–1389, 2014, doi: 10.1016/j.ijsu.2014.10.030.

[62] A. Carter and C. J. Skilbeck, “Sutures, ligatures and knots,” *Surg. (United Kingdom)*, 2014, doi: 10.1016/j.mpsur.2013.12.016.

[63] S. K. Saha and W. O. Schiehlen, “Recursive kinematics and dynamics for parallel structure closed-loop multibody systems,” *Mech. Struct. Mach.*, vol. 29, no. 2, pp. 143–175, Aug. 2001, doi: 10.1081/SME-100104478.

[64] N. T. Nguyen *et al.*, “Laparoscopic Suturing Evaluation among Surgical Residents,” vol. 136, pp. 133–136, 2000, doi: 10.1006/jsre.2000.5969.

[65] T. Göpel, F. Härtl, A. Schneider, M. Buss, and H. Feussner, “Automation of a suturing device for minimally invasive surgery,” *Surg. Endosc.*, vol. 25, no. 7, pp. 2100–2104, Jul. 2011, doi: 10.1007/s00464-010-1532-x.

[66] A. Talasaz, A. L. Trejos, and R. V Patel, “Effect of force feedback on performance of robotics-assisted suturing,” in *2012 4th IEEE RAS & EMBS International Conference on Biomedical Robotics and Biomechatronics (BioRob)*, Jun. 2012, pp. 823–828, doi: 10.1109/BioRob.2012.6290910.

[67] E. H. Murai, S. Homer-Vanniasinkam, P. G. Silveira, J. S. Dai, D. Martins, and H. A. Wurdemann, “Towards a Modular Suturing Catheter for Minimally Invasive Vascular Surgery,” *Proc. - IEEE Int. Conf. Robot. Autom.*, pp. 44–49, 2018, doi: 10.1109/ICRA.2018.8460823.

[68] J. Joseph, Y. Leung, L. Eichel, K. Scheidweiler, E. Erturk, and R. Wood, “Comparison of the Ti-knot Device and Hem-o-lok Clips with Other Devices Commonly Used for Laparoscopic Renal-Artery Ligation,” *J. Endourol.*, vol. 18, no. 2, pp. 163–166, Mar. 2004, doi: 10.1089/089277904322959806.

[69] P. W. Y. Chiu, S. J. P. Z. Wang, Z. S. Carmen, and C. P. T. Yamamoto, “Feasibility of full-thickness gastric resection using master and slave transluminal endoscopic robot and closure by overstitch : a preclinical study,” *Surg Endosc*, pp. 319–324, 2014, doi: 10.1007/s00464-013-3149-3.

[70] S. Leonard, K. L. Wu, Y. Kim, A. Krieger, and P. C. W. Kim, “Smart tissue anastomosis robot (STAR): A vision-guided robotics system for laparoscopic suturing,” *IEEE Trans. Biomed. Eng.*, vol. 61, no. 4, pp. 1305–1317, 2014, doi: 10.1109/TBME.2014.2302385.

[71] B. Roth, F. D. Birkhäuser, G. N. Thalmann, and P. Zehnder, “Novel prototype sewing device , EndoSew ® , for minimally invasive surgery : an extracorporeal ileal conduit construction pilot study in 10 patients,” pp. 959–964, 2013, doi: 10.1111/j.1464-410X.2012.11599.x.

[72] A. Talasaz, A. L. Trejos, and R. V Patel, “The Role of Direct and Visual Force Feedback in Suturing Using a 7-DOF Dual-Arm Teleoperated System,” *IEEE Trans. Haptics*, vol. 10, no. 2, pp. 276–287, Apr. 2017, doi: 10.1109/TOH.2016.2616874.

[73] S. Perreault, A. Talasaz, A. L. Trejos, C. D. W. Ward, R. V. Patel, and B. Kiaii, “A 7-DOF haptics-enabled teleoperated robotic system: Kinematic modeling and experimental verification,” in *2010 3rd IEEE RAS & EMBS International Conference on Biomedical Robotics and Biomechatronics*, Sep. 2010, pp. 906–911, doi: 10.1109/BIOROB.2010.5625949.

[74] S. Leonard, A. Shademan, Y. Kim, A. Krieger, and P. C. W. Kim, “Smart Tissue Anastomosis Robot (STAR): Accuracy evaluation for supervisory suturing using near-infrared fluorescent markers,” in *Proceedings - IEEE International Conference on Robotics and Automation*, 2014, pp. 1889–1894, doi: 10.1109/ICRA.2014.6907108.

[75] D. B. Camarillo, T. M. Krummel, and J. K. Salisbury, “Robotic Technology in Surgery : Past , Present and Future,” 2016.

[76] R. H. Taylor and D. Stoianovici, “Medical Robotics in Computer-Integrated Surgery,” vol. 19, no. 5, pp. 765–781, 2003.

[77] V. Verma *et al.*, “IoT and Robotics in Healthcare,” in *Medical Big Data and Internet of Medical Things*, Boca Raton : Taylor & Francis, [2019]: CRC Press, 2018, pp. 245–269.

[78] A. M. Djuric, R. Al Saidi, and W. ElMaraghy, “Global Kinematic Model generation for n-DOF reconfigurable machinery structure,” in *2010 IEEE International Conference on Automation Science and Engineering*, Aug. 2010, pp. 804–809, doi: 10.1109/COASE.2010.5584632.

[79] R. Al Saidi and B. Minaker, “Analysis and Development of Self-Reconfigurable Open Kinematic Machinery Systems,” in *IEEE International Conference on Automation Science and Engineering (CASE)*, 2013, pp. 966–971.

[80] J. Dempster, T. Dempsey, W. Nh, J. Dempster, and H. Ns, “Laparoscopic Entry : A Review of Techniques , Technologies , and Complications,” *J. Obstet. Gynaecol. Canada*, vol. 29, no. 5, pp. 433–447, 2007, doi: 10.1016/S1701-2163(16)35496-2.

[81] M. T. Das and L. C. Dülger, “Mathematical modelling, simulation and experimental verification of a scara robot,” *Simul. Model. Pract. Theory*, vol. 13, no. 3, pp. 257–271, 2005, doi: 10.1016/j.simpat.2004.11.004.

[82] Akash Gupta, Varnita Verma, Adesh Kumar, Paawan Sharma, M. K. Gupta, and C. S. Meera, “Stabilization of Underactuated Mechanical System Using LQR Technique,” in *Advances in Intelligent Systems and Computing*, vol. 479, 2017, pp. 601–608.

[83] A. Mohan and S. K. Saha, “A recursive, numerically stable, and efficient simulation algorithm for serial robots,” *Multibody Syst. Dyn.*, vol. 17, no. 1, pp. 291–319, 2007, doi: 10.1007/s11044-

008-9122-6.

[84] A. Mohan and S. K. Saha, *A recursive, numerically stable, and efficient simulation algorithm for serial robots with flexible links*, vol. 21, no. 1. 2009.

[85] P. I. Corke, “A symbolic and numeric procedure for manipulator rigid-body dynamic significance analysis and simplification,” *Robotica*, vol. 16, no. 5, pp. 589–594, 1998, doi: 10.1017/s0263574798000769.

[86] M. S. ju and J. M. Mansour, “Comparison of Methods for Developing the Dynamics of Rigid-Body Systems,” *Int. J. Rob. Res.*, vol. 8, no. 6, pp. 19–27, 1989, doi: 10.1177/027836498900800602.

[87] J. M. Hollerbach, “A Recursive Lagrangian Formulation of Maniputator Dynamics and a Comparative Study of Dynamics Formulation Complexity,” *IEEE Trans. Syst. Man. Cybern.*, vol. SMC-10, no. 11, pp. 730–736, 1980, doi: 10.1109/TSMC.1980.4308393.

[88] R. Featherstone and D. Orin, “Robot Dynamics : Equations and Algorithms Foundational Work in Robot Dy,” *Tensor*, vol. 1, no. April, pp. 826–834, 2000, doi: 10.1109/ROBOT.2000.844153.

[89] M. Afrough and A. A. Hanieh, “Identification of Dynamic Parameters and Friction Coefficients: of a Robot with Planar Serial Kinemtic Linkage,” *J. Intell. Robot. Syst. Theory Appl.*, vol. 94, no. 1, pp. 3–13, Apr. 2019, doi: 10.1007/s10846-018-0778-8.

[90] A. Akbarzadeh and J. Enferadi, “A virtual work based algorithm for solving direct dynamics problem of a 3-RRP spherical parallel manipulator,” *J. Intell. Robot. Syst. Theory Appl.*, vol. 63, no. 1, pp. 25–49, Jul. 2011, doi: 10.1007/s10846-010-9469-9.

[91] D. M. Katić, A. D. Rodić, and M. K. Vukobratović, “Hybrid dynamic control algorithm for humanoid robots based on reinforcement learning,” *J. Intell. Robot. Syst. Theory Appl.*, vol. 51, no. 1, pp. 3–30, Jan. 2008, doi: 10.1007/s10846-007-9174-5.

[92] S. K. Saha and W. O. Schiehlen, “Recursive kinematics and dynamics for parallel structure closed-loop multibody systems,” *Mech. Struct. Mach.*, vol. 29, no. 2, pp. 143–175, Aug. 2001, doi: 10.1081/SME-100104478.

[93] M. S. Tsai and W. H. Yuan, “Dynamic modeling and decentralized control of a 3 PRS parallel mechanism based on constrained robotic analysis,” *J. Intell. Robot. Syst. Theory Appl.*, vol. 63, no. 3–4, pp. 525–545, Sep. 2011, doi: 10.1007/s10846-010-9526-4.

[94] A. Djuric, R. Al Saidi, and W. Elmaraghy, “Dynamics solution of n -DOF global machinery model,” *Robot. Comput. Integr. Manuf.*, vol. 28, no. 5, pp. 621–630, 2012, doi: 10.1016/j.rcim.2012.02.011.

[95] L. Kelmar and P. . Khosla, “Automatic Generation of Forward and Inverse Kinematics for a Reconfig ura ble Modular Manipulator System,” *J. Robot. Syst.*, vol. 7, no. 4, pp. 599–619,

1990.

[96] P. K. Khosla and S. Diego, “Automatic generation of kinematics for a reconfigurable modular manipulator system,” in *IEEE International Conference on Robotics and Automation*, 2014, no. May 1988, pp. 663–668, doi: 10.1109/ROBOT.1988.12135.

[97] L. T. Wang and B. Ravani, “Recursive Computations of Kinematic and Dynamic Equations For Mechanical Manipulators,” *IEEE J. Robot. Autom.*, vol. 1, no. 3, pp. 124–131, 1985, doi: 10.1109/JRA.1985.1087016.

[98] J. J. Craig, P. Prentice, and P. P. Hall, *Introduction to Robotics Mechanics and Control Third Edition*. 2005.

[99] S. Guo, Q. Chen, N. Xiao, and Y. Wang, “A Fuzzy PID Control Algorithm for The Interventional Surgical Robot with Guide Wire Feedback Force,” pp. 426–430, 2016.

[100] S. Yamacli and H. Canbolat, “Simulation of a SCARA robot with PD and learning controllers,” *Simul. Model. Pract. Theory*, vol. 16, no. 9, pp. 1477–1487, 2008, doi: 10.1016/j.simpat.2008.08.004.

[101] F. Piltan, A. Taghizadegan, and N. B. Sulaiman, “Modeling and Control of Four Degrees of Freedom Surgical Robot Manipulator Using MATLAB/SIMULINK,” *Int. J. Hybrid Inf. Technol.*, vol. 8, no. 11, pp. 47–78, 2015, doi: 10.14257/ijhit.2015.8.11.05.

[102] T. M. Guess and L. P. Maletsky, “Computational modelling of a total knee prosthetic loaded in a dynamic knee simulator,” *Med. Eng. Phys.*, vol. 27, no. 5, pp. 357–367, Jun. 2005, doi: 10.1016/j.medengphy.2004.11.003.

[103] A. Shademan *et al.*, “Supervised autonomous robotic soft tissue surgery.,” *Sci. Transl. Med.*, vol. 8, no. 337, 2016, doi: 10.1126/scitranslmed.aad9398.

[104] A. Shademan, R. S. Decker, J. D. Opfermann, S. Leonard, A. Krieger, and P. C. W. Kim, “Supervised autonomous robotic soft tissue surgery,” *Sci. Transl. Med.*, vol. 8, no. 337, pp. 337ra64-337ra64, May 2016, doi: 10.1126/scitranslmed.aad9398.

[105] A. Issa, M. O. A. Aqel, A. Tubail, Y. Alkayyali, A. Alay, and M. Ferwana, “Vision Assisted SCARA Manipulator Design and Control Using Arduino and LabVIEW,” in *2017 International Conference on Promising Electronic Technologies (ICPET)*, Oct. 2017, pp. 54–59, doi: 10.1109/ICPET.2017.16.

[106] M. Homayounzade and A. Khademhosseini, “Disturbance Observer-based Trajectory Following Control of Robot Manipulators,” *Int. J. Control. Autom. Syst.*, vol. 17, no. 1, pp. 203–211, Jan. 2019, doi: 10.1007/s12555-017-0544-x.

[107] A. Mohammadi, H. J. Marquez, and M. Tavakoli, “Disturbance observer-based trajectory following control of nonlinear robotic manipulators,” *Proc. 23rd Can. Congr. Appl. Mech.*, no.

June 2014, pp. 779–782, 2011.

[108] M. C S, M. K. Gupta, and S. Mohan, “Disturbance observer-assisted hybrid control for autonomous manipulation in a robotic backhao,” *Arch. Mech. Eng.*, vol. 66, no. 2, pp. 153–169, 2019, Accessed: Jul. 12, 2019. [Online]. Available: http://www.czasopisma.pan.pl/dlibra/publication/128442/edition/112047/content.

[109] M. Homayounzade and A. Khademhosseini, “Disturbance Observer-based Trajectory Following Control of Robot Ma- nipulators,” *Int. J. Control. Autom. Syst.*, vol. 17, no. 1, pp. 203–211, 2019.

[110] S. D. Olabarriaga and A. W. M. Smeulders, “Interaction in the segmentation of medical images : A survey,” *Med. Image Anal.*, vol. 5, pp. 127–142, 2001.

[111] Z. Peng, Q. Shj, S. Qu, and Q. Li, “Interactive image segmentation using geodesic appearance overlap graph cut,” *Signal Process. Image Commun.*, vol. 78, pp. 159–170, 2019, doi: 10.1016/j.image.2019.06.012.

[112] A. Protiere and G. Sapiro, “Interactive image segmentation via adaptive weighted distances,” *IEEE Trans. Image Process.*, vol. 16, no. 4, pp. 1046–1057, Apr. 2007, doi: 10.1109/TIP.2007.891796.

[113] N. A. bin Abdul Rahman, K. C. Wei, and J. See, “RGB-H-CbCr Skin Colour Model for Human Face Detection,” *Proc. MMU Int. Symp. Inf. Commun. Technol. (M2USIC 2006)*, pp. 90–96, 2006, [Online]. Available: http://ac.aua.am/skhachat/Public/Papers on Face Detection/RGB-H-CbCr Skin Colour Model for Human Face Detection.pdf%5Cnhttp://ac.aua.am/skhachat/Public/Papers on Face Detection/RGB-H-CbCr Skin Colour Model for Human Face Detection.pdf%5Cnpapers2://publica.

[114] M. Abdullah-Al-Wadud and O. Chae, “Region-of-Interest Selection for Skin Detection Based Applications,” in *International Conference on Convergence Information Technology*, Apr. 2008, pp. 1999–2004, doi: 10.1109/iccit.2007.267.

[115] S. Kolkur, D. Kalbande, P. Shimpi, C. Bapat, and J. Jatakia, “Human Skin Detection Using RGB, HSV and YCbCr Color Models,” in *International Conference on Communication and Signal Processing*, 2017, vol. 137, pp. 324–332, doi: 10.2991/iccasp-16.2017.51.

[116] F. Gasparini and R. Schettini, “Skin segmentation using multiple thresholding,” in *Internet Imaging VII*, Jan. 2006, vol. 6061, no. 60610, p. 60610F, doi: 10.1117/12.647446.

[117] B. L. Price, B. Morse, and S. Cohen, “Geodesic graph cut for interactive image segmentation,” in *Proceedings of the IEEE Computer Society Conference on Computer Vision and Pattern Recognition*, 2010, pp. 3161–3168, doi: 10.1109/CVPR.2010.5540079.

[118] S. Marcel, O. Bernier, J.-E. Viallet, and D. Collobert, “Hand Gesture Recognition using Input-

Output Hidden Markov Models," 2000, Accessed: Apr. 13, 2019. [Online]. Available: http://www.idiap.ch/resource/gestures/papers/marcel-fg-00.pdf.

[119] V. Verma, A. Rajput, P. Chauhan, H. Rathore, P. Goyal, and M. K. Gupta, "7. Machine vision for human–machine interaction using hand gesture recognition," in *Intelligent Decision Support Systems*, De Gruyter, 2019, pp. 155–181.

[120] C. Rother, V. Kolmogorov, and A. Blake, "'GrabCut' - Interactive foreground extraction using iterated graph cuts," in *ACM Transactions on Graphics*, 2004, vol. 23, no. 3, pp. 309–314, doi: 10.1145/1015706.1015720.

[121] M. J. Fard, S. Ameri, R. B. Chinnam, and R. D. Ellis, "Soft Boundary Approach for Unsupervised Gesture Segmentation in Robotic-Assisted Surgery," *IEEE Robot. Autom. Lett.*, vol. 2, no. 1, pp. 171–178, 2016, doi: 10.1109/LRA.2016.2585303.

[122] S. K. K., J. C. F., and E. R. B., "Unsupervised Wound Image Segmentation," *ICTACT J. Image Video Process.*, vol. 04, no. 03, pp. 737–747, Feb. 2014, doi: 10.21917/ijivp.2014.0107.

[123] S. K. Ueng and C. Y. Chang, "Skin color model adaptation under varying lighting conditions," *Adv. Mech. Eng.*, vol. 8, no. 9, pp. 1–8, 2016, doi: 10.1177/1687814016668999.

[124] H. Lombaert, Y. Sun, and … L. G., "A multilevel banded graph cuts method for fast image segmentation," in *Tenth IEEE International Conference on Computer Vision (ICCV'05)* , 2005, pp. 259–265, Accessed: Mar. 03, 2020. [Online]. Available: https://ieeexplore.ieee.org/abstract/document/1541265/.

[125] S. Sankaran, J. R. Hagerty, M. Malarvel, G. Sethumadhavan, and W. V. Stoecker, "A comparative assessment of segmentations on skin lesion through various entropy and six sigma thresholds," in *Lecture Notes in Computational Vision and Biomechanics*, vol. 30, Springer Netherlands, 2019, pp. 179–188.

[126] A. Blake, C. Rother, M. Brown, P. Perez, and P. Torrmicrosoft, "Interactive image segmentation using an adaptive GMMRF model," in *European conference on computer vision*, 2004, vol. 3021, pp. 428–441, doi: 10.1007/978-3-540-24670-1_33.

[127] N. Selvarasu, A. Nachiappan, and N. M. Nandhitha, "Abnormality detection from medical thermographs in human using Euclidean distance based color image segmentation," in *2010 International Conference on Signal Acquisition and Processing, ICSAP 2010*, Feb. 2010, pp. 73–75, doi: 10.1109/ICSAP.2010.63.

[128] L. Canalini, J. Klein, D. Miller, and R. Kikinis, "Registration of ultrasound volumes based on euclidean distance transform," in *Lecture Notes in Computer Science (including subseries Lecture Notes in Artificial Intelligence and Lecture Notes in Bioinformatics)*, Oct. 2019, vol. 11851 LNCS, pp. 127–135, doi: 10.1007/978-3-030-33642-4_14.

[129] W. J. Niessen, B. M. Ter, H. Romeny, and M. A. Viergever, “Geodesic Deformable Models for Medical Image Analysis,” *IEEE Trans. Med. Imaging*, vol. 17, no. 4, 1998.

[130] N. A.Ibraheem, R. Z. Khan, and M. M. Hasan, “Comparative Study of Skin Color based Segmentation Techniques,” *Int. J. Appl. Inf. Syst.*, vol. 5, no. 10, pp. 24–39, 2013, doi: 10.5120/ijais13-450985.

[131] G. Q. Ma, Z. L. Yu, G. H. Cao, Y. Bin Zheng, and L. Liu, “The Kinematic Analysis and Trajectory Planning Study of High-Speed SCARA Robot Handling Operation,” *Appl. Mech. Mater.*, vol. 687–691, pp. 294–299, 2014, doi: 10.4028/www.scientific.net/amm.687-691.294.

[132] A. Visioli and G. Legnani, “On the trajectory tracking control of industrial SCARA robot manipulators,” *IEEE Trans. Ind. Electron.*, vol. 49, no. 1, pp. 224–232, 2002, doi: 10.1109/41.982266.

[133] N. N. Son, C. Van Kien, and H. P. H. Anh, “A novel adaptive feed-forward-PID controller of a SCARA parallel robot using pneumatic artificial muscle actuator based on neural network and modified differential evolution algorithm,” *Rob. Auton. Syst.*, vol. 96, pp. 65–80, 2017, doi: 10.1016/j.robot.2017.06.012.

[134] J. Weng, “Design and Implementation of the SCARA Robot Arm,” no. Icarob, pp. 71–74, 2017.

[135] V. Verma, P. Chauhan, and M. K. Gupta, “Disturbance Observer-assisted Trajectory Tracking Control for Surgical Robot Manipulator,” *J. Eur. des Syst. Autom.*, vol. 52, no. 4, pp. 355–362, 2019, doi: 10.18280/jesa.520404.

[136] E. Sariyildiz, R. Oboe, and K. Ohnishi, “Disturbance Observer-based Robust Control and Its Applications: 35th Anniversary Overview,” *IEEE Trans. Ind. Electron.*, vol. PP, no. c, pp. 1–1, 2019, doi: 10.1109/tie.2019.2903752.

[137] S. Hao, L. Hu, and P. X. Liu, “Sliding Mode Control for a Surgical Teleoperation System via a Disturbance Observer,” *IEEE Access*, vol. 7, pp. 1–1, 2019, doi: 10.1109/access.2019.2901899.

[138] N. A. Anang *et al.*, “Tracking performance of NPID controller for cutting force disturbance of ball screw drive,” *J. Mech. Eng. Sci. ISSN*, vol. 11, no. 4, pp. 3227–3239, 2017, doi: 10.15282/jmes.11.4.2017.25.0291.

[139] B. M. Pillai and J. Suthakorn, “Motion control applications : observer based DC motor parameters estimation for novices,” *Int. J. Power Electron. Drive Syst.*, vol. 10, no. 1, pp. 195–210, 2019, doi: 10.11591/ijpeds.v10n1.pp195-210.

[140] Y. Singh and M. Santhakumar, “Inverse dynamics and robust sliding mode control of a planar parallel (2-PRP and 1-PPR) robot augmented with a nonlinear disturbance observer,” *Mech. Mach. Theory*, vol. 92, pp. 29–50, 2015, doi: 10.1016/j.mechmachtheory.2015.05.002.

[141] S. Huang, W. Liang, and K. K. Tan, “Intelligent Friction Compensation : A Review,”

IEEE/ASME Trans. Mechatronics, vol. 24, no. 4, pp. 1763–1774, 2019, doi: 10.1109/TMECH.2019.2916665.

[142] T. N. Do, T. Tjahjowidodo, M. W. S. Lau, and S. J. Phee, "Nonlinear friction modelling and compensation control of hysteresis phenomena for a pair of tendon-sheath actuated surgical robots," *Mech. Syst. Signal Process.*, pp. 1–15, 2015, doi: 10.1016/j.ymssp.2015.01.001.

[143] W. H. Chen, J. Yang, L. Guo, and S. Li, "Disturbance-Observer-Based Control and Related Methods - An Overview," *IEEE Trans. Ind. Electron.*, vol. 63, no. 2, pp. 1083–1095, 2016, doi: 10.1109/TIE.2015.2478397.

[144] A. Mohammadi, H. J. Marquez, and M. Tavakoli, "Disturbance observer-based trajectory following control of nonlinear robotic manipulators," in *Proceedings of the 23rd CANCAM*, 2011, pp. 779–782, doi: 10.1.1.416.7576.

[145] A. Mohammadi, M. Tavakoli, H. J. Marquez, and F. Hashemzadeh, "Nonlinear Disturbance Observer Design For Robotic Manipulators," doi: 10.1016/j.conengprac.2012.10.008.

[146] A. Nikoobin and R. Haghighi, "Lyapunov-based nonlinear disturbance observer for serial n-Link robot manipulators," *J. Intell. Robot. Syst. Theory Appl.*, vol. 55, no. 2–3, pp. 135–153, Jul. 2009, doi: 10.1007/s10846-008-9298-2.

[147] A. Mohammadi, M. Tavakoli, H. J. Marquez, and F. Hashemzadeh, "Nonlinear disturbance observer design for robotic manipulators," *Control Eng. Pract.*, vol. 21, no. 3, pp. 253–267, Mar. 2013, doi: 10.1016/j.conengprac.2012.10.008.

[148] A. Ogulmus, A. Cakan, and M. Tınkır, "Modeling And Position Control Of Scara Type 3D Printer," *Int. J. Sci. Technol. Res.*, vol. 5, no. 12, pp. 140–143, 2016.

[149] L. Angel and J. Viola, "Fractional order PID for tracking control of a parallel robotic manipulator type delta," *ISA Trans.*, pp. 1–17, 2018, doi: 10.1016/j.isatra.2018.04.010.

[150] M. Santhakumar, "A nonregressor nonlinear disturbance observer-based adaptive control scheme for an underwater manipulator," *Adv. Robot.*, vol. 27, no. 16, pp. 1273–1283, Nov. 2013, doi: 10.1080/01691864.2013.819608.

[151] V. Venkatesan, S. Mohan, and J. Kim, "Disturbance observer based terminal sliding mode control of an underwater manipulator," in *2014 13th International Conference on Control Automation Robotics & Vision (ICARCV)*, Dec. 2014, pp. 1566–1572, doi: 10.1109/ICARCV.2014.7064549.

[152] M. R. Soltanpour and S. E. Shafiei, "Robust Adaptive Control of Manipulators in the Task Space by Dynamical Partitioning Approach," *Elektron. ir Elektrotechnika*, vol. 101, no. 5, pp. 73–78, 2010, doi: 10.5755/J01.EEE.101.5.9429.

[153] P. Cao, Y. Gan, and X. Dai, "Finite-Time Disturbance Observer for Robotic Manipulators,"

Sensors (Basel)., vol. 19, no. 8, pp. 1–11, 2019, doi: 10.3390/s19081943.

[154] X. Liu, G. Zuo, J. Zhang, and J. Wang, “Sensorless force estimation of end-effect upper limb rehabilitation robot system with friction compensation,” *Int. J. Adv. Robot. Syst.*, vol. 16, no. 4, p. 172988141985613, Jul. 2019, doi: 10.1177/1729881419856132.

[155] W. H. Chen, “Disturbance observer based control for nonlinear systems,” *IEEE/ASME Trans. Mechatronics*, vol. 9, no. 4, pp. 706–710, 2004, doi: 10.1109/TMECH.2004.839034.

[156] S. Ding, W.-H. Chen, K. Mei, and D. Murray-smith, “Disturbance Observer Design for Nonlinear Systems Represented By Input-Output Models,” *IEEE Trans. Ind. Electron.*, vol. PP, no. c, pp. 1–1, 2019, doi: 10.1109/TIE.2019.2898585.

[157] A. Habibollahi, A. Nikoobin, and A. Dideban, “Lyapunov-Based Nonlinear Disturbance Observer for n-Link Flexible Joint Robot Manipulators,” *Control Eng. Appl. INFORMATICS*, vol. 20, no. 2, pp. 22–32, 2018.

[158] M. Homayounzade and A. Khademhosseini, “Disturbance Observer-based Trajectory Following Control of Robot Manipulators,” *Int. J. Control. Autom. Syst.*, vol. 17, no. 1, pp. 203–211, Jan. 2019, doi: 10.1007/s12555-017-0544-x.

[159] A. Munawar, “Implementation of a Surgical Robot Dynamical Simulation and Motion Planning Framework,” 2015.

APPENDIX A

The generalized dynamic equations for n- DOF robot manipulator were derived in chapter 3.. The equation of dynamics were derived using Newton Euler formulation as mentioned in Eqn. (4.27), as

$$M(q)\ddot{q} + N(q,\dot{q})\dot{q} + G(q) = \tau$$

The ALSR mass matrix (M), Coriolis matrix (N) and gravity matrix (G) of dynamics were illustrated in Eqn.(4.28) to Eqn.(4.30). The dynamic parameters mentioned in Eqn.(4.28) to Eqn.(4.30) were illustrated as ,

$$p_1 = l_1 + l_2 + l_3 + I_4 + m_1 l_1^2 + K1 + K2$$

$$p_2 = 2(2l_1 l_2 m_2 + 4l_1 l_3 (m_3 + m_4))$$

$$p_3 = I_2 + I_3 + I_4 + m_2 l_2^2 + 4l_2^2 (m_3 + m_4)$$

$$p_4 = m_3 + m_4$$

$$p_5 = I_4$$

$$K1 = m_2 (l_2^2 + 4l_1^2)$$

$$K2 = (m_3 + m_4)(4l_1^2 + 4l_2^2)$$

Where Ii is the moment of Inertia around the centroid, m_i is the mass, l_i is the length of link i.

LIST OF PUBLICATIONS

VARNITA VERMA

EDUCATION

2014-2016	M.Tech in Robotics Engineering, University of Petroleum & Energy Studies (UPES), Dehradun, India.
2009-2013	B.Tech in Electronics and Instrumentation Engineering, Uttar Pradesh Technical University, Lucknow, India.

JOURNAL PUBLICATIONS

1. **Varnita Verma**, Akash Gupta, Mukul Gupta, Piyush Chauhan *"Performance estimation of Computed Torque Control for Surgical Robot Application",* Journal of Mechanical Engineering and Science, vol. 14, no. 3, pp. 7017 - 7028, Sep. 2020, https://doi.org/10.15282/jmes.14.3.2020.04.0549
2. **Varnita Verma**, Piyush Chauhan, Mukul Kumar Gupta, "*Disturbance observer-assisted trajectory tracking control for surgical robot manipulator"*. Journal Européen des Systèmes Automatisés, Vol. 52, No. 4, pp. 355-362, 2019. https://doi.org/10.18280/jesa.520404
3. **Varnita Verma**, Anil Kumar, Mukul Gupta, Piyush Chauhan, *"Interactive Segmentation Technique for Ex-Vivo Skin Laceration Detection"*. International Journal on Emerging Technologies, 11(3): 371–376, 2020
4. Akash Gupta, Anshuman Singh, **Varnita Verma**, Amit Kumar Mondal & Mukul Kumar Gupta, "*Developments and clinical evaluations of*

robotic exoskeleton technology for human upper-limb rehabilitation, Advanced Robotics", 2020, DOI: 10.1080/01691864.2020.1749926

BOOK CHAPTERS

1. **Varnita Verma,** Anshuman Rajput, Piyush Chauhan, Harshit Rathore, Piyush Goyal, Mukul Kumar Gupta, "*7. Machine vision for human–machine interaction using hand gesture recognition".* In Surekha Borra, Nilanjan Dey, Siddhartha Bhattacharyya, Mohamed Salim Bouhlel (Eds.), Intelligent Decision Support Systems: Applications in Signal Processing (pp. 155–181), 2019. Berlin, **Boston: De Gruyter**. https://doi.org/10.1515/9783110621105-007
2. **Varnita Verma**, Vinay Chowdary, Mukul Kumar Gupta, and Amit Kumar Mondal. *Chapter 10 "IoT and Robotics in Healthcare"* Page No. (245-270). Hassanien, A. E., Dey, N., & Borra, S. (Eds.). (2018). Medical Big Data and Internet of Medical Things: Advances, Challenges and Applications. **CRC Press.**

URKUND

Document Information

Analyzed document	thesis_phd_final_29.pdf (D82383561)
Submitted	10/22/2020 11:11:00 AM
Submitted by	Varnita Verma
Submitter email	vverma@ddn.upes.ac.in
Similarity	4%
Analysis address	vverma.upes@analysis.urkund.com

Sources included in the report

W	URL: https://doi.org/10.15282/jmes.14.3.2020.04.0549 Fetched: 10/22/2020 11:13:00 AM	4
SA	**Thesis3144611.pdf** Document Thesis3144611.pdf (D20955442)	2
SA	**C&A-371.pdf** Document C&A-371.pdf (D54848733)	2
W	URL: https://www.researchgate.net/publication/337276998_Disturbance_Observer-assisted_T ... Fetched: 10/22/2020 7:37:19 AM	25
W	URL: https://core.ac.uk/download/pdf/80148954.pdf Fetched: 3/24/2020 8:24:56 PM	4
SA	**J.Senthil Kumar Thesis.pdf** Document J.Senthil Kumar Thesis.pdf (D25565154)	1
W	URL: https://www.researchgate.net/publication/319417730_Regularization_of_the_different ... Fetched: 10/22/2020 11:13:00 AM	1
SA	**Msc_Project_Report-Binbin TAN-2186870.pdf** Document Msc_Project_Report-Binbin TAN-2186870.pdf (D21438264)	1
W	URL: https://doi.org/10.1515/9783110621105-007 Fetched: 10/22/2020 11:13:00 AM	2
J	**Nonlinear Disturbance Observers: Design and Applications to Euler?Lagrange Systems** URL: e6a169b5-cab4-4dc3-8444-14c8ddfdf86b Fetched: 4/2/2019 3:57:54 PM	3